This is to certify that the

dissertation entitled

Interfacial Changes During the Processing of a Typical Carbon Fiber/Epoxy Composite Material

presented by

Venkatesh Rao

has been accepted towards fulfillment
of the requirements for

Ph.D. degree in Chemical Engr.

Lawrence T. Drzal
Major professor

Date November 12, 1991

INTERFACIAL CHANGES DURING THE PROCESSING OF A TYPICAL CARBON FIBER/EPOXY COMPOSITE MATERIAL

by

Venkatesh Rao

A DISSERTATION

Submitted to
Michigan State University
in partial fulfillment of the requirements
for the degree of

DOCTOR OF PHILOSOPHY

Department of Chemical Engineering

1991

ABSTRACT

INTERFACIAL CHANGES DURING THE PROCESSING OF A TYPICAL CARBON FIBER/EPOXY COMPOSITE MATERIAL

By

Venkatesh Rao

The effect of the processing cycle on the interfacial shear strength of a thermoset mPDA/DGEBA matrix reinforced with carbon, AS4 fibers was investigated. The processing cycle of a thermoset can be conveniently divided into three different regimes: the fluid regime (up to the point of matrix gelation), the ambient temperature regime (room temperature), and the elevated temperature regime. In each of these regimes, readily measurable material properties of the matrix will be related to the fiber-matrix interfacial shear strength using model single fiber techniques to quantify the interfacial shear strength.

In the fluid regime, the kinetics of crosslinking are used to determine gelation times. A modified Williams-Landel-Ferry (WLF) equation is then used to model the viscosity changes as a function of the extent of cure. Gravimetric pull-out tests are conducted to relate the viscoelastic properties of the matrix to an interfacial pull-out strength. Results indicate that in the fluid regime, the interfacial strength begins to develop and increases with increasing viscosity of the reacting matrix. A modified WLF-type model is used to describe the dependence of interfacial pull-out strength on extent of cure.

At ambient conditions, constant interfacial and matrix chemistry is used to systematically vary the matrix properties from ductile to brittle in order to simulate the actual processing cycle. These matrix properties are then related to the interfacial shear strength (the single fiber fragmentation test is used to quantify the interfacial shear strength). Different length polyether diamine curing agents are used to alter the matrix properties while keeping the chemical bonding and chemistry at the interface constant. It will be shown that the interfacial shear strength decreases monotonically with decreasing modulus of matrix. A shear lag model is shown to model the changes in interfacial shear strength as a function of matrix properties down to a matrix shear modulus of 1 GPa. Radial compressive stresses as well as the fiber wettability characteristics are shown to play a minor role in comparison to the changing material properties of the matrix in determining the level of adhesion at the interface.

At elevated temperatures, interfacial (single fiber) shear strength measurements confirm the reduction in interfacial shear strength with a reduction in matrix modulus. As the glass transition of the matrix is approached, a large decrease in interfacial shear strength is noted parallel to the decrease in matrix modulus. The results were used to generate a master curve capable of predicting the changes in interfacial shear strength as a function of temperature. Additionally, epoxy sized fibers were used to study and model the formation of an interphase by preferential diffusion of the curing agent into the coating and creating an interphase with different mechanical properties than the bulk matrix. A model for the formation of the interphase is presented.

TO:

MY DAD AND MOM

Dr. S. Tyagaraja Rao and Lalitha Rao

ACKNOWLEDGEMENTS

As with any undertaking of this size and magnitude, many people need to be thanked and form the backbone necessary for proper completion of the task. I start with my sincere appreciation to Dr. Lawrence T. Drzal for his guidance, support, encouragement, and flexibility throughout the duration of this project. It has been a pleasure to work with him and I have certainly learned a great deal during my stay here at Michigan State University.

I also wish to thank my fellow chemical engineering graduate students at the Composites center past and present--Raj, Shri, Javad, Brent, Craig, Greg, Ed, Sanjay and many others for their assistance and friendship and for making my stay here a very enjoyable one. In addition, I wish to thank Mike Rich, Brian Rook, Hassan Al-Moussawi, Pedro Franco-Herrera and Shekar for their help in equipment operation, experimental analysis as well as their friendship. My thanks also go to Steve Kahl and Ethan Russell for their help in some of the data acquisition.

I am thankful to the other members of my committee--Dr. E. A. Grulke, Dr. M. Hawley, Dr. S. Selke and Dr. D. Liu for the time they dedicated to this dissertation.

I thank my parents and family for their emotional and financial support and their never-ending encouragement throughout my educational career.

Finally, I thank my wife Revathy for her love and support in enabling me to complete this work and for her ability to adjust to a new lifestyle in this country while at the same time enduring my sometimes long, irregular work hours over the past two years.

TABLE OF CONTENTS

LIST OF TABLES

LIST OF FIGURES

NOMENCLATURE

a	Dimensionless parameter $(k/D)^{0.5}$, defined by Equation D2
A_t	WLF shift factor
C	Concentration of curing agent (in interphase region)
C_{bulk}	Bulk concentration of curing agent
$C_{1,2}$	WLF constants defined by Equations 3.1 and 3.2
d, d_f	Diameter of fiber
d_{avg}	Average diameter of fiber
D, D_e	Average, effective diffusion coefficients
D(C)	Concentration dependent diffusion coefficient
DSC	Differential scanning calorimeter
DMA	Dynamic mechanical analyzer
erf	Error function
erfc	Complimentary error function (1-erf)
E_i	Immersion depth
E_f	Tensile modulus of fiber
E, E_m	Tensile (Young's) modulus of matrix
E/R	Ratio of activation energy to gas constant defined in Table 3.1
F	Pull-out or debonding force

F_{ss}	Steady-state pull-out force defined by Equation 2.4
g	Acceleration due to gravity (9.80665 m/sec^2)
G, G_m	Shear modulus of matrix
G'	Storage modulus of matrix
G"	Loss modulus of matrix
ISS	Interfacial shear strength
k	Pseudo first order rate constant of epoxy/amine reaction
$k_{1,2}$	Arrenhius based reaction rate constants
l_c	Critical length defined by Equation 2.1
L	Embedment length
m	Kinetic exponent defined by Equation 3.3
n	Kinetic exponent defined by Equation 3.3
P,p	Applied load
r_i	Radial distance from center of fiber to edge of interphase region
r_f	Radius of fiber
R	Universal gas constant (1.987 Kcal/mole-K)
R	Interfiber spacing in composites as defined by Equation 5.1
R(C)	Concentration dependent reaction rate defined by Equation 6.1
t	time
t_{gel}	Gelation time (time required to reach gel point)
t_p	Time to reach peak in reaction rate
T	Temperature

T_g	Glass transition temperature
T_o	Reference temperature chosen for shifting data (346°K)
TMA	Thermal mechanical analyzer
x,z,r	Radial distance parameters

GREEK SYMBOLS

α, α_{weib}	Weibull model scale parameter defined by Equation 2.2
α	Extent of reaction (conversion) defined by Equation 3.3
α_p	Conversion at peak reaction rate
$\dot{\alpha}$	Reaction rate, $d\alpha/dt$
$\dot{\alpha}_p$	Peak (maximum) reaction rate
β, β_{weib}	Weibull model shape parameter defined by Equation 2.2
B	Fiber scaling parameter defined by Equation 5.1
ϵ_f	Fracture strain of matrix
ϵ_b	Strain at which final break occurs in fragmentation test
ξ	Dimensionless distance defined by Equation 4.4
π	"pi", 3.14151629
ζ	Dimensionless distance defined by Equation B2
η	Viscosity defined by Equations 3.1 and 3.2
η_g	Viscosity of fully cured matrix, 10^{15} cP, defined by Equation 3.1
Δr	Interphase thickness
ΔT	$T-T_g$

σ_f	Tensile strength of fiber
ϕ	Dimensionless modulus defined by Equation 6.5
ψ	Dimensionless radial distance defined by Equation 6.5
$\gamma^t, \gamma_{l,t}$	Total surface free energy of material
γ^d, γ_d	Dispersive component of surface free energy
γ^p, γ_p	Polar component of surface free energy
θ	Contact angle in Wilhelmy experiments
δ	Partial differential operator
μ	micrometers (microns)
ν	Poisson's ratio
Γ	Gamma function defined by Equation 2.2

CHAPTER 1

BACKGROUND AND INTRODUCTION

There are three main points to be included in the definition of an acceptable composite material for use in structural applications [1]:

(1) It consists of two or more physically distinct and mechanically separable materials.

(2) It can be made by mixing the separate materials in such a way that the dispersion of one material in another can be done in a controlled way to achieve optimum properties.

(3) The properties are superior, and possibly unique in some specific respects to the properties of the individual components.

The last point provides the main impetus for the development of composite materials. They may be broadly classified as fibrous composites (consisting of fibers embedded in a matrix), laminated composites (layers of various fibrous composites), and particulate composites (consisting of particles in a matrix). The discussion in this work will be restricted to fibrous composites.

Fibrous composites are composed of fibers, which are usually aligned and embedded in a polymeric matrix. The fibers themselves can be of various types, the most prominent being carbon, glass and Kevlar fibers. Comparison of the typical properties of these fibers [1] are illustrated in Table 1.1 below.

All polymers are potential candidates for matrix materials. But limitations such as end properties and processability rule out quite a number of them [2]. Epoxy resins are the most widely used thermosetting matrices, due to their ease of processability and good properties at low to moderate temperatures. Typical mechanical and thermal properties [3] of an epoxy resin are illustrated in Table 1.2 below.

A typical process for producing epoxy/carbon fiber composites involves drawing carbon fibers through a vat of epoxy resin and winding the epoxy coated fibers onto a

Table 1.1: Properties of carbon, glass and Kevlar 49 fibers at 20°C

Property	Carbon Fibers (PAN Based)	E Glass Fibers	Kevlar 49 Fibers
Diameter (microns)	7-8	8-14	11-12
Density (10^3 kg-m^{-3})	1.75	2.56	1.45
Young's Modulus (GN-m^{-2})	250	76	125
Transverse Modulus (GN-m^{-2})	20	76	---
Tensile Strength (GN-m^{-2})	2.70	1.4-2.5	2.8-3.6
Strain to Failure (%)	1.0-1.5	1.8-3.2	2.2-2.8

mandrel. The mandrel containing the wound fibers in epoxy matrix is then subject to a thermally driven processing cycle which initiates devolatilization [4]. The curing occurs in two stages. In stage I, the material is reacted to produce a lightly crosslinked structure at moderate temperatures. In stage II, the material is post cured at higher

Table 1.2: Properties of a typical Epoxy Resin

Property	Typical Epoxy Resin
Density ($Mg\text{-}m^{-2}$)	1.1-1.4
Tensile Modulus ($GN\text{-}m^{-2}$)	3-6
Poisson's Ratio	0.38-0.40
Tensile Strength ($MN\text{-}m^{-2}$)	35-100
Compressive Strength ($MN\text{-}m^{-2}$)	100-200
Strain to Failure (%)	1-6
Coefficient of Thermal Expansion (10^{-6} °C^{-1})	60-65
Heat Distortion Temp. (C)	50-300
Shrinkage upon Curing (%)	1-2

temperatures and longer times to arrive at the final composite. After curing and post curing are completed, the composite is cooled to ambient conditions.

There is a major problem associated with epoxy/carbon fiber composites and any thermoset composite made in this fashion. During processing, defects are produced and

appear as large wavy regions of fibers in the interior of the composite (see Figure 1.1 below).

When exposed to high pressure differences between the interior and exterior, it is possible that these defects cause the composite to crack and fail in a direction normal to the wavy regions, due to compression and shear [5]. It is believed that these defects are formed during the curing process.

Upon cooling, especially below the glass transition temperature (T_g), internal stresses build up as a result of the different volume expansions in regions of differing temperature and extent of cure [6]. During the curing process, large temperature gradients occur in the composite caused by the heat transfer to the material through both the inner and outer surfaces of the cylinder and by the exotherm of the curing reaction. A temperature front begins at both inner and outer surfaces and travels towards the interior during curing. It is likely that a region of high temperature greater than the processing temperature exists where the two fronts meet in the interior of the composite. These high temperatures may lead to decomposition and/or charring of the matrix material and stress build-up during cooling. The region of maximum temperature during curing will remain the region of maximum temperature during cooling. The regions near the inner and outer surfaces during cooling will be at or below T_g, whereas at some region within the composite the temperature is at or above T_g. The stress build up in the regions near the surface may cause the material within the inner high temperature region to deform into the observed wavy patterns or delaminate the composite in this region. These defects are especially evident in the production of thick section composite structures ($>$ 0.5" thick) used in a variety of aerospace and naval applications [7,8].

It is the ability of the matrix to transmit stresses from fiber to fiber (through the interface) at the microscopic level that is responsible for internal stress development in a composite, which in turn is responsible for causing the generated defects.

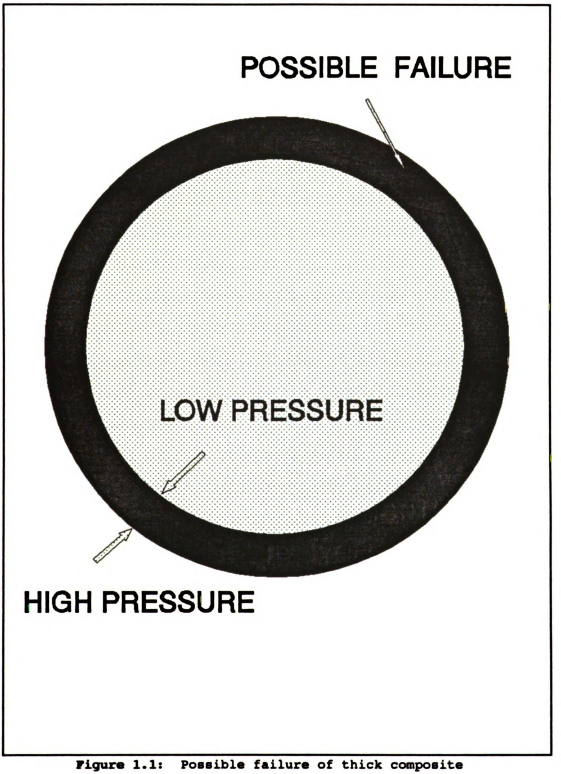

Figure 1.1: Possible failure of thick composite

Experimentally verified data on the generation of interfacial stresses and their variation

with temperature, extent of cure and time is needed. Interfacial properties are dependent on the matrix modulus and the interactions at the fiber-matrix interface. During processing there is a simultaneous increase in modulus with time and temperature. A typical time-temperature transformation (TTT) diagram [9,10] is shown in Figure 1.2 for a reacting thermoset system. It is critical that the mechanism by which the interfacial and mechanical properties are generated is understood and the mechanical properties known as a function of temperature, extent of cure and processing time. Interfacial shear strength and interfacial normal strength measurements have not been determined as a function of processing conditions.

While it is not possible to directly probe the in-situ stresses within a composite with high enough resolution, a separate study is required to generate this data. It is the objective of this study to measure interfacial shear properties during the entire processing cycle of a carbon fiber/thermoset material. In this study, single fiber methods [11], which allow for the isolation and measurement of interfacial properties will be combined with processing data to obtain the variation in interfacial (shear and normal) properties as a function of extent of processing. The interfacial shear strength will be directly measured as a function of the relevant material properties of the matrix being processed. As a result of this study, it will be possible to predict the interfacial shear strength given the changing material properties of the matrix during processing. This will ultimately allow for probing of the processing cycle in an attempt to identify where defects may begin occurring in the composite material.

The chapters in this thesis are generally arranged according to the regime of the processing cycle being discussed. The appendices contain some of the mathematical derivations as well as some of the experimental data. All the chapters are self contained in that there is an introduction section to overview the existing literature, an experimental section, a results and discussion section, a modeling section and finally, a set of

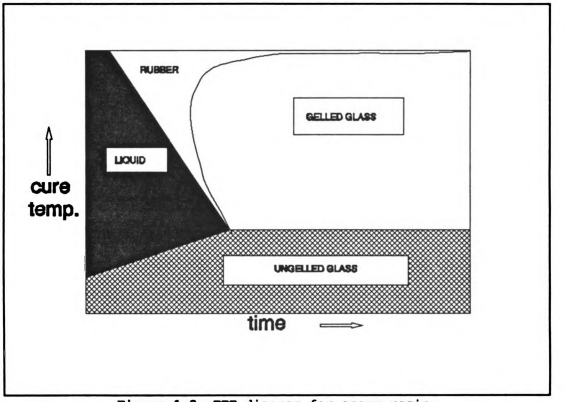

Figure 1.2: TTT diagram for epoxy resin

conclusions. Specifically, the chapters are arranged in the following order:

(1) Chapter 2 discusses the materials used and the experimental techniques employed in this study.

(2) Chapter 3 focuses on the kinetics of crosslinking, time to gelation, and in general, how the interface behaves in the viscous regime (up to the point of matrix gelation). Interfacial parameters are quantified with a single fiber gravimetric pull-out test.

(3) Chapter 4 deals with the microbond test for measuring the interfacial shear strength of brittle systems. It will be shown that diffusion of curing agent in small sized samples can alter the mechanical properties of the droplet specimens leading to misleading measurements of interfacial shear strength.

(4) Chapter 5 describes how the interface behaves at ambient conditions (after matrix gels and sets) as a function of bulk matrix and interfacial properties. Interfacial shear strength is quantified using the single fiber fragmentation test.

(5) Chapter 6 examines the role of elevated temperatures on interfacial shear strength. Single fiber fragmentation tests are conducted in a specially designed temperature chamber. Arguments will be made, using the data, for the formation of an interphase region.

(6) Chapter 7 describes normal strength measurements of the interface.

(7) Chapter 8 describes interfacial shear strength measurements on a thermoplastic system (Polycarbonate--Lexan) as a function of temperature.

(8) Chapter 9 presents the conclusions in a manner to coherently tie together the material in Chapters 3, 4 and 6. Also, Chapter 9 attempts to provide proper guidelines for future work that needs to be addressed in determining and modeling the changes at the interface during processing.

Additionally, in chapters 3-6 mathematical models will be presented for the prediction of interfacial properties based on material properties of the matrix. In chapter 3, a modified WLF equation [12] will be used to predict the interfacial pull-out force as a function of the changing viscosity of the reacting fluid medium. In chapter 4, an unsteady state Fickian-type [13] diffusion model will be used to analyze the transient diffusion characteristics of the curing agent out of the samples. In chapter 5, an existing shear-lag model proposed by Cox and modified later by Cooke [14] will be used to model the interfacial shear strength as a function of the changing material properties of the matrix. Finally, in Chapter 6, a predictive model will be presented for the description of the interfacial shear strength as a function of the modulus (or T_g) of the matrix. In addition, the steady-state Fickian diffusion equation (with a reaction term

[15]) will be used to mathematically explain the formation of an interphase region, whose properties (different from the bulk matrix) play a major role in determining the level of fiber/matrix adhesion. The elevated temperature interfacial shear strength data will be used to predict an effective diffusion coefficient in the interphase region, the thickness of the interphase region as well as to validate the model.

CHAPTER 2

EXPERIMENTAL MATERIALS AND METHODS

2.1 MATERIALS SELECTION

2.1.1 EPOXY RESINS

The term "epoxy" refers to a reactive chemical group consisting of an oxygen atom bonded to two other atoms already united in some way [16]. Since their discovery, epoxy resins have been the subject of a plethora of patents and technical publications. There has been more written about these products per pound of sales [3] than any other commercially available thermosetting resins. This broad interest in epoxy resins comes from the wide variety of chemical reactions and materials that can be used for the curing and the wide spectrum of different properties that result. The chemistry is unique among the thermosetting resins. In contrast to formaldehyde resins [3], for example, an addition reaction takes place instead of a condensation reaction insuring that no volatiles are given off during cure. This means that only minimum pressures are required for the fabrication techniques normally used on these materials. The volumetric shrinkage [17] during curing is also much less than encountered in many other systems. This means reduced stresses in the cured final product. Moreover, a knowledge of the chemistry involved permits the user to process epoxy resins over a wide range of temperatures and to control the degree of crosslinking. As will be seen in later chapters, this last point plays an important role in the physical and interfacial properties of epoxy thermosets.

Considering the range of attainable properties, the versatility of epoxy resins becomes even more apparent. Depending on the chemical nature and structure of the curing agent and curing conditions, it is possible to obtain mechanical properties with a wide range of flexibility, strength, hardness, adhesive strength and electrical resistance [3]. Uncured, the resins have a variety of physical forms, ranging from low viscosity liquids

to tack-free solids, that, along with the curing agent, afford the experimentalist a wide range of processing conditions. In the absence of curing agents, the epoxies are also useful as plasticizers and coatings [3].

Two different types of epoxy resins were used as representative composite matrices in this particular study. A diglycidyl ether of Bisphenol-A (DGEBA)--EPON 828-Shell Chemical Company--was used for the majority of the study as the representative difunctional (with and Epoxy Equivalent Weight of about 180) epoxy resin while MY720 (Araldite, Ciba Geigy, EEW of about 125) was used as the representative tetrafunctional epoxy resin. The structures of both these compounds are illustrated in Figure 2.1.

2.1.2 CURING AGENTS

Epoxides are notable for their high degree of reactivity towards a variety of nucleophilic and electrophilic reagents. Extensive and detailed reviews of curing agents are available elsewhere, see for example Tanaka and Mika [18] and Mika [19]. In general, epoxy resin curing reactions involve opening of the epoxide ring followed either by a homopolymerization reaction with further epoxides or reaction with the "curing agent" to form addition products.

Amongst the curing agents of greatest technological and structural importance [20] are the polycarboxylic anhydrides, polyamines, and anionic or cationic catalysts. In this work, all curing agents used were polyamines (diamines and triamines).

Figure 2.2 shows the chemical structures of all the curing agents employed in this study. Meta-phenylenediamine (mPDA) was used as the baseline curing agent. The other curing agents used were diamino-diphenyl sulfone (DDS) and a series of polyetheramines (Jeffamines, Texaco Co.) having oxypropylene units of varying length between the end amines. These different curing agents resulted in final properties of the matrix varying from brittle to ductile while at the same time preserving the interfacial

to tack-free solids, that, along with the curing agent, afford the experimentalist a wide range of processing conditions. In the absence of curing agents, the epoxies are also useful as plasticizers and coatings [3].

Two different types of epoxy resins were used as representative composite matrices in this particular study. A diglycidyl ether of Bisphenol-A (DGEBA)--EPON 828-Shell Chemical Company--was used for the majority of the study as the representative difunctional (with and Epoxy Equivalent Weight of about 180) epoxy resin while MY720 (Araldite, Ciba Geigy, EEW of about 125) was used as the representative tetrafunctional epoxy resin. The structures of both these compounds are illustrated in Figure 2.1.

2.1.2 CURING AGENTS

Epoxides are notable for their high degree of reactivity towards a variety of nucleophilic and electrophilic reagents. Extensive and detailed reviews of curing agents are available elsewhere, see for example Tanaka and Mika [18] and Mika [19]. In general, epoxy resin curing reactions involve opening of the epoxide ring followed either by a homopolymerization reaction with further epoxides or reaction with the "curing agent" to form addition products.

Amongst the curing agents of greatest technological and structural importance [20] are the polycarboxylic anhydrides, polyamines, and anionic or cationic catalysts. In this work, all curing agents used were polyamines (diamines and triamines).

Figure 2.2 shows the chemical structures of all the curing agents employed in this study. Meta-phenylenediamine (mPDA) was used as the baseline curing agent. The other curing agents used were diamino-diphenyl sulfone (DDS) and a series of polyetheramines (Jeffamines, Texaco Co.) having oxypropylene units of varying length between the end amines. These different curing agents resulted in final properties of the matrix varying from brittle to ductile while at the same time preserving the interfacial

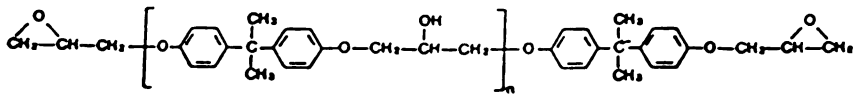

DIGLYCIDYL ETHER OF BISPHENOL A (DGEBA)
(DIFUNCTIONAL RESIN)

N,N,N',N'-Tetraglycidyl-4,4'-methylenebisbenzenamine

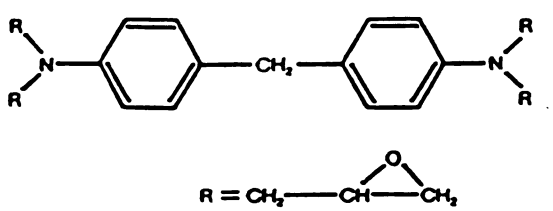

MY720 ARALDITE RESIN
(TETRAFUNCTIONAL RESIN)

Figure 2.1: Chemical structure of resins

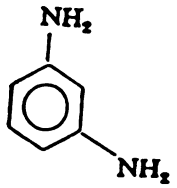

mPDA

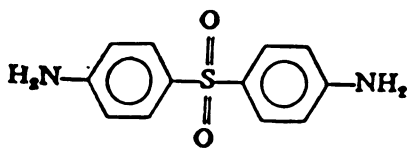

DDS

JEFFAMINE CURING AGENTS:

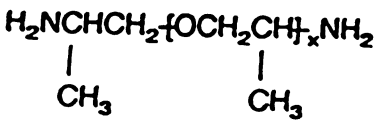

DI-AMINES

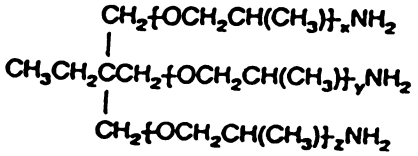

TRI-AMINES

Figure 2.2: Chemical structure of curing agents

chemistry. Unless otherwise noted, the standard curing cycles used for the various systems is listed below in Table 2.1.

Table 2.1: Curing schedules used in study

CURING AGENT	CURING SCHEDULE
mPDA	75°C-2hr, 125°C-2hr
DDS	180°C-1hr, 220°C-2hr
All Jeffamines	80°C-2 hr, 125°C-3hr

Unless otherwise noted, all matrix formulations in this study employed a stoichiometric amount of curing agent based on the epoxy equivalent weight of the resin and the amine equivalent weight of the curing agent. Table 2.2 below shows the proportions used for the different curing agents employed in this study.

Table 2.2: Stoichiometry of curing agents used

CURING AGENT	AMOUNT USED (phr)
mPDA	14.5
DDS	35.8
J230	33.0
J400	56.0
J403	45.0
J700	117.0

One note of caution must be mentioned about the longer chained Jeffamine curing agents. Our results have shown that these curing agents have a tendency to degrade over time [21] leading to differing mechanical properties of the final, neat specimens. Care must be exercised in storing these curing agents properly in dark, airtight containers.

2.1.3 FIBER REINFORCEMENTS

By 1960, it had been shown that cellulose textile fibers could be carbonized in reasonably large quantities to give low-grade carbon fibers [22]. The original carbon fibers were made from textile grades of PAN (poly-AcryloNitrile) and fortuitously many of their features proved to be advantageous. PAN has a $-CH_2-CH$ backbone with CN side groups [23]. The polarity of the nitrile side groups produces relatively strong intermolecular forces resulting in an amorphous structure.

The properties of the fiber-matrix interface are most significant. Carbon fibers straight from the final heat treatment furnace do not adhere well to polymeric matrices. They are usually given an oxidative surface treatment which increases the fiber-matrix bond strength but which can reduce the composite toughness. The level of surface treatment needs to be adjusted to give optimum overall properties. Fitzer [24] has presented an excellent review of the production of high performance carbon fibers and their applications.

The carbon fibers chosen for this study are the "A" type. These are produced by high temperature inert gas graphitization of PAN fiber. The morphology of the resulting carbon fiber is axially and radially symmetric composed of ribbons of graphitic crystals formed in turbostatic layers oriented almost parallel to the fiber axis as well as varying in orientation across the fiber diameter. Adhesion to these fibers, as mentioned above, in their untreated state by a typical amine cured epoxy results in very low values of interfacial shear strength [25]. Many surface treatments for improving the adhesion to carbon fibers have been proposed and various commercial ones are extensively described in existing patent literature [26].

The specific PAN based carbon fibers used in this study are the "A-4" type (Hercules Co.) having a fiber tensile modulus of about 238 GPa and a tensile strength of 3.5 GPa when measured at a 25 mm gage length. They are circular in cross section. The fibers

used in this study had two different surface conditions: (1) "AS4" fibers are surface treated with an electrochemical oxidation process which optimizes their adhesion to epoxy matrices and (2) "AS4-C" fibers, in addition to being surface treated, are coated with a 100-200 nm layer of epoxy applied from a organic solvent directly onto the AS4 fiber surface. A typical SEM micrograph showing the surface morphology of AS4 fibers is shown in Figure 2.3. The surface energetics and details on the surface morphology have been studied in detail by Drzal et al. and reported elsewhere [27].

2.2 EXPERIMENTAL METHODS

Many methods are available for determining the interfacial shear strength in a single fiber composite. Extensive reviews are available [11,28,149]. In this section, three different protocols for determining the interfacial shear strength of single fiber systems will be outlined. Also, in this section, experimental procedures for determining the material, thermal and optical properties of the matrices will be given. Finally, an experimental protocol will be given for determination of the surface free energies of the matrices and fibers used.

2.2.1 SINGLE FIBER FRAGMENTATION TEST

The single fiber fragmentation test was originally used by Kelly and Tyson [29] who used some brittle fibers embedded in a copper matrix. They observed that upon application of a tensile load to the matrix, a multiple fiber fracturing phenomenon took place. Since then, many experimenters [30,31,32,33,34] have used this technique to study fiber/matrix adhesion in single filament thermoset as well as thermoplastic systems.

In general, the fragmentation test involves fabrication of single fiber specimens. This is achieved by mixing of the curing agent and resin in proper proportions and pouring into a mold with a fiber aligned axially within it followed by appropriate curing. The mold itself is a silicone room temperature vulcanizing (RTV 664) eight cavity mold.

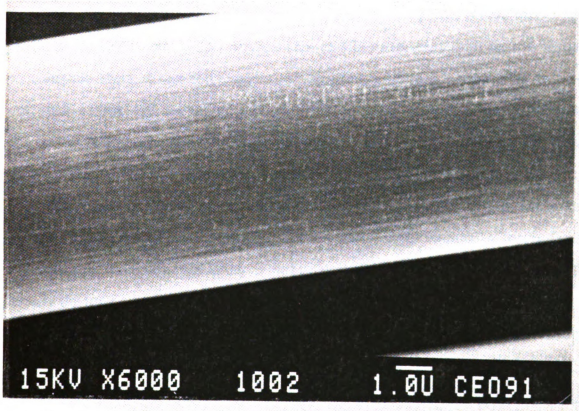

Figure 2.3: Scanning electron micrograph of carbon, AS4 fiber

Standard ASTM 64 mm "dogbone" specimen cavities with a 3.18 mm wide by 1.59 mm thick by 25.4 mm gage section are molded into a 76.2 x 203.2 x 12.7 mm silicone piece. Sprue slots are molded in the middle of each dog bone to a depth of 1/32" and through the end of the silicone piece. A more detailed description of the dimensions of the molds used has been given by Herrera-Franco et al. [28].

Single fibers approximately 5" length are selected by hand from a fiber bundle kept inside of aluminum foil. Single filaments are carefully separated from the tow without touching the fibers, except at the ends. Once selected, a filament is mounted in the mold and held in place with a small amount of rubber cement at the end of the sprue. After the rubber cement sets, the liquid matrix is carefully pipetted into the molds and cured. More details on this procedure have been provided by Herrera-Franco et al. [28,35].

After the fiber is totally encapsulated in a matrix coupon and cured, a tensile load is applied to the coupon, and an interfacial shear stress transfer mechanism is relied upon to transfer the coupon tensile forces to the encapsulated fiber through the interface. The tensile jig used for straining the specimens is shown in Figure 2.4. As the load is increased on the specimen, shear forces are transmitted to the fiber along the interface. The fiber tensile stress increases to the point where the fracture strength of the fiber is exceeded and the fiber breaks inside the matrix. This process is repeated producing shorter and shorter fragments until the remaining fragment lengths are no longer sufficient in size to produce additional fracture through this stress transfer mechanism. At this point, the critical length (l_c) is said to have been reached. This fragment process is shown schematically in Figure 2.5. The fragment critical length-to-diameter (l_c/d) is measured with the aid of the optical microscope, under which all the tests are conducted. A shear lag analysis is completed (force balance at the interface) on the fragments in order to calculate an interfacial shear strength, τ, according to:

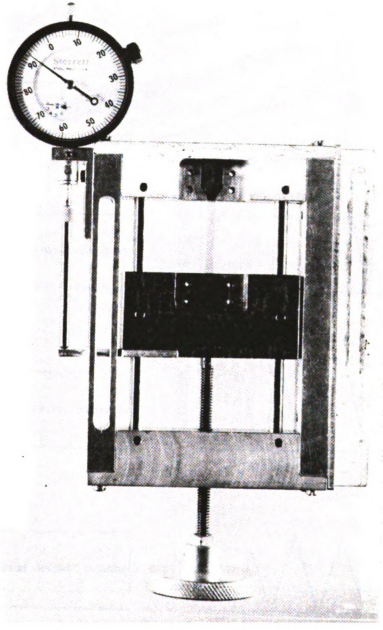

Figure 2.4: Tensile jig used for conducting fragmentation tests

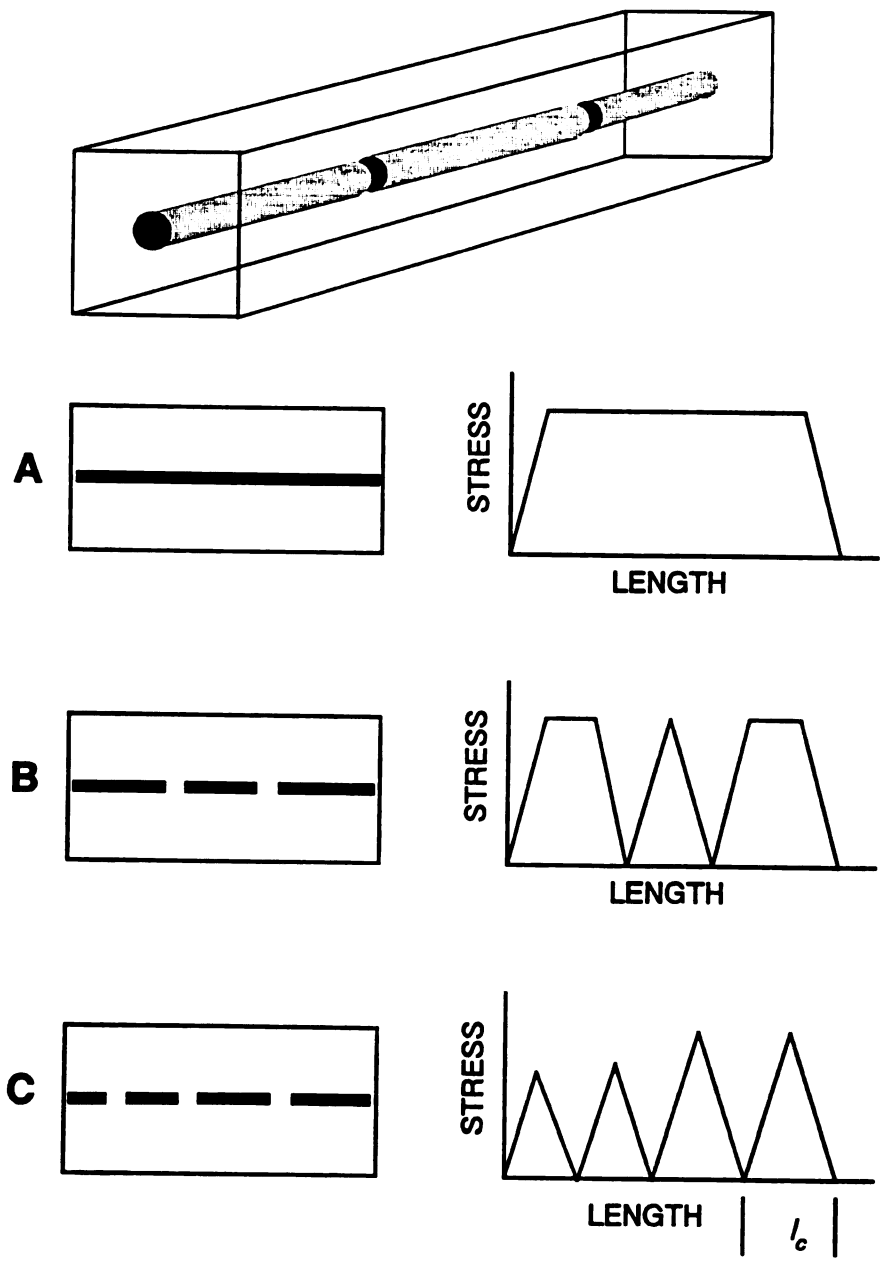

Figure 2.5: Process of fragmentation

$$\tau = \frac{\sigma_f}{2}\frac{d}{l_c} \qquad (2.1)$$

Different statistical analyses exist and have been used for fitting the distribution of critical lengths [28,36,37]. Throughout this work, the distribution of critical lengths will be fit to a two-parameter Weibull statistical model [30,36,51] and the following equation will be used to calculate τ, the interfacial shear strength. Where α and B are the shape

$$\tau = \frac{\sigma_f}{2\beta}\Gamma\left(1-\frac{1}{\alpha}\right) \qquad (2.2)$$

and scale parameters, respectively, and Γ is the Gamma function. σ_f represents the fiber tensile strength at the gage length in question and for this work was obtained from the literature [38] for all fibers used.

The embedded single fiber technique has several advantages. A large number of data points can be gathered in each observation, the failure process itself can be observed in transmitted (polarized) light, the locus of failure is identified and the process replicates the in-situ events in the actual composite itself. A plethora of experimental data has been generated with this method and published elsewhere [31,32,34,39,40].

A specially designed heated cell was constructed to conduct the single fiber measurements at elevated temperatures. The dimensions of the cell (2"x1.25"x1") are such that it fits snugly around the dogbone coupon and in the straining device shown in Figure 2.4. The cell is constructed entirely out of teflon which has thermal capabilities up to 300°C. Two aluminum blocks, which house the "firerods" (1/4"x1" and 40 Watts, Watlow Co.) used for heating the interior of the cell, are built into the two outside teflon walls. Quartz glass windows above and below the specimen allow for experimental observation under an optical microscope. Elongated dogbone shaped specimens (2" gage

length) are inserted in the chamber and the gage length is heated to the desired temperature. Tests are conducted as mentioned previously. Temperature calibration runs have shown that the entire gage length attains constant temperature to within 5% of the set point temperature after equilibration. The time for equilibration is dependant upon the set point temperature and ranges from 5-15 minutes. Even at the highest temperatures used in this study (about 120°C), the equilibration time is less than 15 minutes.

2.2.2 MICROBOND TEST

The procedure used to fabricate samples for the microbond test is similar to that described by Miller et al. [41,42]. It involves deposition of a small amount of resin onto a clean surface of a fiber in the form of several microdroplets. The droplets form concentrically around the fiber in the shape of ellipsoids and retain their shape after appropriate curing. Once cured, the microdroplet specimens and fiber diameter are measured with the aid of an optical microscope. The embedded length is fixed by the diameter of the microdroplet along the fiber axis, which is dependant on the amount of resin deposited on the fiber. In these experiments, 6" lengths of fibers were stretched across a rectangular frame and held in tension (with tape) while random drops of various sizes were deposited on the fibers with the aid of a very thin (30 gage) needle, the fiber collection was then appropriately cured. The practical minimum limit for embedment length using this technique is about 70 microns.

In this work, a fiber holder and straining device, mounted horizontally and positioned under an optical microscope, was used to collect the data. One end of the fiber specimen is fixed adhesive to a metal tab which is connected to a loadcell (the microdroplets are sheared off the fiber at a rate of about 100 microns/min using a moveable stage). To grip the droplet, an adjustable micrometer equipped with flat, rectangular cross-section blades is used. The blades of the micrometer are first positioned on one side of the

droplet, then the blades are brought into contact with the fiber and then opened slightly to let the fiber, but not the droplet, move between them. This process reproducibly positions the blades properly in relation to the droplet and fiber. The moveable stage is used to translate the fiber and droplet laterally in the horizontal plane. As the blades continue to move, they make full contact with the droplet and an axial force is exerted on the droplet. The axial force on the droplet is then transformed to the fiber through a shearing force at the fiber/matrix interface. When the shearing force exceeds the interfacial bond strength, detachment occurs, and the droplet is displaced horizontally along the axis of the fiber. The maximum in the force curve is taken as the point at which the droplet has debonded from the fiber. A simple force balance at the interface gives the following relation for determining the interfacial shear strength. Here, F is the

$$\tau = \frac{F}{\pi d L} \qquad (2.3)$$

maximum force recorded, d is the fiber diameter, and L is the embedment length. Figures 2.6 and 2.7 show typical droplets on fibers and the apparatus used.

2.2.3 INTERFACIAL PULL-OUT TEST

To determine the interfacial characteristics of the matrix when in a fluid state, pull-out experiments were conducted with a gravimetric electrobalance (see section 2.2.8 for a more detailed description of the electrobalance itself) apparatus. A schematic of the apparatus is shown below in Figure 2.8.

The pull-out tests were conducted as follows:

(1) Immerse a single filament of carbon fiber to a known depth (controlled by the motor and usually about 7 mm) in the resin which is maintained at a temperature, T and viscosity, η.

(2) Pull out the filament at an approximate rate of 25 microns/min (preset by motor). Alternatively, it was also found that it was as convenient to manually move the stand that the resin rests upon. Either technique resulted in very reproducible results.

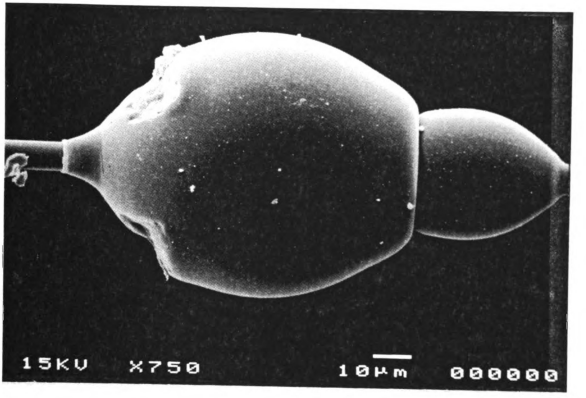

Figure 2.6: Scanning electron micrograph of microdrops on fibers

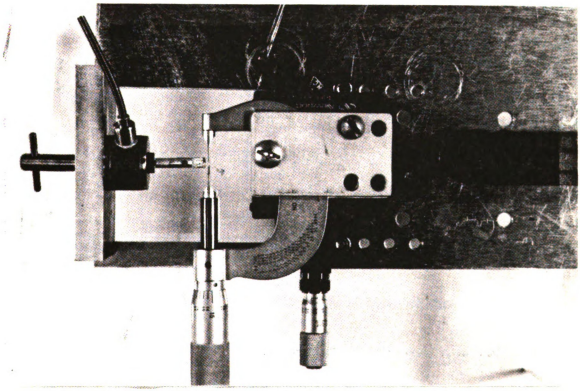

Figure 2.7: Schematic of microbond apparatus

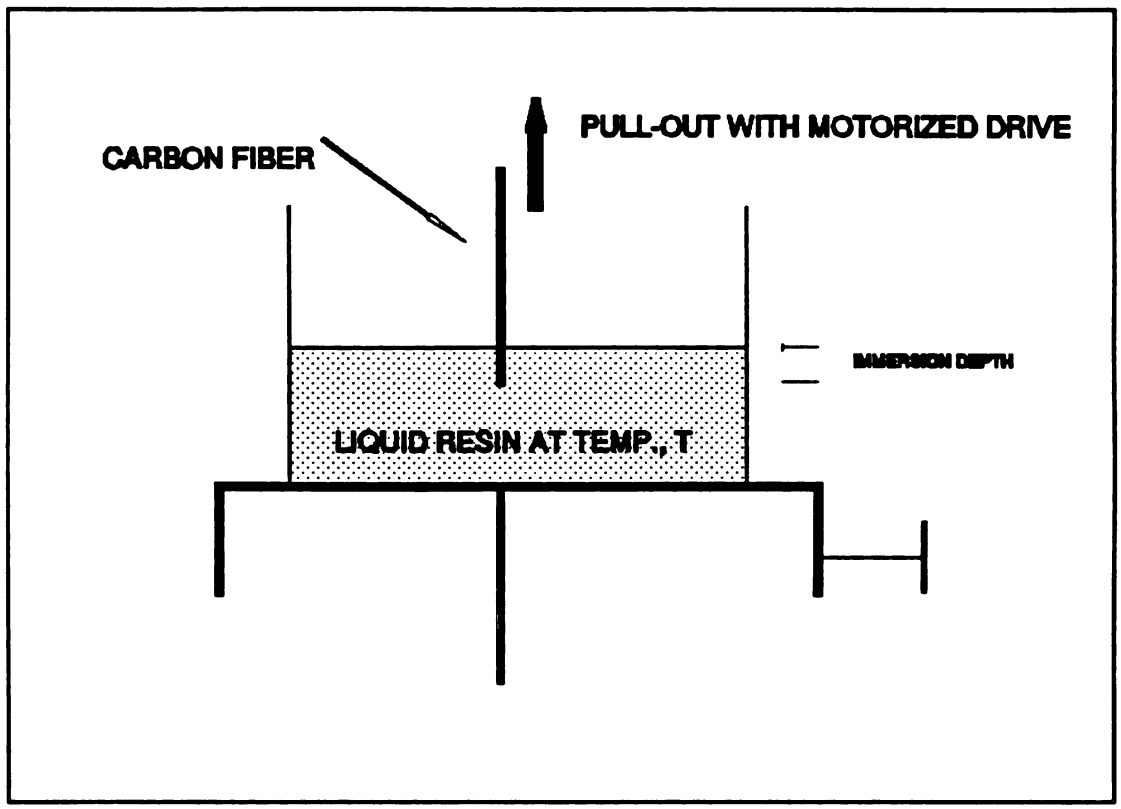

Figure 2.8: Schematic of pull-out experiment apparatus

(3) Take the steady-state value (after initial transient behavior dies out) in the force versus time curve as force at pull out.

(4) Calculate an approximate interfacial pull-out (shear) strength, τ, according to:

$$\tau = \frac{F_{ss}}{\pi d_f E_i} \tag{2.4}$$

where,

τ = Interfacial pull-out strength (Pa)
F_{ss} = Steady-State pull-out force (gms)
d_f = Diameter of fiber (about 7.4 microns)
E_i = Immersion depth (usually about 7 mm)

(5) Relate τ of the known viscoelastic properties of the matrix.

Piggott et al. [43] and Gent et al. [44] have used this type of experimental methodology to calculate interfacial tensions and pull-out forces in cured epoxies and polymers.

Two types of pull-out experiments were conducted. Neat DGEBA resin was used to conduct pull-out tests at various temperatures (and thus, at different viscosities). Additional experiments were conducted after the matrix was allowed to react for a given amount of time at an isothermal temperature. These samples were quenched at specific times (at known extent of cures) and pull-out experiments were conducted.

2.2.4 INTERFACIAL TRANSVERSE STRENGTH MEASUREMENTS

Normal strength measurements of the interface were made by aligning the fiber in a direction perpendicular to the plane of load application. Figure 2.9 shows a schematic of the samples. Sample preparation technique was similar to the single fiber fragmentation sample preparation technique discussed in section 2.2.1. Once the dog bone shaped samples are cured, they are polished and subject to a tensile load. In this set of experiments, however, a pneumatic controller was used to apply load in order to measure the amount of load applied to the sample. An optical microscope was used to detect the first signs of debonding. Once detected, the load is recorded and multiplied by an appropriate stress concentration factor [45] to arrive at a load at debonding.

2.2.5 MATERIAL PROPERTIES OF THE MATRIX

The matrix property data (Young's modulus, strain to failure and Poisson's ratio of the matrix materials) used in this study was obtained using a Materials Testing System (MTS). The specific instrument used was a MTS-880 servo-hydraulic instrument equipped with a biaxial extensiometer. Samples were cured into standard 4.5" gagelength (or 1" gagelength) hourglass shaped specimens suitable for material property testing. Load/displacement data was obtained directly from the MTS at a rate of approximately 0.02 inches/min.

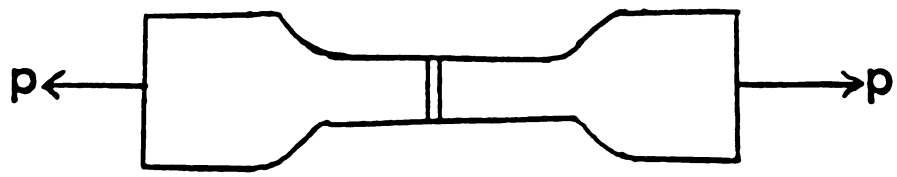

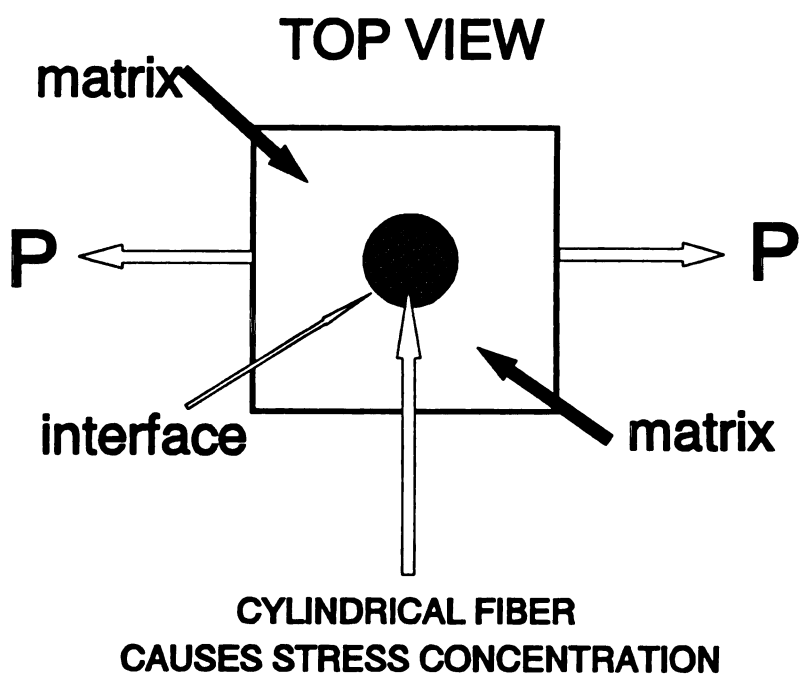

Figure 2.9: Schematic of transverse strength specimens

The Young's modulus, E, was computed by extending the initial portion of the stress/strain curves and by measuring the slopes of these relatively linear regions. The shear modulus, G, was then estimated by measuring the Poisson's ratio, ν, of the matrix material and by assuming the matrix material to be isotropic; whereby the following relation can be used [46]:

$$G=\frac{E}{2(1+\nu)} \qquad (2.5)$$

The strain to failure, ϵ_f, of the various matrices were determined directly from the endpoints of the stress/strain curves and by knowing the exact gage length of the specimens. The strain at final fiber (i.e. at critical length) break, ϵ_b, represents the strain at which the final break occurs in the fragmentation test (section 2.2.1) and is always less than ϵ_f.

2.2.6 THERMAL PROPERTIES OF THE MATRICES

Two methods were used to determine the glass transition temperature (T_g) of samples used in this work. For bulk samples, a Differential Scanning Calorimeter (DSC, DuPont 9900) was used. DSC scans of cured matrices, as well as cured droplets were made at 5°C/min under nitrogen purge using open pans. The T_g's were estimated from the midpoints of the transition regions.

For individual as well as clusters of droplets (section 2.2.2) too small to test on DSC, a Thermal Mechanical Analyzer (TMA, DuPont 9900) was used. In this method, the thermal expansion coefficient is used as an indicator of thermal transitions. This method is a novel application of TMA, not attempted or found successful by others, for measuring thermal properties of very small quantities of polymer. Individual droplets were prepared on fibers as mentioned in section 2.2.2 and subsequently, after

measurement of droplet dimensions, cut from fibers and placed under the TMA probe for T_g determination. For droplets less than about 600 microns (0.6 mm) in diameter, a cluster of droplets of similar size was used to generate the necessary signal (which is approximately 0.8-1.0 mm) for determining the T_g. Care must be taken with this technique since the small quantities of polymer have a tendency to adhere to the TMA probe which would necessitate a bakeout of the probe before the next set of experiments can be conducted. A careful check was made between these two experimental techniques (DSC and TMA) to assure that consistent T_g's were obtained for identical bulk samples.

DSC was also used to carry out kinetic experiments. Sample size was 15-35 mg. Isothermal runs were used to calculate extent of reaction (cure). Samples were cured outside the calorimeter at the desired temperature. After various times, the samples were quenched with ice (water) and residual cure was measured by DSC at a heating rate of 5°C/min. The fraction reacted, α, was calculated as that fraction of the total possible enthalpy of exothermic reaction [48,64,78]. DSC was also used to determine T_g as a function of extent of cure, α. Samples were quenched after exposure to a temperature for a given time and subsequently analyzed (as described previously) for T_g.

A Dynamic Mechanical Analyzer (DMA, DuPont 9900) coupled to the Dupont 9900 Thermal Analyzer System was used to carry out viscoelastic experiments on the matrices [47]. Loss (G') and storage modulus (G") data was obtained as a function of temperature. The instrument was operated at a fixed frequency of 1 Hz. and amplitude of 0.6 mm. The modulus data reported here refer to flexural moduli, which are closer to tensile modulus than to the shear modulus because of the sample dimension utilized. The sample dimensions were approximately 3.5x0.5x0.2 inches. Dynamic Viscoelastic experiments were performed at an initial ambient temperature up to the matrix T_g at a rate of 5°C/min. The experiments were discontinued at temperatures close to the T_g due to the fact that large scale deformations are expected to occur in the vicinity of T_g.

2.2.7 VISCOSITY MEASUREMENTS

Viscosity measurements were made with two different pieces of equipment. A tabletop Brookfield Viscometer was used to gather data at low viscosities (< 500 cp). Different spindle sizes were used to get the maximum amount of sensitivity. The bulk of the viscosity and gelation measurements, however, were made using a Rheometrics Mechanical Spectrometer (RMS 800). Simple temperature sweeps were made at isothermal temperatures and a fixed frequency of 1 rad/sec. Parallel plate geometry (with a gap width of about 1 mm) in the dynamic, oscillating mode was then used to measure dynamic properties (viscosity, storage modulus and loss modulus) as a function of time at a fixed frequency (1 rad/sec) and temperature. Further details on the experimentation technique is available elsewhere [48].

2.2.8 SURFACE ENERGY MEASUREMENTS

Surface energy measurements were done by measurement of dynamic contact angles (advancing and receding) for single fibers as well as cured matrices using a micro-Wilhelmy technique with water, methylene iodide and ethylene glycol as characterizing liquids (see Table 2.3 below).

Fibers, about 10 mm in length, were attached with cyanoacrylate ("super glue") adhesive to a nickel hook which hung on a Cahn RG Electrobalance which measured the force on the fiber as it was raised and lowered in the characterizing liquid. Approximately 2.5 mm of the fiber (or matrix sample) was immersed in the liquid of interest before being moved in and out of the liquid at the rate of 25 microns/sec. The nickel hooks were dipped into the matrices of interest and allowed to cure for testing of the various matrix materials. Once cured, the uneven ends were snipped off leaving behind a thin film which was dipped into the liquid of interest and tested.

Table 2.3: Surface energies of characterizing liquids [27]

LIQUIDS	$\gamma_{l,t}$ (mj/m^2)	$\gamma_{l,d}$ (mj/m^2)	$\gamma_{l,p}$ (mj/m^2)
WATER	72.8	21.8	51.8
ETHYLENE GLYCOL	48.3	29.3	19.0
METHYLENE IODIDE	50.8	48.4	2.40

The samples were allowed to stabilize 30 seconds before the static force measurement was taken. The entire apparatus was enclosed in an environmentally controlled chamber to eliminate wind currents, reduce contamination of the characterizing liquid, insulate the apparatus from vibrations, and maintain constant temperature. All glassware (and other materials) was thoroughly cleaned with a strong mineral acid ("Chromerge") and baked out to avoid any type of contamination.

Contact angles (θ) were determined (neglecting the buoyant force) according to the following equation:

$$F=m\cdot g=\gamma_{l,t}\cdot P\cos\theta \qquad (2.6)$$

where m is the mass measured by the electrobalance, g is the acceleration due to gravity, and P is the perimeter ($=\pi d$ for circular cross section samples) of the sample. A minimum of 35 measurements were taken for each sample to assure statistical significance.

Surface energy analyses of the samples was determined from the contact angles in the manner described by Kaelble et al. [49]. This method assumes, for low surface

energy solids such as polymers, that the total surface free energy across the interface, $\gamma_{i,t}$, is composed of a polar, $\gamma_{i,p}$, and dispersive part, $\gamma_{i,d}$: $\gamma_{i,t} = \gamma_{i,d} + \gamma_{i,p}$ where i stands for the fiber, matrix or liquid. Due to the simplicity of this analysis for determining surface free energies, many experimenters have resorted to using it [27,50,105] for determining the surface energy characteristics of both fibers as well as polymeric matrices.

2.2.9 MICROSCOPY

Some common polymeric matrices, when undeformed, can be considered optically isotropic. However, when subjected to stresses, whether due to externally applied loads or thermally induced stresses from differential shrinkage during sample preparation, the material becomes optically anisotropic (birefringent). Since 828 epoxy resin is transparent and exhibits birefringent behavior when subjected to stresses, it would be beneficial, for a better understanding of fiber-matrix interactions, to study the stress birefringence adjacent to the fibers, before, during, and after application of load in the single-fiber embedded test described above. Drzal et al. [51] observed qualitative differences in the stress pattern resulting from interface changes and levels of adhesion when working on carbon fibers and epoxy matrices. Recently, Marshall et al. [52] have reported that visual observation of the events taking place at the interface during a different type of single fiber pull-out test is also valuable in determining the type of adhesion that exists there. Scanning electron microscopy (SEM, JEOL 2200) was also used to identify fracture surfaces and the surface morphology of carbon fibers. Bascom et al. [53] have demonstrated how SEM of fractured surfaces can be used to detect levels of adhesion in thermoplastic composites.

CHAPTER 3

BEHAVIOR OF THE INTERFACE IN THE VISCOUS REGIME

This chapter focuses on the kinetics of crosslinking, time to gelation, and in general, how the interface behaves in the viscous regime (up to the point of matrix gelation). Interfacial parameters are quantified with a single fiber gravimetric pull-out test and the data is modeled with a modified WLF-type equation. This chapter is based on work to be published by Rao et al. [54].

3.1 INTRODUCTION

In order to make optimum use of epoxies as structural materials, it is important to know what the curing process is, to what extent it proceeds, and the structure of the cured material as a function of curing time and temperature. Interfacial properties likewise play a major role in developing the final properties of the epoxy based composite material. Conventional isothermal processing of thick section composites, for example, have been found [5,7] to fail due to interfacial defects formed at some point during the curing process. The development of non-conventional curing methods requires knowledge of the process by which interfacial strength develops during the entire processing cycle of these types of composite materials to be able to determine where these defects initiate and propagate. Moreover, interfacial properties need to be related to readily measurable properties of the reacting matrix material if they are to be used effectively. Extensive studies [14,55,56,57] have been conducted relating interfacial properties to matrix and fiber properties in the solid state (after matrix gels and sets). Recent studies [36,58,59] have investigated the variation of interfacial properties as a function of matrix properties at elevated temperatures. However, very little work has

been done in an attempt to understand the behavior of the interface during the initial stages of cure when the matrix is in a fluid state. Though the matrix will be unable to transfer stress to the interface when the matrix is motionless in the fluid state, as the consolidation process moves fibers past the matrix shear stresses will be introduced. Concurrently the matrix reacts and its viscosity increases the magnitude of these stresses. The ability of the interface to withstand these stresses during the early stages of processing can reduce the tendency to separate matrix from the fiber and hence produce voids. Such information would be desirable for process models. The early stages of cure of the matrix mass will be characterized for extent of cure, viscosity and modulus. These data will then be combined with gravimetric pull-out experiments to measure a "pseudo" interfacial pull-out force based on the changing viscosity of the reacting material. A model for this process has been developed.

3.2 EXPERIMENTAL ANALYSIS

DGEBA resin was processed at stoichiometric conditions with the hardener meta-phenylene diamine (mPDA). The hardener was melted at 70°C before being mixed with the DGEBA resin at about 70°C. Fresh samples were used for all experiments.

The fiber used for the pull-out experiments was a carbon, AS4 fiber described in detail in Section 2.1.3.

All kinetic experiments were carried out on a DuPont 9900 model differential scanning calorimeter as described in Section 2.2.6. DSC was also used to obtain the T_g data as a function of extent of cure of the matrix. Since resin and hardener were mixed at 70°C, most of the discussion in this chapter will center on kinetic data above 70°C. Viscosity and gel point data were collected, as described in Section 2.2.7, on two different pieces of equipment. A Brookfield viscometer was used to gather data at low viscosities. At higher viscosities (> 5000 cp) a Rheometrics RMS was used, in the cone

and plate mode with a gap width of 1 mm, to collect the appropriate data. Isothermal data was collected to the maximum extent of cure possible (i.e. to the point of gelation) for a given temperature. The raw data (obtained from RMS) is shown, for the reacting system, in Figure 3.1 for a temperature of 125°C. Viscosity for the DGEBA resin alone was also measured as a function of temperature. The results are shown in Figure 3.2. As expected, the data in Figure 3.2 show the DGEBA resin to be a Newtonian fluid [12].

Many authors have used [60,61,62] viscosity measurements to track the progress of a reacting, crosslinking system. Most of this work focuses on relating the viscosity to the temperature and degree of cure according to a WLF-type relationship shown below:

$$\log(\eta/\eta_g) = \frac{-C_1(T-T_g)}{C_2+T-T_g} \qquad (3.1)$$

where,

η = viscosity (cP)
η_g = viscosity in "fully cured" state (constant [63,78] at 10^{15} cP)
C_1, C_2 = characteristic "WLF" constants for this system
T = reaction temperature (°C)
T_g = glass transition temp., function of extent of cure, α

In order to evaluate the constants C_1 and C_2, Equation 3.1 is rearranged to give,

$$(T-T_g) = \frac{-C_1(T-T_g)}{\log(\frac{\eta}{\eta_g})} - C_2 \qquad (3.2)$$

Equations 3.1 and 3.2 are the basis of the analysis presented in this particular chapter.

Pull-out experiments were conducted in a gravimetric, Wilhelmy type apparatus described earlier in Section 2.2.8 (Figure 2.8). Similar to the viscosity experiments described above, two types of pull-out experiments were conducted. Neat DGEBA resin was used to conduct pull-out tests at various temperatures (and thus, at various viscosities). This data is shown in Figure 3.3. Additional experiments were conducted

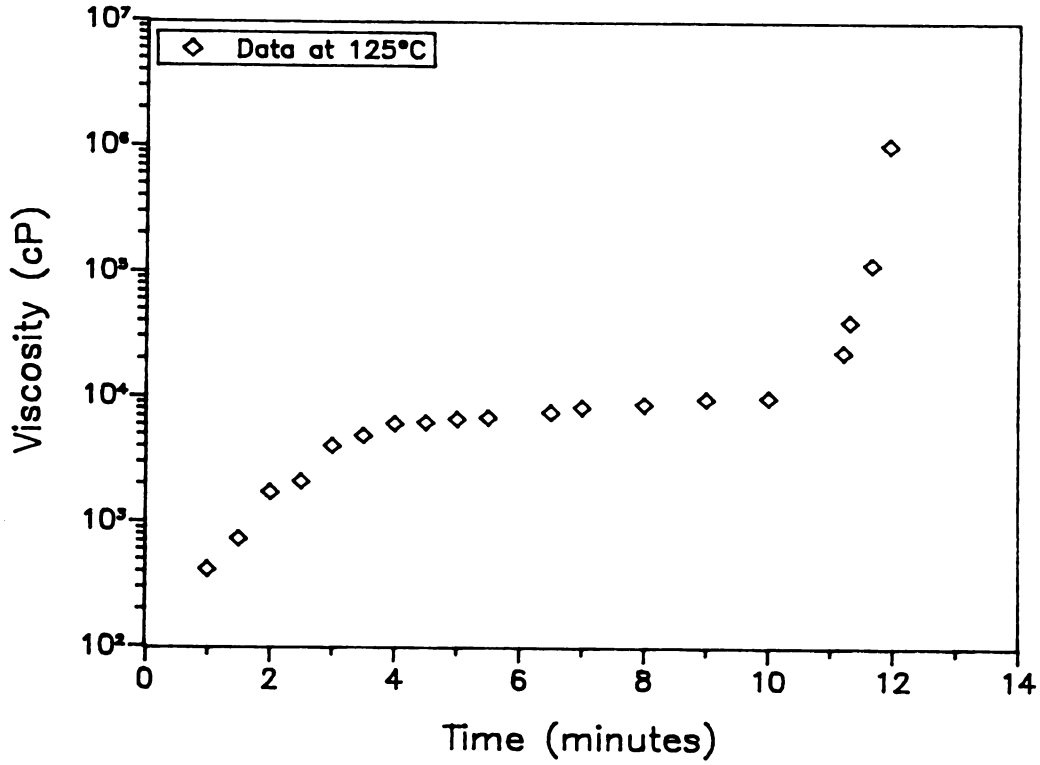

Figure 3.1: Viscosity vs. time for DGEBA/mPDA system at 125°C

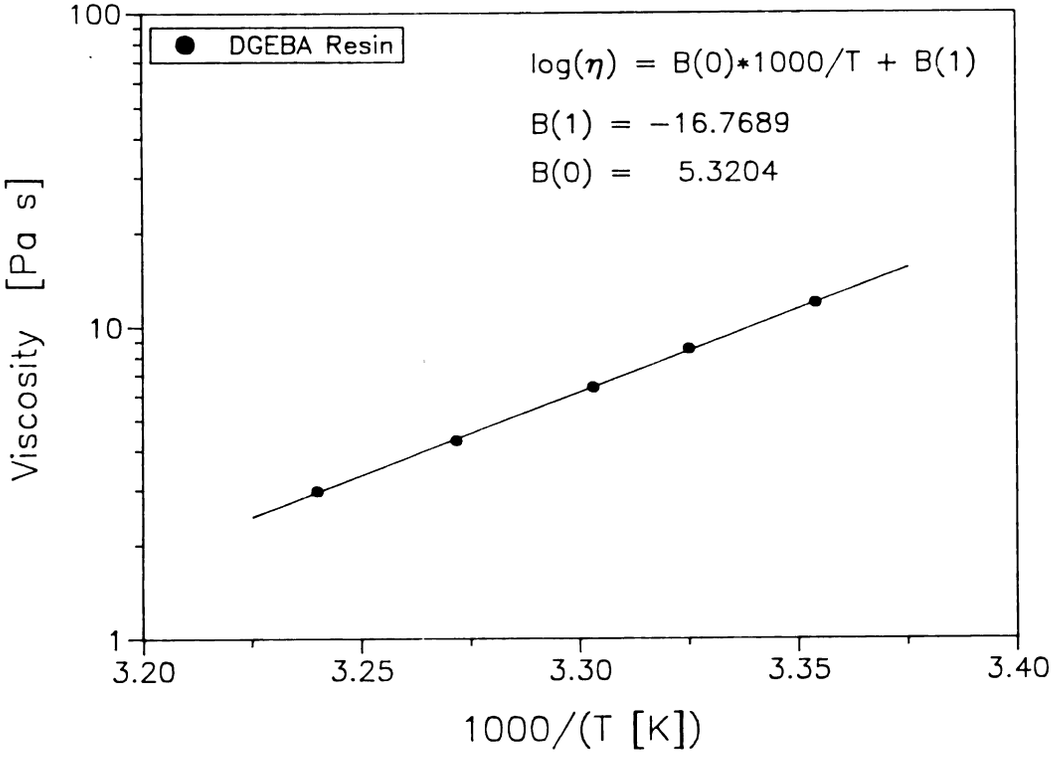

Figure 3.2: Viscosity vs. temperature for neat DGEBA resin

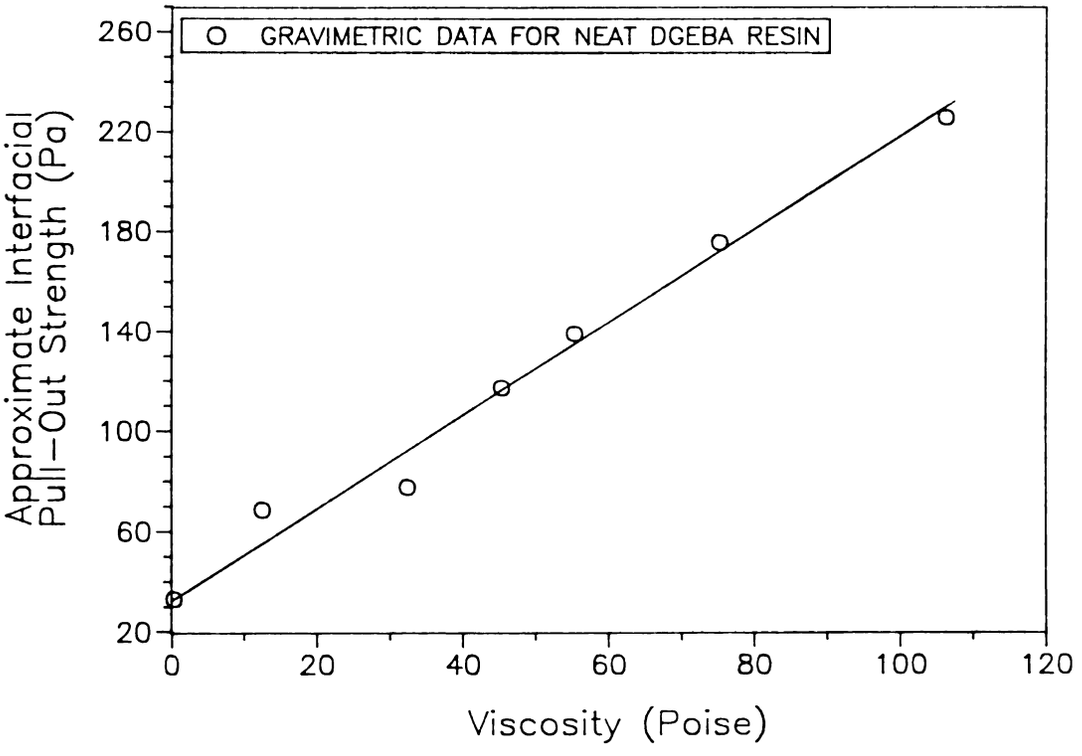

Figure 3.3: Viscosity vs. pull-out force for neat DGEBA resin

after the matrix was allowed to react for a given amount of time at an isothermal temperature. These samples were quenched at specific times (at known extent of cures) and pull-out experiments were conducted up to the gel point of the system. Pull-out experiments (with the reacting system) are tedious to conduct as the gel point of the system is approached. The reacting system has a tendency to exotherm, as the gel point is approached, and instantaneously gel causing the termination of the run and the experimental apparatus to malfunction, usually necessitating recalibration.

3.3 RESULTS AND DISCUSSION

3.3.1 KINETICS OF DGEBA/mPDA

An extensive amount of kinetic studies have been conducted on epoxy reactions [9]. Lee et al. have suggested an autocatalytic mechanism to describe the crosslinking process [64], while others [65,66] have suggested an initial autocatalytic mechanism followed by a pseudo-first order diffusion controlled regime. Prime et al. have conducted an extensive amount of kinetic experiments with this system (DGEBA/m-PDA) at a non-stoichiometric ratio of resin to curing agent. Much of Prime's work [9,67], as well as work done by Kamal [68] indicate that these type of crosslinking epoxy reactions proceed autocatalytically with an overall kinetic order of two until the diffusion-controlled regime is reached, whereby they become pseudo-first order. In this analysis, the autocatalytic model with an overall kinetic exponent of two is used and validated with appropriate DSC data.

Isothermal experiments were carried out as discussed previously and the resulting data is presented in Figure 3.4 as extent of cure, α, versus time. As expected the nature of the curves (at elevated temperatures) indicate an autocatalytic reaction [69] mechanism. The data in Figure 3.4 also show that diffusion limits the maximum extent

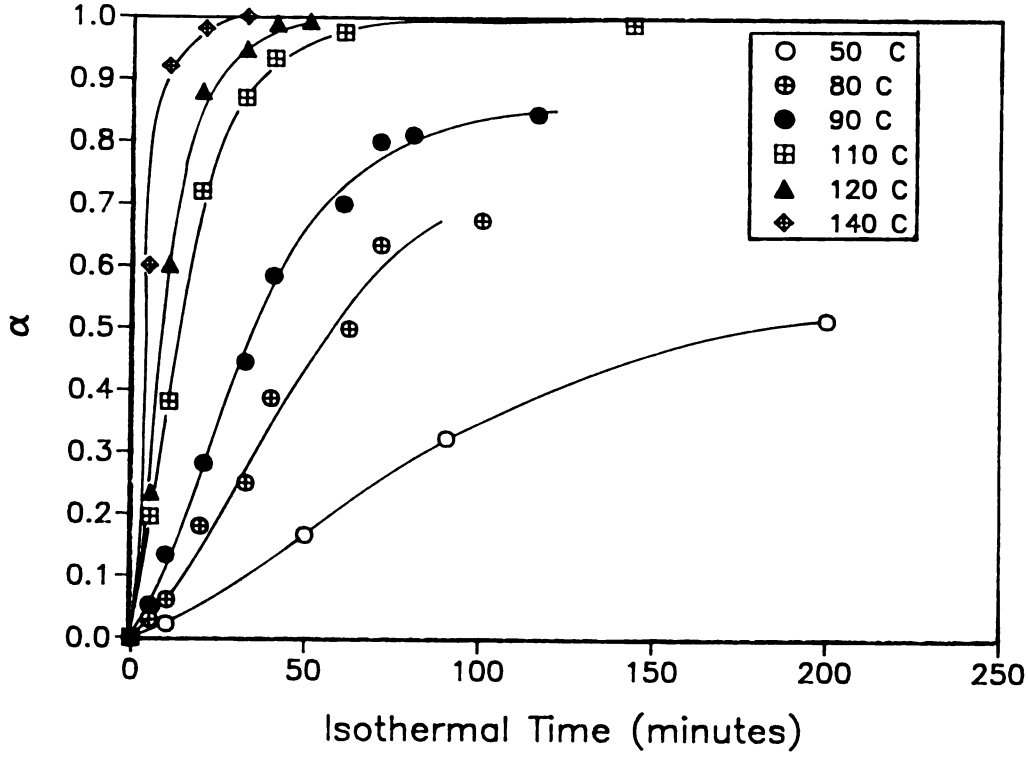

Figure 3.4: Extent of conversion, α, vs. time for isothermal kinetic data

of cure at lower temperatures; only at about 110°C is a cure of 95% achieved. A widely-used [68] three parameter kinetic model was used to monitor reaction rate:

$$\frac{d\alpha}{dt} = (k_1 + k_2 \alpha^m)\ (1-\alpha)^n \qquad (3.3)$$

where,
k_1, k_2 = Arrenhius-based reaction rate constants (min^{-1})
$d\alpha/dt$ = Reduced reaction rate (min^{-1})
m,n = Kinetic exponents (overall order of reaction = m+n)
α = extent of cure

A plot of reduced reaction rate, $d\alpha/dt$, versus time is shown, for various isothermal temperatures ranging from 50-140°C, in Figure 3.5. As expected, the maximum in reaction rate occurs at lower times for higher temperatures. A non-linear regression analysis [15] was used to fit all of the data in Figures 3.4 and 3.5 to Equation 3.3 above. The resulting relevant parameters are shown in Table 3.1.

In Table 3.1 below, the reaction rate constants ($k_{1,2}$) are incorporated into an Arrenhius form while the kinetic exponents are incorporated as a function of temperature. The activation energies determined for this system are in excellent agreement with values in the literature reported for similar systems by Prime et al. [9,67], and Acitelli et al. [70]. A comparison of the model prediction (Equation 3.3 with the appropriate parameters from Table 3.1) and experimental values of the reduced reaction rate (versus time) is shown in Figure 3.6. It can be seen that the agreement is good at high temperatures. This close agreement indicates that the previous assumption of the overall reaction order (m+n) being two is valid. At the lower temperatures (less than about 85°C), however, the reaction is less autocatalytic and the reaction kinetics can be adequately described by a pseudo-first order reaction mechanism (see Appendix A).

An equally elegant alternative way of determining these kinetic parameters from dynamic DSC data has been suggested by Kissinger et al. [71] and used by others

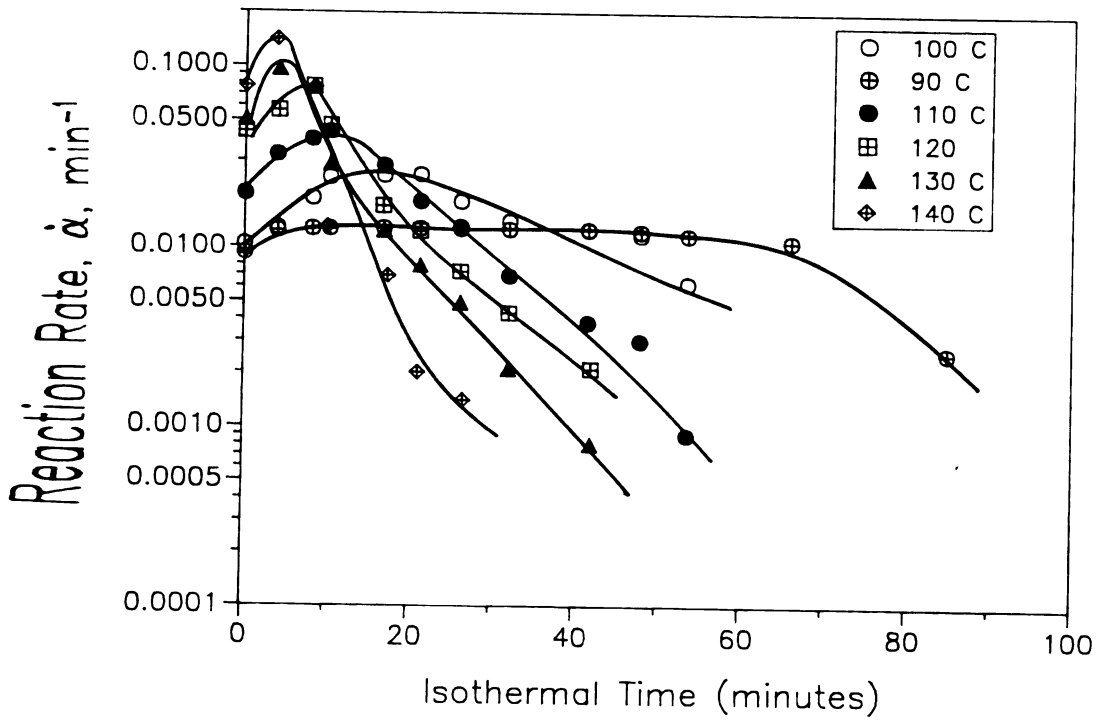

Figure 3.5: Reaction rate, dα/dt, vs. time for isothermal data

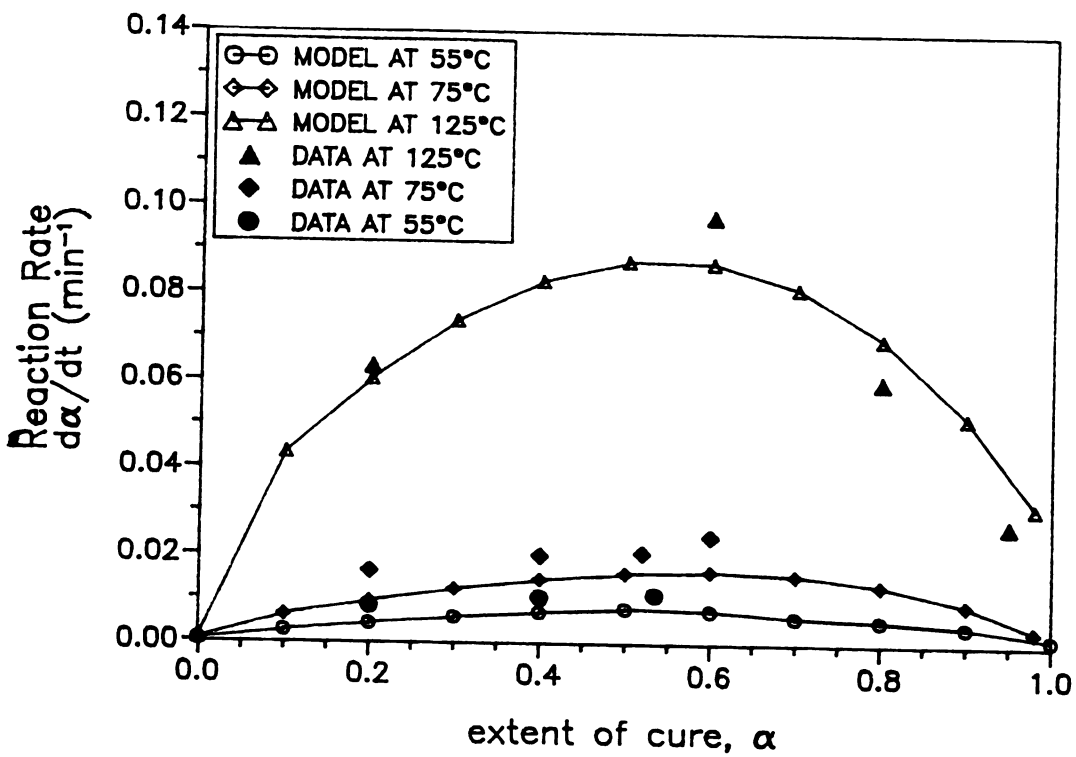

Figure 3.6: Comparison of kinetic model to data at 55°C, 75°C and 125°C

[72,73]. In their method, different heating rates are used to determine "peak" values and these are used, after algebraic manipulation of Equation 3.3, to determine the kinetic parameters in Table 3.1. Appendix A outlines the usage of this method (with isothermal DSC data)

Table 3.1: Kinetic model parameters

Reaction Rate Constants of the form, $k=Ae^{-E/RT}$: $k_1 = 1.693 \times 10^6 e^{(-7034/T)}$ $k_2 = 9.505 \times 10^3 e^{(-4196/T)}$ where,   A, $k_{1,2}$ are in min^{-1} T is in °K   E/R is in Kcal-°K
Kinetic Exponents: $m = -2.75 \times 10^{-3} T + 1.43$, for $T > 85°C$ $n = 2 - m$ where,   T is in °C

to determine the kinetic parameters for this particular system. It will be seen that the agreement, with the isothermal rigorous regression technique used above, is good. Equation 3.3 can be next used to predict the gel time as a function of temperature once the extent of cure at the gel point, α_{gel}, is known.

3.3.2 VISCOSITY AND GEL POINT OF mPDA/DGEBA

In order to use Equation 3.1 to predict viscosities, the constants C_1 and C_2 need to be determined for the system at hand. Equations 3.1 and 3.2 require the knowledge of T_g as a function of extent of cure. The appropriate experiments were conducted as described in Sections 2.2.6 and 2.2.7 and all of the data have been combined and condensed into Figure 3.7. These data agree quite well with the semi-empirical relationship suggested by Pascault et al. [74] for the dependence of T_g on the extent of

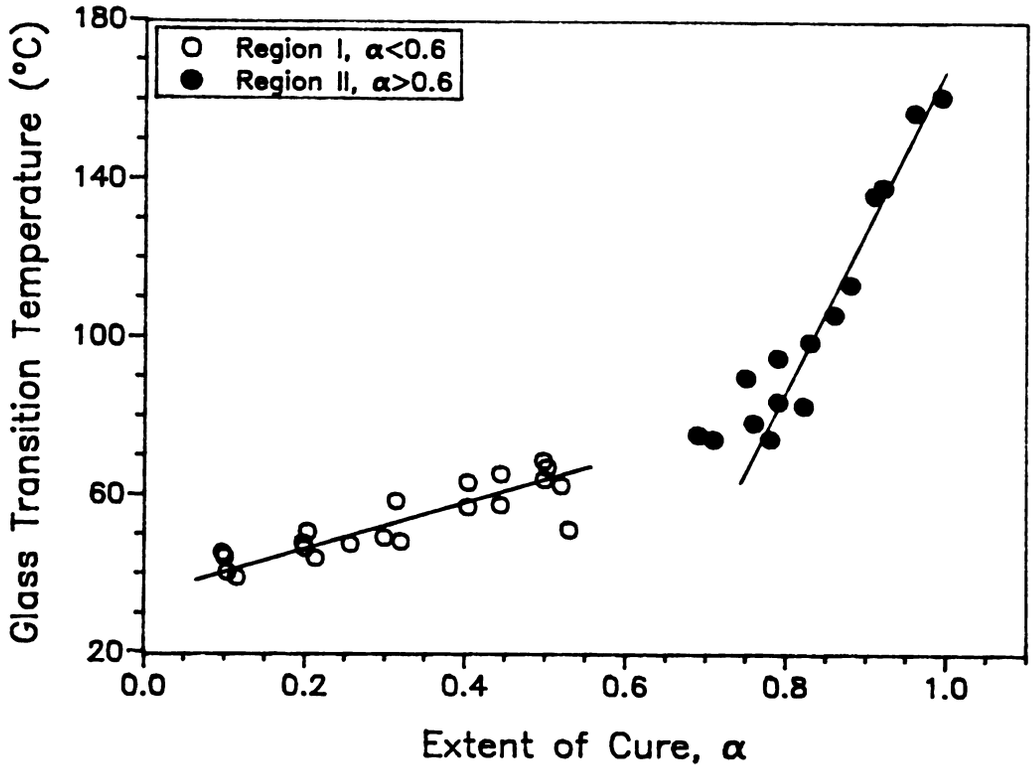

Figure 3.7: T_g vs. extent of cure, α

cure for crosslinking systems. The data in Figure 3.7 fall into two distinct regimes; one for $\alpha<0.6$ and one for $\alpha>0.6$. The appropriate "best-fit" relationships are shown for the two regimes in Table 3.2 below:

TABLE 3.2: T_g as a function of α

FOR $\alpha \leq 0.6$,	$T_g = 35.89+52.1\alpha$
FOR $\alpha>0.6$,	$T_g = 335.6-150.0\alpha$

The dramatic increase in T_g after crossing the gel point of the system is expected and has been observed before for similar epoxy systems [75]. At the lower curing temperatures, measured T_g's exceed the curing temperature at the higher extent of cures due to vitrification [10]. Because the model (Equation 3.2) is very sensitive to changes in $T-T_g$, data that fall into the 'vitrified' regime are not used.

Using the viscosity data from Figure 3.1 (the data for 125°C is shown; however, similar data was generated for different temperatures and used in this analysis) and the T_g data from Table 3.2, the constants C_1 and C_2 can be determined from Equation 3.2. The appropriate linear form of Equation 3.2 is shown in Figure 3.8 for three different temperatures. The constants C_1 and C_2 were determined as slope and Y-intercept of a "best-fit" line through all of the data. The appropriate calculations of slope and intercept result in $C_1=11.30$ and $C_2=0.580$ for this thermoset system. Nielsen [12] has suggested that the constant C_1 should be approximately 14 for many polymeric matrices and the constant C_2 varies depending upon the viscokinetic behavior of the particular polymeric system. It should be noted that if additional data at temperatures down to 80°C are added to Figure 3.8 in appropriate form, the slope and y-intercept change less than 5%.

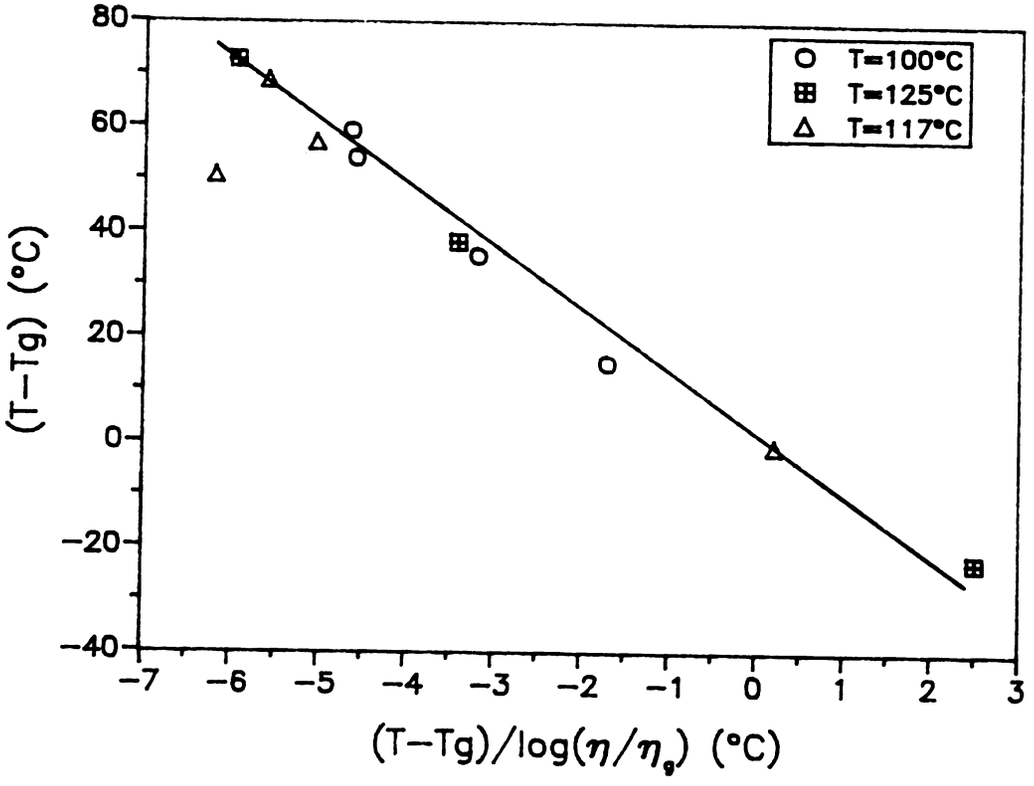

Figure 3.8: Reduced, modified WLF plot of kinetic data

Insertion of the constants C_1 and C_2 and the relationships for the T_g's from Table 3.2 into Equation 3.1 and slight rearrangement gives the following viscosity model for the reacting DGEBA/mPDA system.

For $\alpha \leq 0.6$ and for T in (°C),

$$\log\eta = 15 + \frac{(-11.3)(T-35.89-52.1\alpha)}{(0.58+T-35.89-52.1\alpha)} \qquad (3.4)$$

and for $\alpha > 0.6$,

$$\log\eta = 15 + \frac{(-11.3)(T-335.6\alpha+150)}{(0.58+T-335.6\alpha+150)} \qquad (3.5)$$

Viscosity values predicted by Equations 3.4 and 3.5 at temperatures of 80°C, 117°C and 125°C are shown in Figure 3.9. Actual RMS data (as described in Section 2.2.7) is also shown at these temperatures. At all temperatures, the model predicts changes in viscosity with time and degree of cure. At lower extents of cure (low viscosities) there is seen to be some discrepancy between experimental and predicted viscosities at all temperatures. This is mainly due to the lack of sensitivity in the equipment used to measure very low viscosities (<200 cP). Additionally, there is an initial temperature effect which causes the viscosity to go to a minimum [76] before the crosslinking reaction occurs causing the viscosity to increase.

Three different methods were used to determine the time to gel. In method I, the time at which the storage modulus (G') crosses the loss modulus (G") at a given temperature was used as the characteristic time to gel [75]. A typical plot of G' and G" (RMS data) is shown in Figure 3.10 for a temperature of 80°C. As expected, when all of the data was analyzed for α_{gel}, it was found to be constant between 0.67-0.73. Flory's theory [77] predicts an α_{gel} of about 0.6 for this stoichiometrically cured difunctional

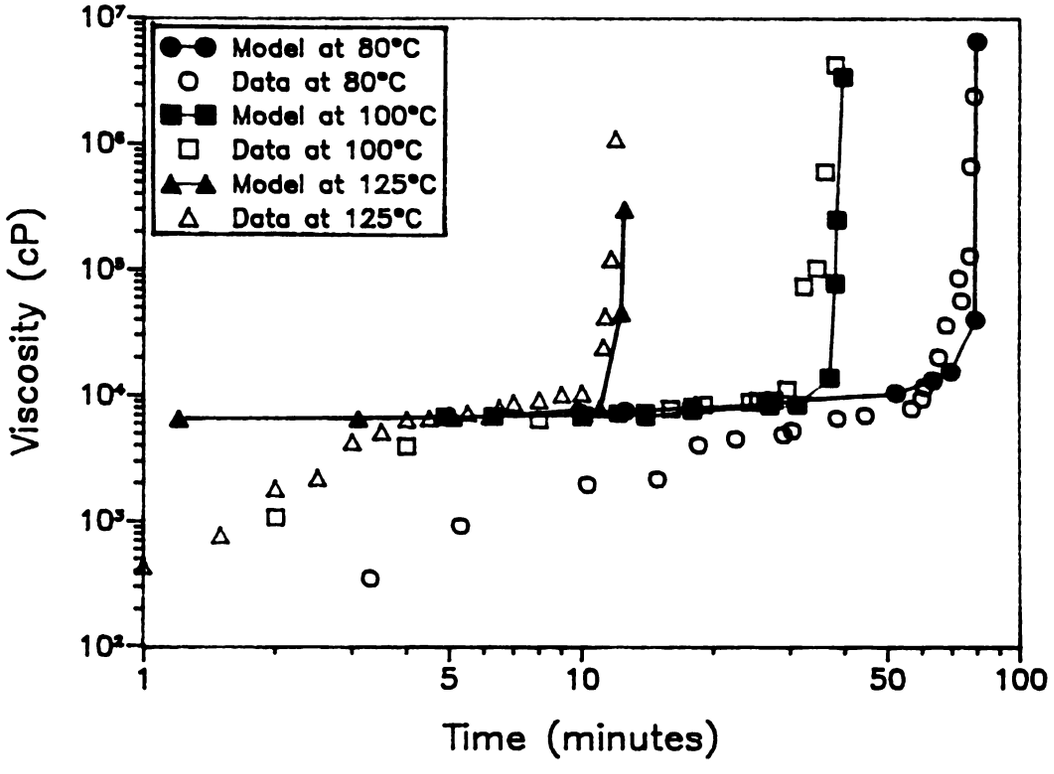

Figure 3.9: Comparison of WLF viscosity model to RMS data at 80°C, 100°C and 125°C

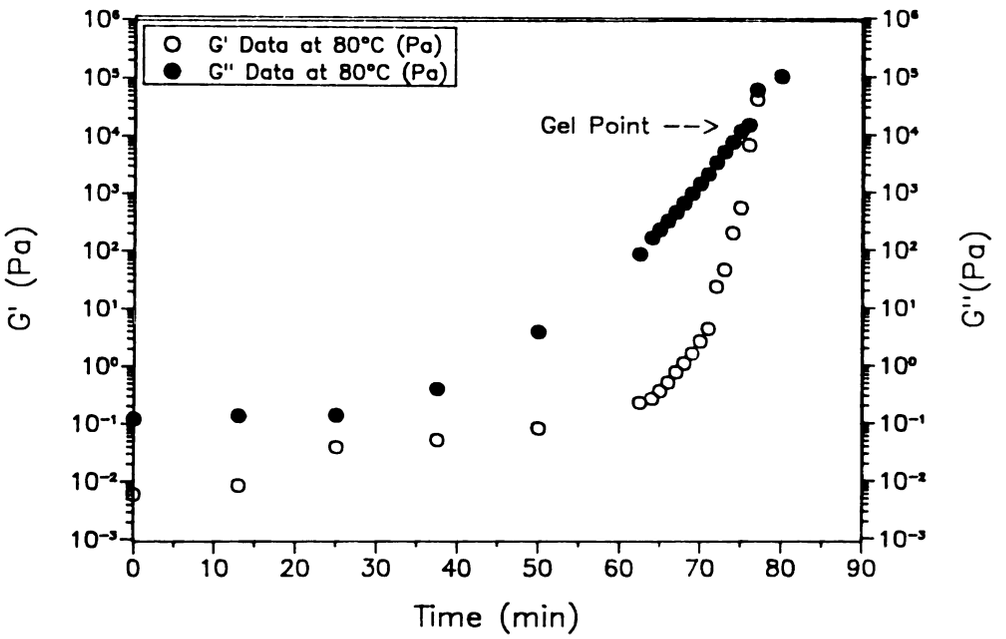

Figure 3.10: G' and G" data for DGEBA/mPDA at 80°C

system. The slight discrepancy between experimental values and the absolute value predicted by Flory's "chain" theory could be due, in part, to slight stoichiometric variations during experimental preparation techniques. In method II for determining t_{gel}, the time to reach a viscosity of 10^6 Pa-S was used as the characteristic time. Finally in method III, α_{gel} was substituted into the kinetic Equation 3.3, with the appropriate parameters from Table 3.1, and the resulting expression numerically integrated for t_{gel} [78]. The calculations from all three methods are summarized in Table 3.3.

The data shown in Table 3.3 is shown graphically in Figure 3.11. It can be seen that the G'=G" data (method I) and the viscosity data (method II) agree closely throughout. The kinetic model predicts slightly lower t_{gel}'s at the lower temperatures. This may be partially due to lack of accurate kinetic and network formation data at these temperatures. In general, the data in Figure 3.11 agree very well with work done by Prime et al. on the same system [9].

TABLE 3.3: Prediction of gel times

METHOD	t_{gel} at 80°C (min)	t_{gel} at 100°C (min)	t_{gel} at 117°C (min)	t_{gel} at 125°C (min)
METHOD I (G'=G")	77.2	32.3	16.2	12.5
METHOD II ($\eta=10^6$Pa-s)	70.2	32.4	15.8	12.5
METHOD III (Kinetic)	52.3	19.3	13.9	12.2

3.3.3 INTERFACIAL PULL-OUT STRENGTH

The viscosity versus pull-out data (for the unreacting, DGEBA resin system) shown in Figure 3.3 was "best-fit" to the following regression line,

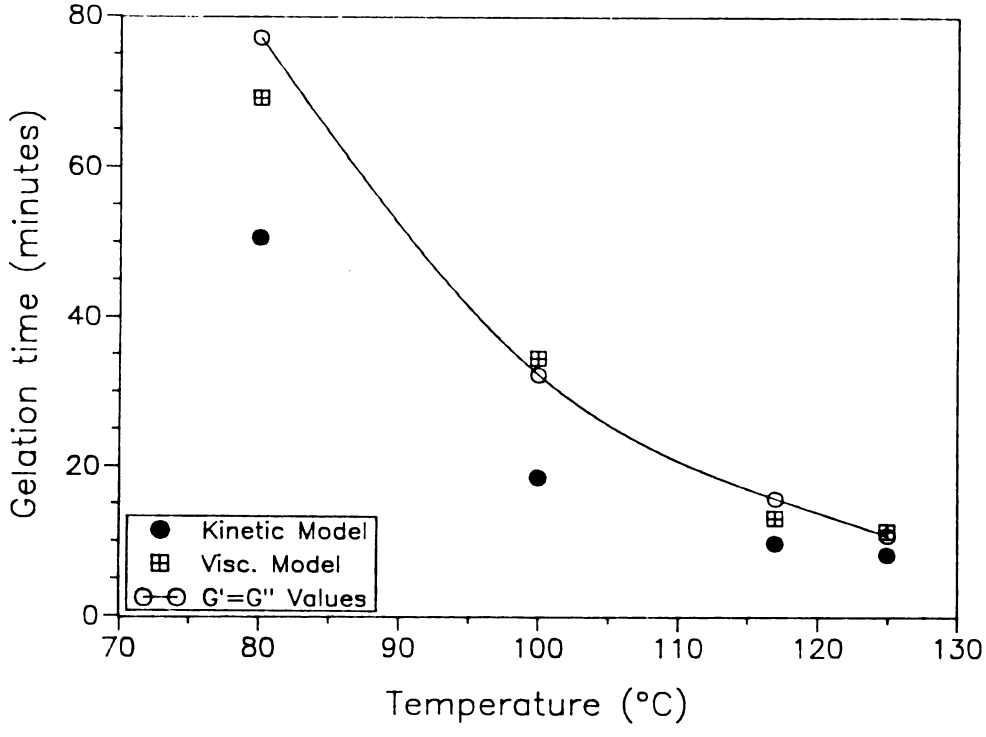

Figure 3.11: Temperature vs. time to gel as predicted by various techniques

$$\eta = 54.48\tau - 2050 \tag{3.6}$$

where,
η is in cP
τ ia in Pa

Insertion of Equation 3.6 into Equations 3.4 and 3.5 yields, for $\alpha \leq 0.6$

$$\tau = \frac{10^{15 + \frac{(-11.3)(T-35.89-52.1\alpha)}{(0.58+T-35.89-52.1\alpha)}} + 2050}{54.48} \tag{3.7}$$

where,
τ is in Pa
T is in °C

and for $\alpha > 0.6$

$$\tau = \frac{10^{15 + \frac{(-11.3)(T-335.6\alpha+150)}{(0.58+T-335.6\alpha+150)}} + 2050}{54.48} \tag{3.8}$$

the units are the same as in Equation 3.7 above. Equation 3.8 cannot be verified experimentally since pull-out experiments cannot be conducted above the gel point of the system (which experimentally occurs between 0.65-0.70 extent of conversion).

Comparison was made between the model prediction for pull-out strength at given extent of cures (Equations 3.7 and 3.8) and actual pull-out data as measured by the gravimetric technique discussed earlier is shown in Figure 3.12. For all temperatures and extent of cures, the agreement is good except at low conversions, where as discussed earlier, viscosities were difficult to measure with any degree of accuracy. Thus, Equations 3.6 and 3.7 as well as Figure 3.12, allow for the estimation of the interfacial pull-out strength of AS4 fiber and mPDA/DGEBA thermosetting matrix at any point during cure. To the best of the authors' knowledge, this type of experimental methodology has not been attempted before to relate the pull-out strength to matrix

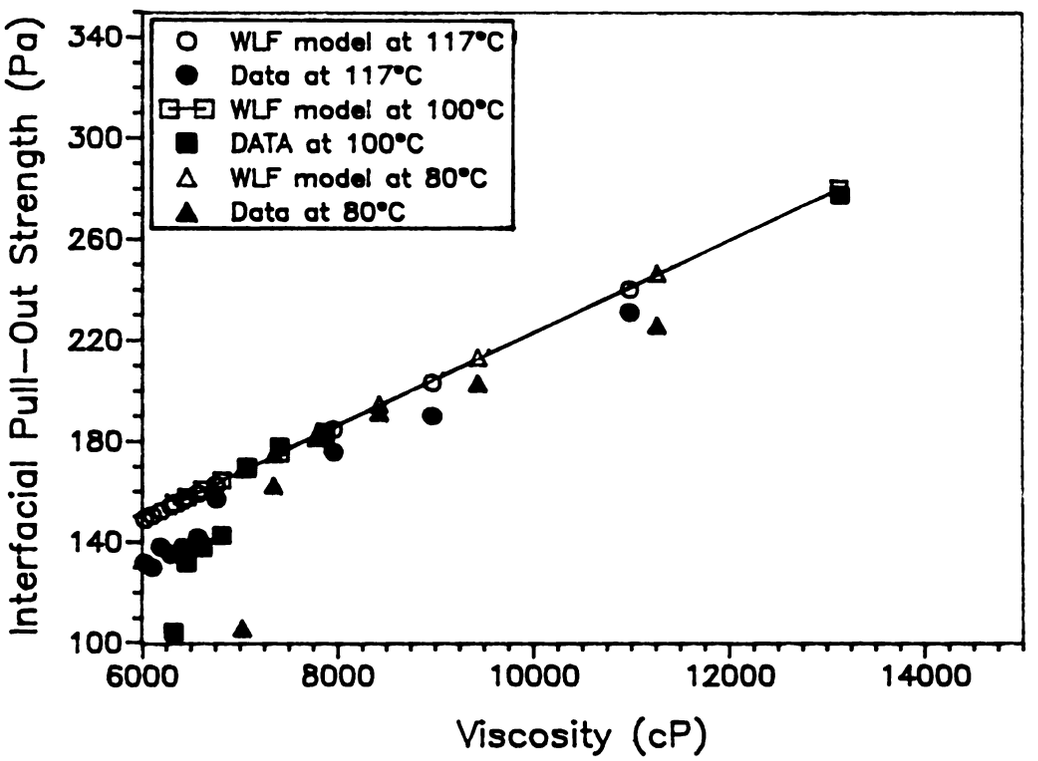

Figure 3.12: Comparison of pull-out model to gravimetric data

viscosity and extent of cure up to the gel point. These data provide an estimate on the upper bound for the amount of stress the interface can withstand in this regime as a function of viscosity. Imposed stresses that exceed these values in the early stages of processing may lead to fiber/matrix separation causing void formation in the final product. As expected, the measured pull-out forces are quite small (in the order of Pascals--whereas solid state interfacial shear strengths are on the order of million Pascals for this same system).

3.4 CONCLUSIONS

In this chapter, an extensive viscokinetic model was constructed for the reacting mPDA/DGEBA system. This model predicts the viscokinetic behavior up to the gel point of the matrix. The crosslinking kinetics were found to be adequately described by a three parameter autocatalytic model at temperatures above about 85°C and by a pseudo first order model below 85°C. The changing viscosity was modeled using a modified WLF-type relationship. The kinetic and viscosity models were then combined with gravimetric pull-out experiments to predict the relationship between extent of cure and the interfacial pull-out strength (using carbon AS4 fibers). Pull-out experiments at various stages of cure revealed the data to match up satisfactorily with model predictions.

CHAPTER 4

MICROBOND TECHNIQUE

In this chapter, results will be reported on the use of the microbond technique for determining the interfacial shear strength of mPDA/DGEBA matrix with AS4 carbon fibers. Results will be presented which show that diffusion of the curing agent, mPDA, at early stages of the cure cycle leads to mechanical property variations in the droplets and low values of interfacial shear strengths when compared to results obtained for the same system with the fragmentation test.

A distinct relationship between the glass transition temperature of the droplets and their size have been found. Smaller droplets (< 150 microns) have very low T_g's and are incompletely cured. It will also be shown that alteration of the curing cycle and droplet environment has little effect on reducing the loss of curing agent. Additionally, for the mPDA/DGEBA system, films in thicknesses up to 3 mm also are susceptible to loss of curing agent by diffusion and evaporation. The research reported in this chapter has been published previously as two different journal articles by Rao et al. [79,80] and one by Herrera-Franco et al. [81].

4.1 INTRODUCTION

The interface between polymer matrix and reinforcing fiber plays a key role in determining the final mechanical properties of the composite material. "Good" adhesion and bonding at the interface is paramount for achieving high interfacial shear and off-axis strength. "Good" adhesion is also necessary for efficient load transfer and long term property retention. Since the interface plays a key role in transferring stress from matrix to the fiber, it is important to be able to characterize the interface and level of adhesion

to understand composite performance properly. Thus, it is essential to have reliable laboratory techniques to study fiber-matrix interfacial interactions.

Several techniques have been developed in an effort to measure the interfacial shear strength directly. In one technique, a single fiber embedded in an epoxy material is loaded in tension in the fiber direction. The fiber repeatedly fractures until a final critical length is reached (see Section 2.2.2). These fragmentation tests have been used to study glass fiber/resin interactions by Frazer et al. [82], carbon fiber/epoxy interactions by Drzal et al. [30,83] and highly cross-linked brittle systems by Lee et al. [84]. A second method is the single fiber pull-out test. A small length of fiber is embedded in a thin disk of resin and the force needed to extract the fiber from the resin is measured and used to calculate the interfacial shear strength, τ, using the equation:

$$\tau = \frac{F}{\pi d L} \qquad (4.1)$$

This test has also been used, with some success, to study the adhesion of thermosetting resins to glass and carbon fibers [85,86]. A limitation inherent in these types of pull-out tests is met when small fibers having diameters of 10 microns or less are used. If the pull-out force exceeds the fiber tensile strength, the fiber breaks before successful pull-out occurs. Thus, very short embedment lengths (.04-.05 mm) are necessary to complete these pull-out tests successfully. Such small embedment lengths are difficult to work with in practice, although some investigators have reported limited success with specially designed apparatus [87] for such tests.

Due to problems inherent with conventional pull-out methods and with other interfacial testing methods, a modified pull-out test version has been developed by Miller et al. [41,42] and used by others [88,89,90]. This method provides a more convenient method for measurement of interfacial shear strengths of fiber/resin interfaces. Because

this method uses very small amounts of resin, it is commonly referred to as the microbond pullout technique or test.

The study in this chapter was undertaken to examine the microbond technique as it applies to determination of interfacial shear strengths of carbon fibers (AS4) with epoxy thermoset matrices as well as to compare it to the more established fragmentation test described earlier.

4.2 EXPERIMENTAL

The experimental methods involved are outlined in detail in Chapter 2 (section 2.2.2). In this chapter, two different curing cycles are used. The "normal" curing cycles (2 hr-75°C, 2 hr-125°C) and for the mPDA/DGEBA system a modified curing cycle (room temperature-24 or 36 hr, 75°C-2 hr, 125°C-2 hr).

Thin film samples were prepared by combining the resin with the appropriate amount of curing agent and mixing well. Hooks were then dipped into these mixtures and allowed to cure vertically in a glass chamber. Repeated dippings resulted in maximum sample thickness of about 4 mm.

4.3 RESULTS AND DISCUSSION

Initially an attempt was made to perform the microbond test after curing the mPDA/DGEBA droplets with the "normal" curing cycle listed in Table 2.1. For the AS4 fiber/mPDA/DGEBA system the critical length in the fragmentation test is found [51,30] to be about 300 microns, so that the droplet sizes cannot be greater than about 200 microns for the microbond test to be conducted. However, the experiments could not be conducted because the smaller droplets (< 110 microns) were incompletely cured as evidenced by the fact that they were "tacky" to the touch or "distorted" during initial stages of testing. This phenomenon is clearly illustrated in the two micrographs shown

in Figure 4.1. It can be seen that the smaller droplets are incompletely cured. For the larger droplets, as soon as the blades make contact with the droplet, large droplet deformations take place.

To investigate this phenomenon more closely, the T_g of mPDA/DGEBA droplets cured with the "normal" curing cycle was measured using the Thermal Mechanical Analyzer (TMA) and Differential Scanning Calorimeter (for larger droplets) as described in Chapter 2. The results are plotted in Figure 4.2 (triangular points) as droplet size versus T_g of the droplets. It can be seen that there is a strong correlation between droplet size and T_g. At small droplet sizes, the curing agent diffuses out of the samples, and the difference between the bulk T_g (T_g for the fully cured bulk DGEBA/mPDA matrix is about 135-140°C) and T_g of the droplet is about 70°C. As the droplet size increases, the T_g of the droplet also increases until at a droplet size of about 600 microns the difference between bulk T_g and the droplet T_g is about 30°C. Since T_g reflects the matrix structure and hence its mechanical properties, the droplet mechanical properties also must change with size. Therefore, measurement of fiber-matrix adhesion by the microbond test can produce artifacts at small droplet size in systems with volatile components because of changes in droplet stoichiometry. A recently published study by Rao and Drzal [55] has demonstrated that matrix modulus itself directly affects the interfacial shear strength. Thus, microbond tests will produce artifacts and cannot get representative values of interfacial shear strength for these systems unless account is taken of the change in material properties.

Since microbond tests failed when run with droplets cured with the "normal" curing cycle, an attempt to retard the process of diffusion and loss of the curing agent at high temperatures of cure was made. Droplets were cured with different, modified curing cycles as well as in mPDA-rich curing environments. The experimental procedure, in the case of the systems in which a mPDA atmosphere was used, was altered slightly.

Droplets Less than 100 Microns

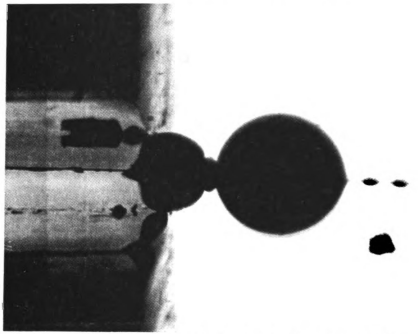

Droplets of 200 Microns Ready to be Tested

Figure 4.1: Schematic of incompletely cured microdroplets

Droplet specimens were prepared as usual and mounted on frames; these frames were, in turn, placed inside a sealed glass chamber containing an excess of mPDA at the bottom of the chamber. At processing temperatures the mPDA melted and its vapor saturated the chamber. The droplets were then cured either with the normal or modified curing cycles in contact with the mPDA vapor. The various curing schemes are shown in Table 4.1. In Table 4.1, all mixes contain a stoichiometric amount of mPDA except curing scheme C, which contains twice the stoichiometric amount. Interfacial shear strength for all the systems listed in Table 4.1, determined from the fragmentation test is 65-70 MPa.

The variation of T_g with droplet size, for the different curing schemes, is

TABLE 4.1: Curing schedules and conditions

CURING SCHEME	CURING CONDITIONS	AMT. OF MELTED mPDA	MICROBOND ISS (MPa)
A	NORMAL	6.667 g	38.9
B	NORMAL	37.42 g	36.8
C	NORMAL	6.787 g	35.7
D	25°C-24 hr NORMAL	6.699 g	45.3
E	25°C-24 hr NORMAL	NONE	41.6
F	25°C-24 hr NORMAL	NONE	54.7

shown in Figure 4.2. It can be seen that, at small droplet sizes (< 150 microns), regardless of whether a mPDA atmosphere or a modified curing cycle is used, the T_g is lower that the bulk T_g (even though it has increased when compared with the data from the "normal" curing cycle alone). At larger droplet sizes, the T_g has increased. However, the values are still low when compared with bulk values of T_g for this particular system. To estimate how much of the amine curing agent is diffusing out of

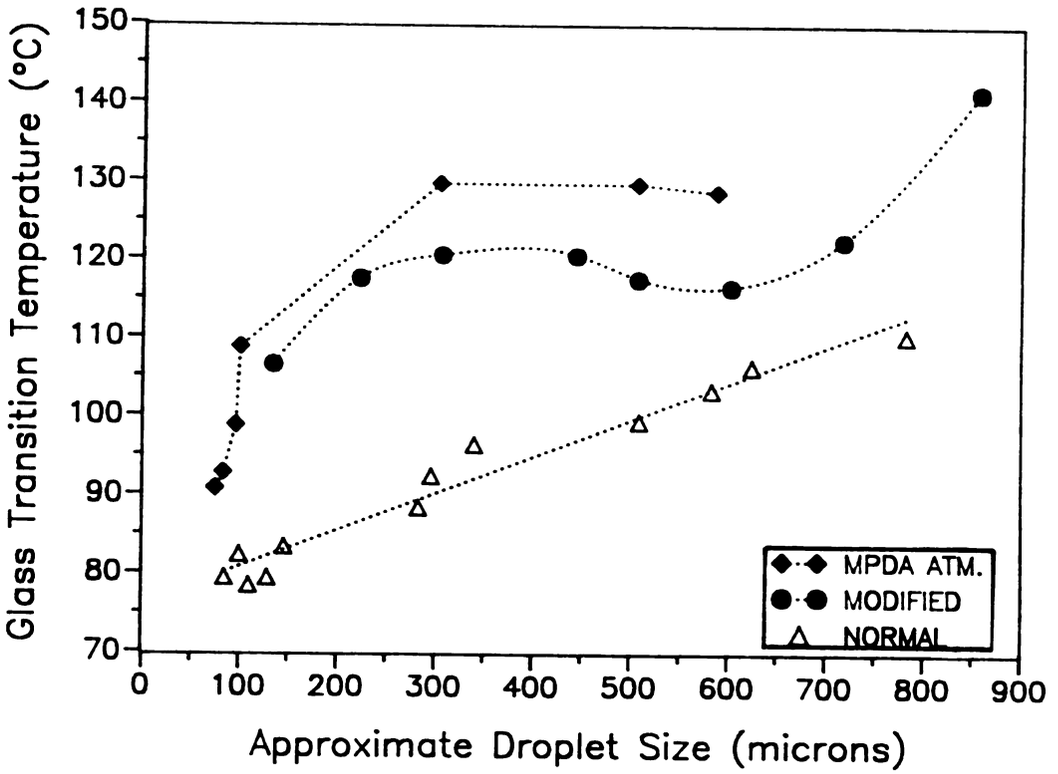

Figure 4.2: T_g as a function of microdroplet size for various curing schemes

the droplets, a relationship between T_g and amount of curing agent (mPDA) in the sample is necessary. The plot shown in Figure 4.3 used DSC to determine the relationship between amount of mPDA in the bulk sample and T_g of the sample. By combining the data from Figures 4.2 and 4.3 an estimate can be made of the droplet mPDA content as a function of droplet size. These data are plotted in Figure 4.4 where it is evident that, for the "normal" curing cycle, close to 40% of the amine curing agent may have been lost in small droplets. Even with the "modified" curing cycle, at small droplet sizes, about 25% of the amine curing agent is estimated to have been lost by diffusion. Ozzello et al. [91] and Haaksma et al. [92] have also made references to diffusion being a problem when conducting microbond tests though no attempts were made to quantify the phenomenon. Because the modified curing cycle as well as the mPDA-rich curing environment data showed less dependency of T_g on droplet size when compared with the normal curing cycle data, microbond experiments were conducted with various combinations of these conditions (Table 4.1) to compare the fragmentation test with the microbond test. Figure 4.5 shows the relationship between embedment area and debonding force, according to Equation 15, for the various curing schemes. In Figure 4.5, data is shown only for a limited range of embedment lengths. This is due to the fact that the carbon fibers tend to rupture if droplet sizes greater than about one-half of the critical length determined from the fragmentation test. The range of data shown in Figure 4.5 corresponds to embedment lengths generally between one-third and one-half of the critical length. It can be seen that all the plots are linear in the range of testing and the values of interfacial shear strength (τ) shown in Table 4.1 represent the slope of the "best-fit" line forced through the origin.

Figure 4.5 represents microbond data taken using curing schemes A through F listed in Table 4.1 and plotted separately in Figure 4.6. From Figure 4.6 it is evident that the microbond interfacial shear strength calculated for all cases is low when compared with

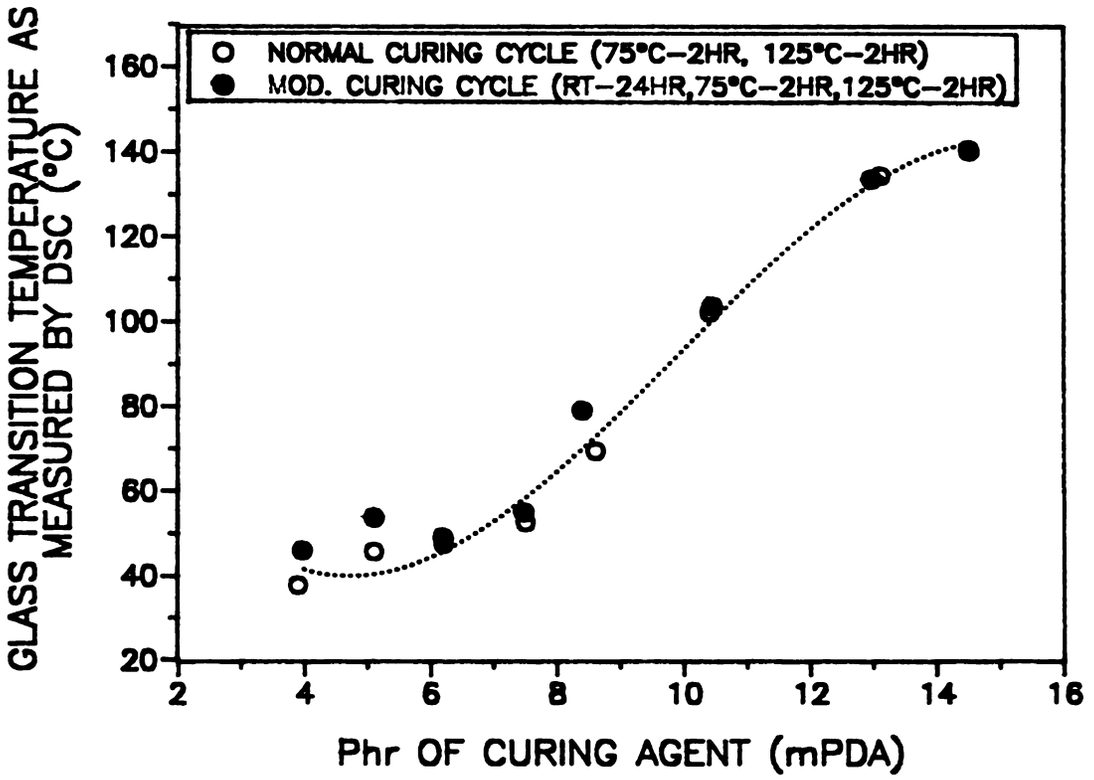

Figure 4.3: T_g vs. amount of mPDA in bulk samples

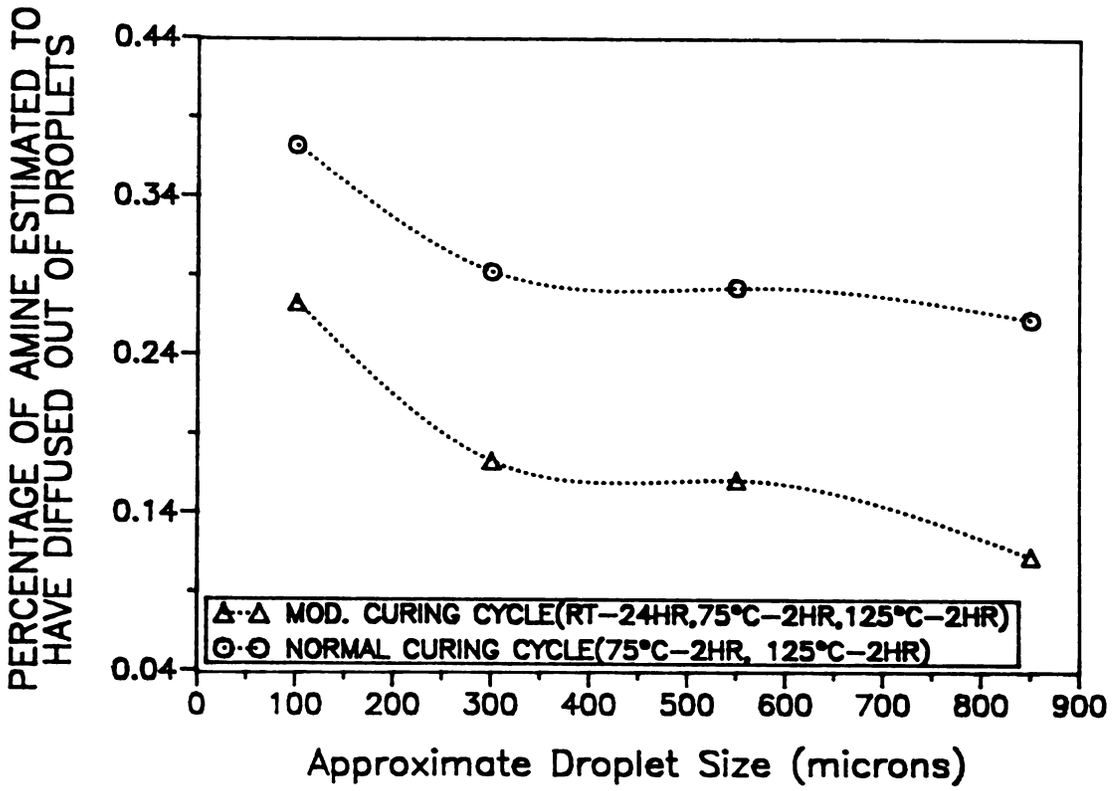

Figure 4.4: Amount of curing agent, mPDA, lost as a function of microdroplet size

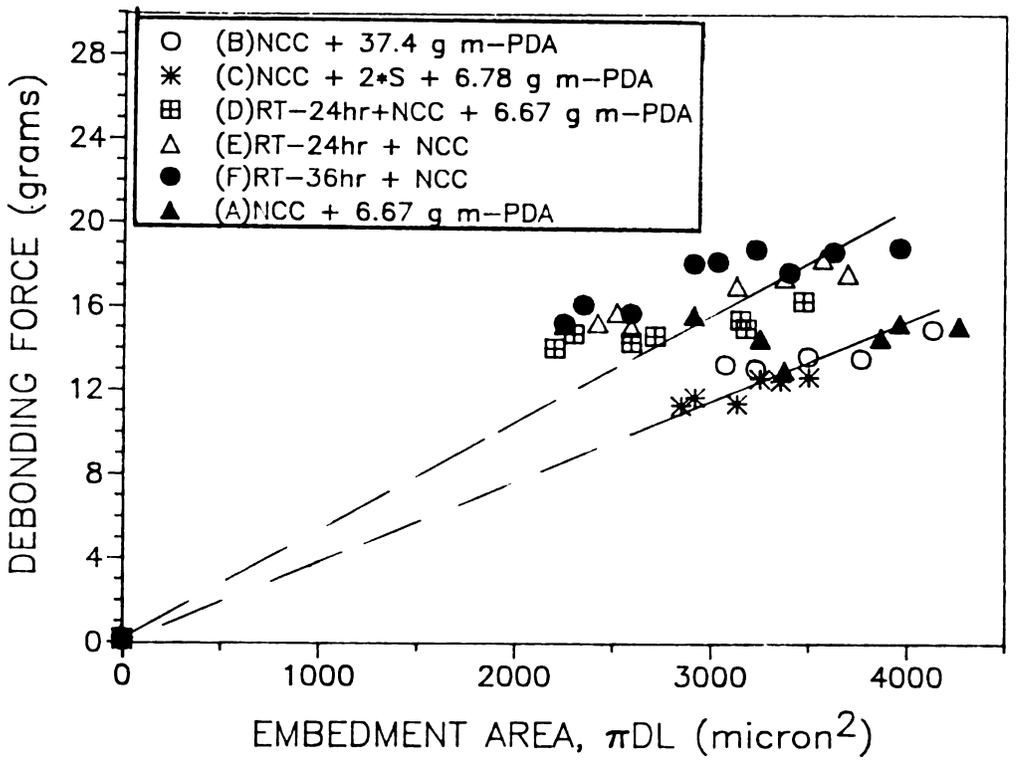

Figure 4.5: Microbond data for mPDA/DGEBA formulation with various curing schemes and atmospheres

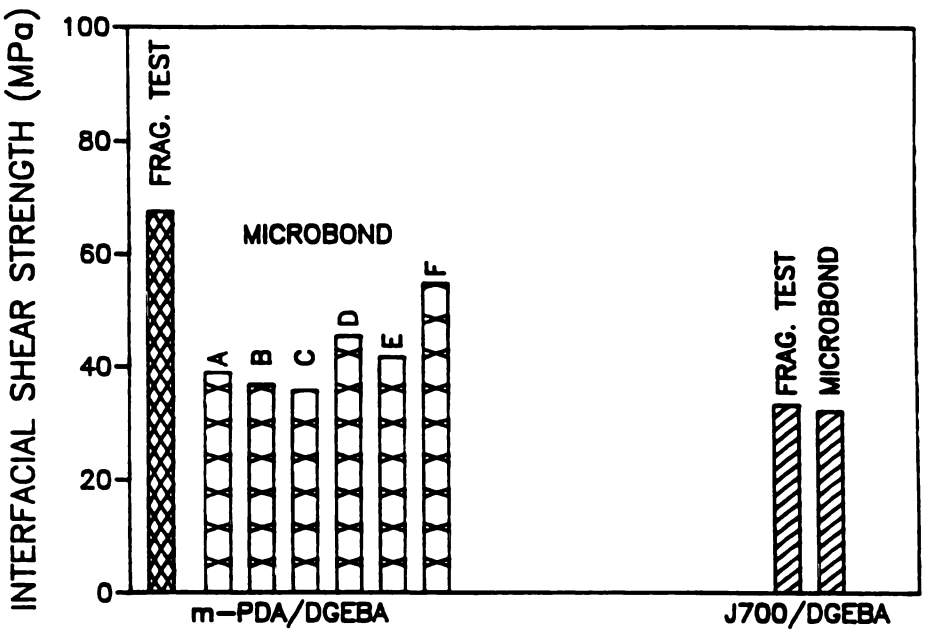

Figure 4.6: A comparison of the microbond test and the fragmentation test for mPDA/DGEBA matrix and J700/DGEBA matrix

the corresponding fragmentation test result of about 65-70 MPa (fragmentation tests conducted on specimens subjected to curing schemes A-F all showed a interfacial shear strength between 65 and 70 MPa). The two lines shown in Figure 4.5 are representative of the data with (curing schemes A, B, and C) without (curing schemes D, E, and F) a room temperature cure portion. The lines illustrate the fact that with the room temperature cure the microbond interfacial shear strength (the slope) has increased.

The mPDA environment (curing schemes A, B, and C) is not able to retard the loss of mPDA due to diffusion to any great extent. Changing the initial stoichiometry of the droplet (curing scheme C) also does not compensate for the amount of curing agent loss by the diffusion process. In curing schemes D-F, the "normal" curing cycle is preceded by a room temperature cure portion. It can be seen from Figures 4.5 and 4.6 that the interfacial shear strengths calculated for these curing schemes are slightly higher and thus closer to the interfacial shear strength values measured using the fragmentation test. The room temperature step allows some reaction to occur between amine and epoxy which retards the diffusion process as indicated by the higher interfacial shear strength results. Providing a mPDA atmosphere does not seem to influence the results as evidenced by the fact that the data from scheme D (with melted mPDA environment) results in lower interfacial shear strength when compared with scheme E (with no melted mPDA). Scheme F, which has a 36 hour room temperature cure--compared with 24 hours in schemes D and E--results in the highest microbond interfacial shear strength measured. This again points to the fact that allowing the droplets to cure at room temperature before being exposed to a high temperature environment effectively causes the system to gel so that the loss of curing agent at high temperatures is reduced.

Figure 4.6 also shows microbond data taken from another diamine curing agent system. In this case, a high molecular weight polyether diamine curing agent (Jeffamine 700) with reduced volatility was used (with curing schedule listed in Table 3) and hence

retarded the diffusion process. The data are shown in Figure 4.7 as embedment area versus force of debonding. The slope of the best-fit line through the origin results in a microbond interfacial shear strength of about 35 MPa. From Figure 4.6 it can be seen that this is within 5% of the interfacial shear strength measured using the fragmentation test for this system [55]. These results are consistent with the fact that the J700 curing agent has a lower vapor pressure and thus the amount of curing agent lost by diffusion and vaporization is minimized when compared with a more volatile system such as mPDA/DGEBA. Figure 4.7 also shows that the range of embedment lengths tested with the J700 system is greater than with the mPDA systems. This is due to the J700/DGEBA matrix being more compliant (the J700 matrix has a strain to failure of about 90% while the mPDA matrices have strain to failures of about 6%) leading to lower fiber-matrix adhesion. This lower adhesion allows larger drops to be tested (because the fiber does not tend to break) while the viscous nature of the J700 curing agent allows for smaller drops to be tested.

Recent work done, using photoelastic and finite element analysis, by Herrera-Franco et al. [81] has shown that the method of loading the microdrop in the droplet test affects the measured debonding force and can lead to a large amount of scatter in the data. The relative position of the blades with respect to the center of the drop (the contact angle between the blade and the microdrop) changes the stress distribution on the microdroplet. Thus, gripping the microdrop "incorrectly" may affect the measured debonding force by introducing large scatter in the data. This is especially true for the brittle mPDA systems studied; the J700 curing agent gives a much more compliant matrix making blade position and location less critical.

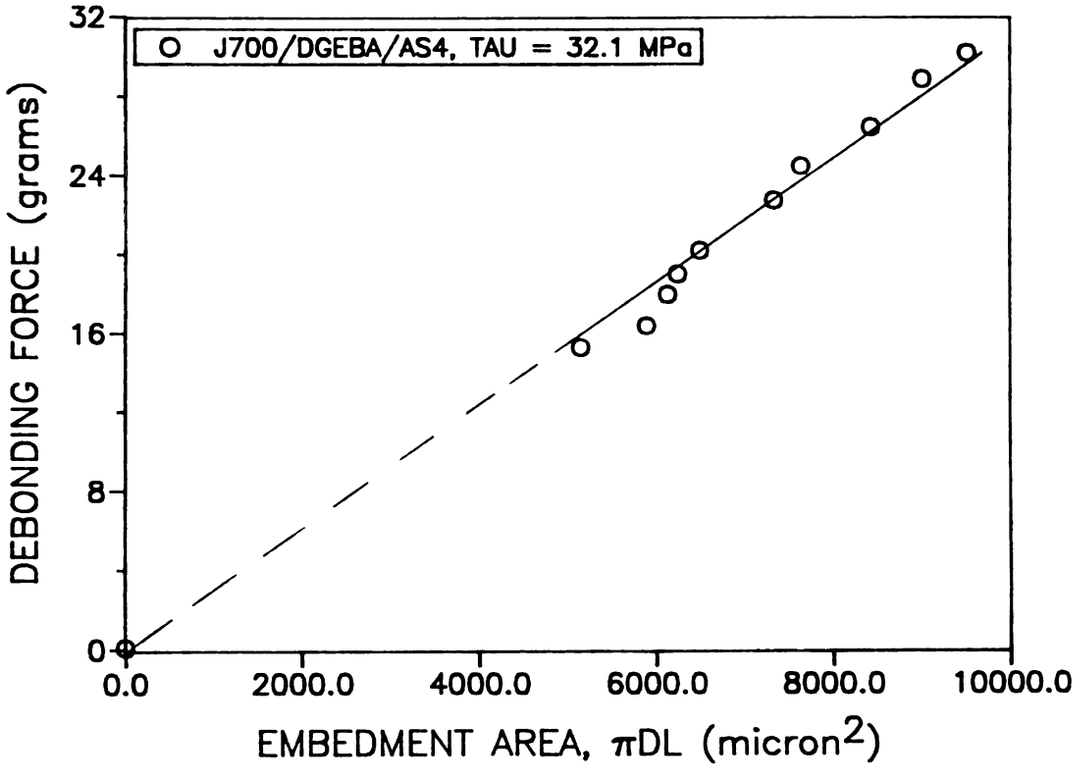

Figure 4.7: Microbond data for J700/DGEBA formulation

4.4 THIN FILMS

Thin films of upto 4 mm in size were prepared and tested (as described in Chapter 2 and above) to discern the amount of curing agent being lost by diffusion for the three of the matrices used in this work. The three different systems chosen for this portion of the study are all based on DGEBA resin cured with stoichiometric amounts of amine curing agents mPDA, J403 and J700. Glass transition temperatures of the "fully" cured samples were used as a measure of how much curing agent was lost during the curing process. As reported in Chapter 2, glass transition temperatures were measured both with a Thermal Mechanical Analyzer (TMA) as well as with Differential Scanning Calorimeter (DSC). The fully cured glass transition temperatures for the three different systems studied are shown below in Table 4.2.

Table 4.2: Fully cured T_g's of the matrices

SYSTEM	T_g (C)
mPDA/DGEBA	137±7
J403/DGEBA	75±3
J700/DGEBA	20±3

The data shown in Figure 4.8 are a combination of the data shown in Figure 4.2 (for the normal curing cycle, mPDA/DGEBA system) and the data obtained from the thin film experiments described earlier. As expected, the two Jeffamine-based systems (which have a higher viscosity and lower volatility when compared to the mPDA system) show nearly constant glass transition temperature throughout the testing regime. On the other hand, the mPDA system, even at sizes of about 3000 microns (3 mm), shows that the measured T_g deviates from the bulk T_g by about 10°C. This indicates that even at such

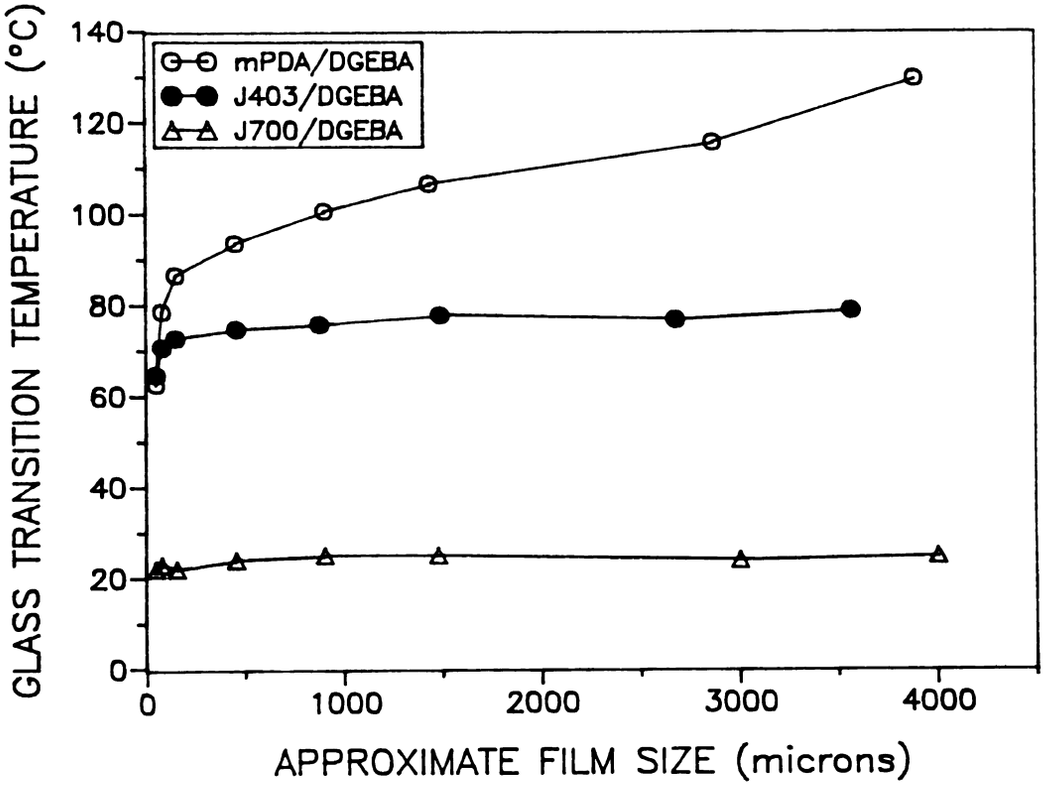

Figure 4.8: T_g as a function of film size for mPDA/DGEBA, J403/DGEBA and J700/DGEBA formulations

large film sizes, the mechanical properties could be different from those of the bulk matrix. Thus, extreme care must be taken to ensure careful measurement of mechanical properties os small dimension samples for the mPDA/DGEBA system or any system where a volatile curing agent is used.

4.5 MODELING OF THE DIFFUSION PROCESS

The diffusion in a semi-infinite slab has been extensively studied by many authors [13]. The slab initially contains a uniform concentration of solute. At some time, chosen conveniently as time zero (t=0), the concentration at the interface is suddenly and abruptly increased. In the case of droplet testing, t=0 would correspond to the time at which the droplets are placed on the fiber. This sudden concentration increment ate the fiber/matrix interface produces a time dependent concentration profile that develops as the solute (curing agent) diffuses out of the droplet.

If a mass balance of the diffusing species is combined with Fick's law, and assuming that the diffusion coefficient is independent of concentration (i.e. constant), we can arrive at the following well-known relation for diffusion of the curing agent:

$$\frac{\delta C}{\delta t} = D_e \frac{\delta^2 C}{\delta z^2} \qquad (4.2)$$

where, C is the concentration of the curing agent, and z is radial distance from interface out, and D_e is the effective diffusion coefficient. In this case, the boundary conditions become:

$$\text{at } t=0, \text{ all } z, \; C=C_\infty=0$$

$$\text{at } t>0, \; z=0, \; C=C_{bulk}$$

$$\text{at } t>0, \; z=\infty, \; C=C_\infty=0$$

It can be shown [12,13] (Appendix C) that the solution of this differential equation with the above boundary conditions is:

$$\frac{C}{C_{bulk}} = 1 - erf(\xi) \qquad (4.3)$$

$$\xi = \frac{z}{\sqrt{4D_e t}} \qquad (4.4)$$

If a diffusion coefficient of 10^{-7} cm^2/sec is assumed for the mPDA/DGEBA system [93] (see Appendix B), the time required to reach 10% of the bulk concentration in a 200 micron droplet is about 2 seconds. Whereas, for the Jeffamine based curing agents, the diffusion coefficient is expected to be lower (in the order of 10^{-8} cm^2/sec) and thus the time to reach the same concentration profile (and ratio) would be an order of magnitude or greater. This analysis validates and explains some of the curing observations made earlier with the volatile mPDA system.

4.6 CONCLUSIONS

In this chapter, experiments were conducted to compare the fragmentation test with the microbond test for determining the interfacial shear strength of carbon fibers in two different epoxy-amine thermoset matrices. Lack of agreement in the interfacial shear strength between the two testing methods has been attributed to loss of curing agent by diffusion from small droplets of resin which significantly changes the droplet mechanical properties. There is a strong correlation between droplet size and the amount of curing agent (mPDA) lost. Droplets less than about 150 microns in diameter lose up to 40% of the curing agent by diffusion and evaporation during the "normal" curing cycle in which the droplets are exposed immediately to a high temperature. This loss of curing agent lowers the T_g of the droplets by 60°C. Adding excess curing agent to the curing atmosphere does not seem to reduce the loss of curing agent from the small drops.

Modifying the cure cycle to include a protracted room temperature portion reduces the loss of curing agent.

A model developed here indicates that the diffusion of amine out of the droplets, at high temperatures, is very fast when the curing agent is the volatile mPDA curing agent. The use of less volatile curing agents (e.g. J700) with the same epoxy resin and fiber result in close agreement between the two tests without modification of the cure cycle or the cure atmosphere.

CHAPTER 5

THE DEPENDENCE OF INTERFACIAL SHEAR STRENGTH ON MATRIX AND INTERPHASE PROPERTIES AT AMBIENT CONDITIONS

This chapter focuses on the dependence of interfacial shear strength (ISS) on the bulk material matrix properties (at ambient conditions) using model compounds based on epoxy/amine chemistry discussed earlier. Carbon, AS4 fibers were used as the subject for these measurements with both a difunctional epoxy (DGEBA) as well as a tetrafunctional epoxy (MY720) system. Amine curing agents were carefully chosen to produce matrices which resulted in a range of matrix properties from brittle, elastic (shorter chained curing agents) to ductile, plastic (longer chained curing agents). The fiber-matrix interfacial chemistry was kept constant throughout this study (this chapter) by always using a stoichiometric amount of curing agent. The interfacial shear strength was quantified using the single fiber fragmentation test. This work has been previously published by Rao and Drzal [55].

5.1 INTRODUCTION

The determination of interfacial shear strength between fiber and matrix in composite materials is possible with a variety of methods ranging from single fiber to composite specimens [25,30,31,94]. While advances are being made in experimental methods that probe the fiber-matrix interface, the ultimate goal is to predict interfacial shear strength and to relate interfacial shear strength to fiber, matrix and interphase properties.

Many authors have proposed theoretical relationships between interfacial properties and bulk material properties. These models allow the local stresses to be computed based on the constituent properties. One of the first approaches was developed by Cox

[95] and later again by Cooke [14] who considered an elastic fiber of length, l, embedded in an elastic matrix, under general strain, ϵ. Cox and Cooke assumed "perfect bonding" between the two phases, as well as lateral contraction of the fiber and matrix. Using the assumption of load transfer through the ends of the fiber, leads to the following equation [14,95]:

$$\tau = E_f \epsilon_m \left(\frac{G_m}{2E_f \ln\left(\frac{R}{r}\right)} \right)^{0.5} \frac{\sinh\beta(0.5L-x)}{\cosh\beta L/2} \qquad (5.1)$$

where, E = Tensile modulus of fiber
ϵ_m = Strain in the matrix
G_m = Shear modulus of matrix
R = Interfiber spacing
r = Radius of the fiber
B = Scaling factor
L = Length of embedded fiber
x = Radial distance outward
τ = Interfacial shear stress at fixed point

As is evident from Equation 5.1, if the specimen geometry is fixed and the same fiber is used in each case, the theory predicts a direct dependence of the interfacial shear strength on the product of the matrix strain and the square root of the shear modulus of the matrix. This square-root dependency of the interfacial shear strength on the matrix shear modulus has also shown to hold in other single fiber tests. Kendall [96], for example, has shown that in single fiber pull-out tests, the force required to pull a single fiber out of an elastic matrix is directly proportional to the square root of the shear modulus of the matrix. Rosen [97,98] also has analyzed the shear stress field along the fibers between parallel fibers in a composite loaded in tension. His model consists of a fiber surrounded by matrix, which in turn is embedded within a composite material exhibiting average composite properties. The fiber is assumed to carry only extensional loads and the matrix to transmit only shear stresses. He used an equilibrium approach to derive the relationship between, τ, the shear stress at the interface and properties of

the fiber and matrix. Dow [97,99] has evaluated a more general case in which the load is applied to both fiber and matrix. The theory used is similar to that considered by Cox and Cooke, except that no matrix was present at the end of the fiber.

In all of these models, the matrix is the medium by which shear stresses are transferred to the fiber. The models show an explicit dependency on matrix shear properties. Yet, most adhesion studies focus entirely on the interfacial interactions (chemical and physical) between fiber and matrix and tend to neglect the matrix itself as having a causal effect on fiber-matrix adhesion.

In other work previously published it has been shown that the maximum extent of chemical bonding between amine and/or epoxy groups with the surface chemical groups present on the fiber surface is less than 5% [100]. Experimental verification of the extent of chemical interaction between epoxy and amine groups with the AS4 fiber surface [100] has been completed in the following fashion. Monofunctional epoxy and amine compounds were dissolved in an inert solvent and placed in a closed container with a aliquot of AS4 carbon fibers. The system was sealed, taken up to the typical processing temperatures encountered in curing epoxy composites, and then cooled to room temperature. The fibers were Soxhlet extracted in pure solvent and the surfaces of the AS4 fibers were compared by Xray photoelectron spectroscopy with the "as-received" fibers. Epoxy and amine chemical bonding to AS4 fiber surfaces has been shown to be less than 5% and occur at temperatures above 100°C supporting the assumption that the extent of chemical bonding in this set of experiments (in this study) to be both small and constant for all of these systems.

It is very tenuous to try to extrapolate interfacial properties from one system to another if the matrix properties are not taken into account. Little experimental verification has been attempted where the interfacial chemistry remains unchanged but the matrix properties are systematically varied. This study presented in this chapter was

undertaken to experimentally investigate the effect of changing matrix properties from stiff and brittle (characteristic of most thermoset matrices) to compliant and ductile (characteristic of thermoplastic matrices) on fiber-matrix interfacial shear strength.

5.2 EXPERIMENTAL

AS4 fibers were used throughout the study presented in this chapter. All curing agents were either di- or tri- amines illustrated in Figure 2.2. Material properties of the different matrices was obtained, as described in Chapter 2, using a MTS-880 system. Thermal analysis (T_g determinations) were performed on a DSC unit.

The single fiber fragmentation test was used (Equation 2.2) to quantify the interfacial shear strength. A single parameter like the interfacial shear strength is of limited value when the mode of failure between fiber and matrix is unknown or changing. A very useful additional feature of the fragmentation test described in Chapter 2 is that *in-situ* observation of the fiber-matrix region can be made during testing. Observation of the fragmentation test with either transmitted or polarized light provides information about local stresses and failure modes. The highly stressed polymer near the ends of the fiber fragments is birefringent and pronounced changes in the photoelastic stress pattern of this region occur with each fiber-matrix combination. The change in this pattern with increasing sample strain has been shown to be a qualitative indicator of different types of fiber-matrix failure modes [30,31].

The wetting characteristics of the fibers and matrices were determined by using a Wilhelmy apparatus for measuring contact angles as described in Chapter 2. A three liquid analysis (deionized water, ethylene glycol and methylene iodide) was completed to compute the polar and dispersive components of the surface free energies.

5.3 RESULTS AND DISCUSSION

5.3.1 EFFECT OF MATRIX PROPERTIES ON ISS

All material and interfacial properties of the different matrices are listed below in Tables 5.1 and 5.2. In Table 5.1, the DDS system did not reach critical length due to the matrix being too brittle. The standard deviations associated with the interfacial shear strengths, τ, measured are on the order of 10-15%. For details on the error in measurements, consult ref. [55]. It can be seen from Table 5.2 that there are fewer data points for the more reactive tetrafunctional MY720 resin system and that all of the mixtures have at least a few phr of J700 curing agent in them. This is due to the fact that the MY720 resin system, which is a gummy solid at room temperature,

TABLE 5.1: Interfacial and material properties of DGEBA system

DGEBA CURED WITH:	τ (MPa)	E (GPa)	υ	G (GPa)	ϵ_f (%)	ϵ_b (%)
mPDA	72.7	3.30	0.35	1.17	5.30	4.10
DDS	64.3	3.40	0.31	1.30	4.40	4.40
J230	56.7	2.95	0.35	1.09	7.10	6.00
J400	51.3	2.73	0.34	1.01	8.00	7.3
J403	47.0	2.31	0.36	0.85	12.2	9.8
J700	39.0	0.67	0.44	0.23	96.3	28.0

reacts very quickly with any of the smaller sized curing agents leading to an uncontrolled exothermic crosslinking reaction upon mixture of the resin and curing agent. Various methods (such as aliquoting the curing agent into the resin, cooling the resin to a lower

TABLE 5.2: Interfacial and material properties of MY720 system

MY720 Cured With:	τ (MPa)	E (GPa)	G (GPa)	ϵ_f (%)	ϵ_b (%)
J700	40.8	1.26	0.45	86.0	25.0
J700/J403	48.8	2.67	0.99	8.30	7.80
J700/J400	53.8	2.92	1.08	7.10	6.50

temperature before mixing, etc.) were attempted with little success. A controlled reaction could be initiated only with the addition of a few phr of J700 to the other curing agents before mixing. The reaction could not be controlled (even after the addition of J700) with the J230, mPDA and DDS curing agents. However, a stable controlled reaction was obtained with the J400 and J403 curing agents.

As can be seen from Tables 5.1 and 5.2, the interfacial shear strength (as calculated using Equation 2.2) is seen to decrease as the modulus of the matrix material decreases. This relationship is seen clearly in Figure 5.1 where the interfacial shear strength, τ, is plotted versus the shear modulus, G, for both the difunctional as well as the tetrafunctional resin systems. From Figure 5.1 it can be seen that, for both systems, as the modulus of the matrix decreases, the interfacial shear strength also decreases in a non-linear fashion. This suggests that as the matrix material near the fiber surface, in which the fiber is embedded, becomes more compliant, the transfer of stress between it and the AS4 carbon fiber is reduced.

Microscopic observation of the single AS4 carbon fiber in various matrices during the interfacial shear strength measurement provides additional insights into the processes

occurring during the interfacial fragmentation test. Figures 5.2-5.6 show a series of photomicrographs, using both transmitted light and transmitted polarized light, depicting the fiber in the various systems studied. For comparative purposes all micrographs were selected at a point at approximately 50% of the strain required to reach critical length. From these micrographs it is possible to identify the failure modes in the various systems.

Figure 5.2 displays a micrograph of the relatively high modulus DGEBA/mPDA system. Under polarized light the stresses that develop around the fiber fragment ends can be easily observed due to the photoelastic nature of the matrix. The large elliptical photoelastically active area represents the tip of a growing interfacial crack. This elliptical region was seen to be initially present at the end of a fiber fragment. With increasing sample strain, this region moves away from the fiber along the fiber-matrix interface leaving behind an intense narrow region between itself and the fiber fragment end. Previous studies [30,101] have used transmission electron microscopic analysis of ultramicrotomed sections to show that this pattern is associated with a fracture path between the fiber and the epoxy matrix which is purely interfacial (this phenomena can be seen in the transmitted light micrograph in Figure 5.2).

In the next two sets of photomicrographs (Figures 5.3 and 5.4), failure modes for two of the Jeffamine based curing agents, which have a lower modulus than the mPDA system, are shown. The tensile modulus of the J230 cured system is 2.95 GPa while for the J403 cured system it is 2.31 GPa (compared to 3.30 GPa for the mPDA cured system). In each case, the photoelastic stress pattern is less intense (indicating lower adhesion) than the mPDA system described above. In the case of the J230 curing agent (Figure 5.3), the polarized light micrograph shows a more diffuse photoelastically active area with a narrow intense region at the interface extending away from the fiber break. These regions again represent the elastic zone at the tip of a growing interfacial crack.

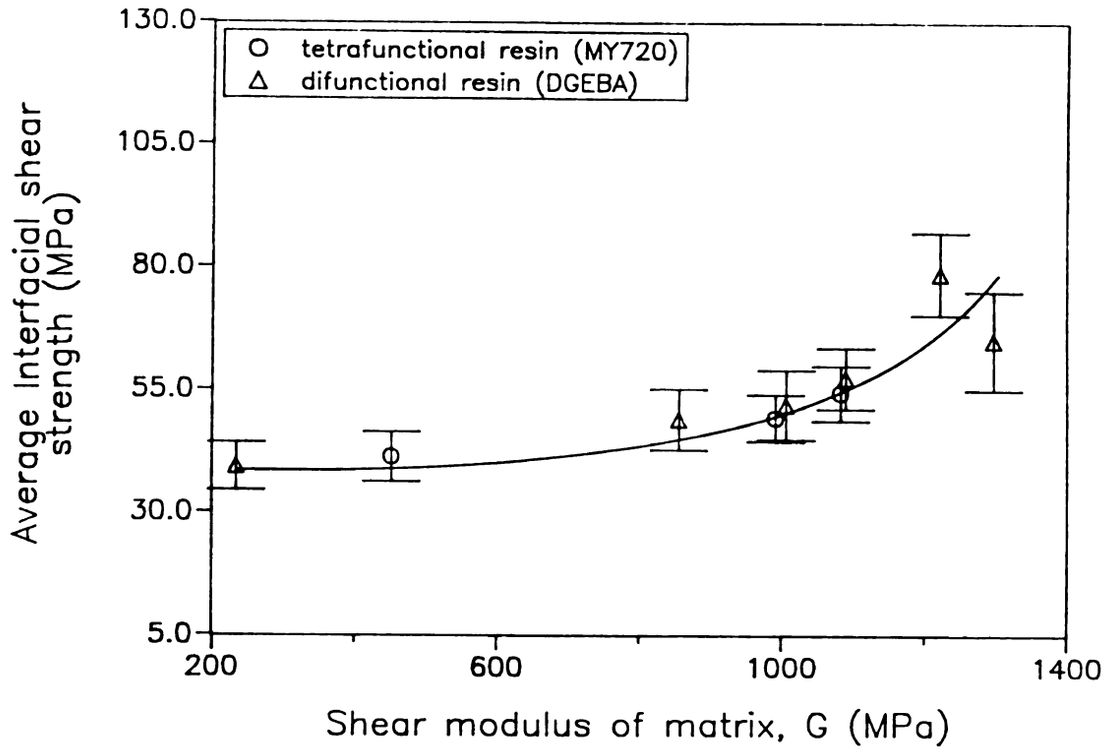

Figure 5.1: Interfacial shear strength as a function of bulk matrix shear modulus

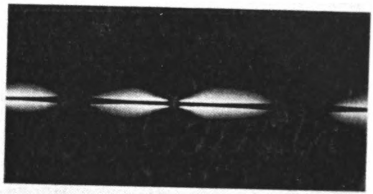

Polarized Light Micrograph

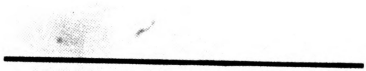

Transmitted Light Micrograph
(fiber diameter ~ 7 μm)

Figure 5.2: Interfacial failure mode of mPDA/DGEBA formulation

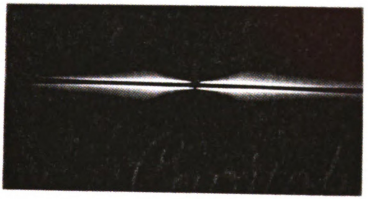

Polarized Light Micrograph

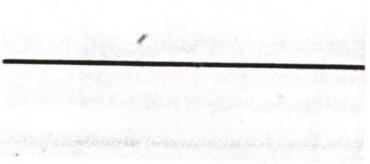

Transmitted Light Micrograph
(fiber diameter $\sim 7\ \mu m$)

Figure 5.3: Interfacial failure mode of J230/DGEBA formulation

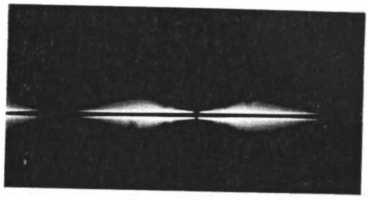

Polarized Light Micrograph

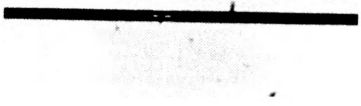

Transmitted Light Micrograph
(fiber diameter ~ 7 μm)

Figure 5.4: Interfacial failure mode of J403/DGEBA formulation

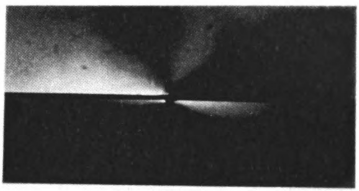

Polarized Light Micrograph

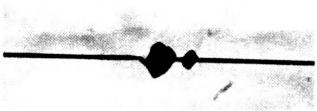

Transmitted Light Micrograph
(fiber diameter $\sim 7\ \mu m$)

Figure 5.5: Interfacial failure mode of J700/DGEBA formulation

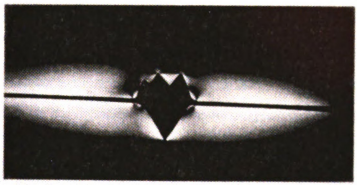

Polarized Light Micrograph

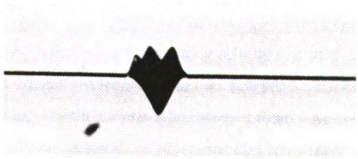

Transmitted Light Micrograph
(fiber diameter $\sim 7\ \mu m$)

Figure 5.6: Interfacial failure mode of J700/MY720 formulation

As with the mPDA curing agent, as the strain is increased, this region moves away from the fiber break leaving behind a less intense narrow region between itself and the fiber fragment end. The transmitted light micrograph reveals that the interface fails with the simultaneous creation of a transverse crack and interfacial debonding. For the DGEBA/J403 system, and for which the micrographs are shown in Figure 5.4, the failure process is similar to those described above as characterized by the photoelastically active area. As before, the debonding is seen to be interfacial along with a small amount of matrix tearing as seen in the transmitted light micrograph. This feature is seen as a small sharp crack going into the matrix in a direction perpendicular to the fiber. This type of matrix failure was completely absent in the mPDA system and was barely detectable in the J230 system.

The micrographs shown in Figure 5.5 is that of the very compliant J700/DGEBA system. This system (along with J700/MY720 (Figure 5.6) which behaves identically) is quite different when compared to the other systems studied. This system shows very large amounts of matrix damage (matrix tearing away from interface) occurring from the initial stages of the single fiber test when the sample strain is very low due to the low yield stress of the matrix. At the point when the first break occurs in the single fiber test, a large amount of matrix damage is already present. As the sample strain is increased the matrix fracture associated with the breaks increases and the fracture opens creating the characteristic double-diamond shaped pattern depicted in the micrograph. The photoelastic stress pattern, representing the plastic zone at the tip of the crack, has no geometrical shape associated with it and is less intense when compared to the other systems studied. The debonding, however, still takes place interfacially.

It is obvious from the failure-mode micrographs that the fracture toughness of the matrices is changing and is partly responsible for the changes which are observed. Since the fiber geometry is constant in these experiments, the stresses at the fiber fracture point

should be similar. The matrix formulations which are lower in toughness would be expected to produce less damage.

The theory presented by Cox and Cooke (Equation 5.1) relates the interfacial shear strength to the material properties of the matrix and properties of the fiber. For a fixed geometry, a linear relationship is predicted between the interfacial shear stress, τ, and the product of the matrix strain and the square root of the shear modulus of the matrix, $\epsilon_m\sqrt{G_m}$, provided that all of the other variables are held constant. In the present work, the interfacial chemistry and specimen geometry are constant. The linear relationship suggested by Cooke is plotted in Figure 5.7 with a minor adjustment. Instead of plotting the quantity $\epsilon_m\sqrt{G_m}$, the group $\epsilon_b\sqrt{G_m}$ is plotted in Figure 5.7 versus the interfacial shear strength. For these experiments, ϵ_b is selected as a better measure of the physical events taking place at the interface than ϵ_m. ϵ_b is the strain in the matrix where the fiber has reached its critical length rather than the yield point of the matrix.

Figure 5.7 shows a nearly linear relationship, for both the difunctional as well as the tetrafunctional resin systems, for all the points except when pure J700 is used as the curing agent. One possible reason for the J700 cured systems not following the linear relationship as the other curing agents could be due to the fact that the modulus of the system is so low that its behavior is more plastic than elastic. Significant necking was seen to occur while conducting the stress/strain experiments for this system. From the stress/strain curves depicted in Figure 5.8, it is evident that the total strain is much greater for this system than for any of the other systems studied. From Figure 5.7 it is seen that the linear dependence between the interfacial shear strength and the product of the strain to failure at the critical length of each system times the square root of the shear modulus of the matrix is valid until the shear modulus of the matrix decreases to below about 1 GPa. Cooke's model uses linear elastic theory to predict the interfacial shear stress as a function of matrix and fiber properties. It is therefore rather surprising that

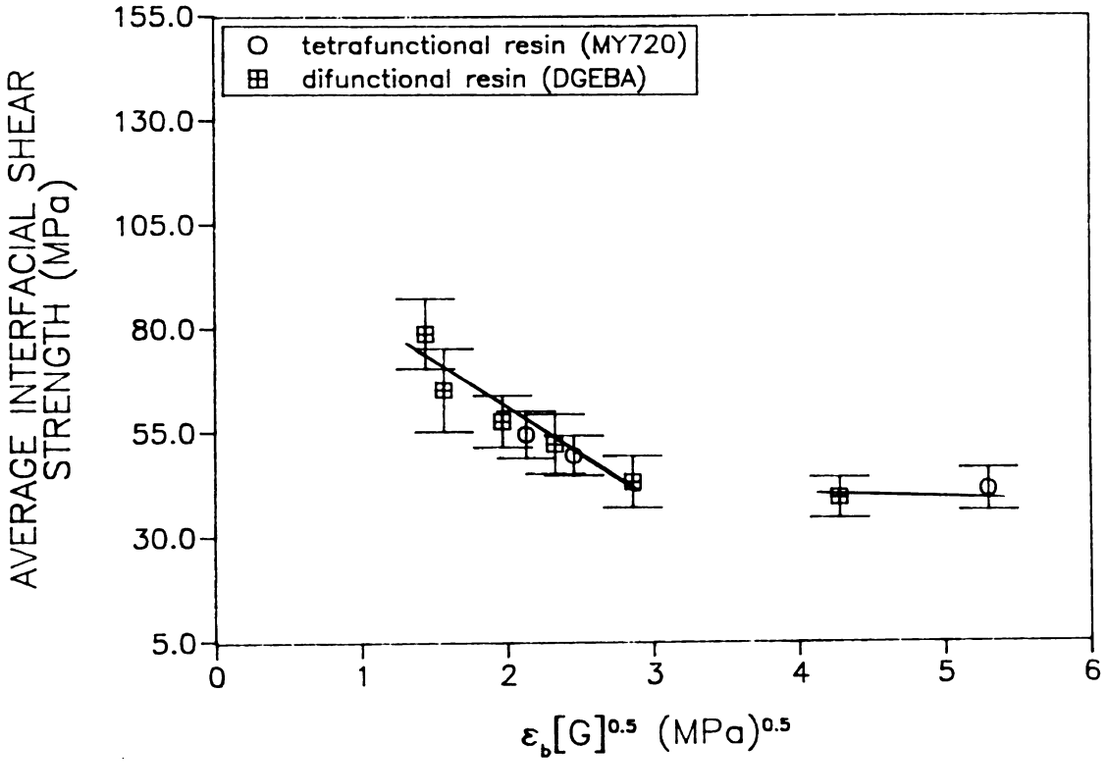

Figure 5.7: Interfacial shear strength as a function of the product of squareroot of matrix shear modulus and strain at final break

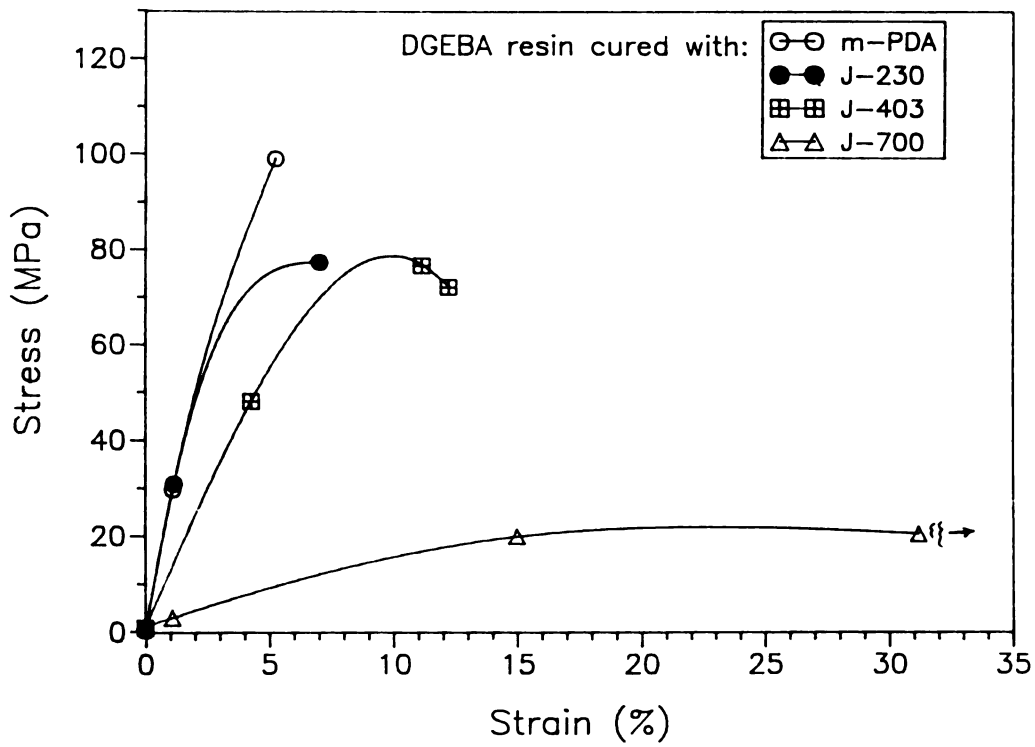

Figure 5.8: Stress/Strain curves for all DGEBA formulations

for the elastic/plastic systems studied, the model seems to predict interfacial phenomena as a function of matrix and fiber properties rather well down to approximately 1 GPa for matrix shear modulus. Figure 5.7 indicates that there is a lower limit of the matrix modulus on fiber-matrix adhesion. Netravali et al. [56] have also shown that the effect of matrix properties (modulus) on interfacial shear strength is minimal for these types of systems below about 1.3 GPa modulus for the matrix material. The matrix material in the interphase may behave in a more linearly elastic manner under the superimposed triaxial compressive interfacial stress. This mechanism will be explained in detail in the next chapter where the effect of elevated temperature on interfacial shear strengths will be discussed.

All experimental values of the interfacial shear strengths have been determined by Equation 2.2. However, the effects of thermal stresses and Poisson's radial contractions are not explicitly present in the equation. Interfacial shear strengths calculated using Equation 2.2 agree well with Cox's and Cooke's model until the matrix begins to become very compliant (about 1000 MPa) at which point the agreement between the two is seen to decrease. Better agreement with Equation 2.2 can be obtained when a three-dimensional model proposed by Whitney and Drzal [102] is used to compute the interfacial shear strengths. This three dimensional stress model proposed by Whitney can be used to compute the complete state of interfacial stresses. For example, the radial compressive stress (which results from thermal stresses and shrinkage in the matrix and fiber), in the various systems studied, is calculated using Whitney's model and tabulated in Table 5.3. These data are plotted in Figure 5.9 as shear modulus of the matrix versus the radial compressive stress. Also shown in Figure 5.9 is the variation of the interfacial shear strength as a function of the shear modulus of the matrix. The vertical line drawn in Figure 5.9 at a shear modulus value of 1180 MPa reflects previous work [39] done on a similar fiber/matrix system in which the effect of cure temperature on interfacial

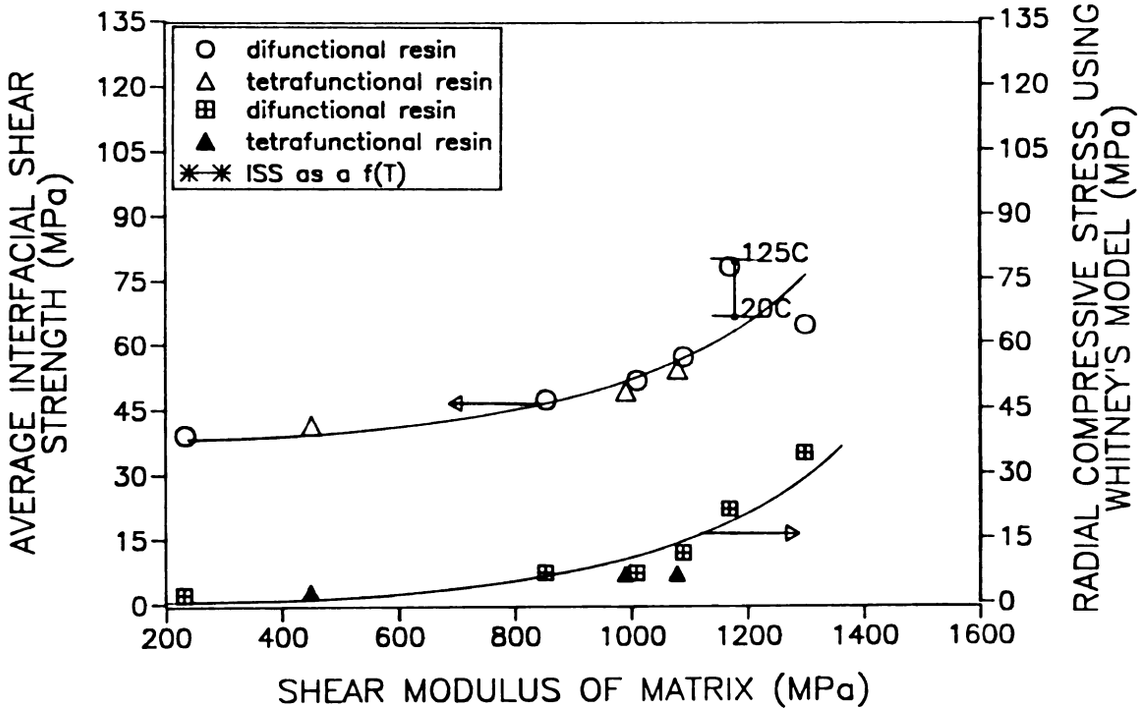

Figure 5.9: Radial compressive stress and interfacial shear strength as a function of matrix shear modulus

strength was studied. The lower point represents the interfacial shear strength for an epoxy/amine system that was fully cured at ambient condition. The difference should be entirely attributable to differences in radial residual compressive stress. Higher cure temperatures produce a higher (beneficial) radial residual compressive stress at the interface. From Figure 5.9 it can be seen that the radial compressive stress, for a given system of modulus G, is only about 25% of the interfacial shear strengths for the high modulus systems and is virtually non-existent for the low modulus systems.

To aid in identifying the role that the radial compressive stress plays determining the

TABLE 5.3: Radial compressive stresses

SYSTEM DGEBA CURED WITH:	T_g (°C)	$T-T_g$ (°C)	ISS (MPa)	RADIAL COMP. STRESS (MPa)
mPDA	130	-110	72.9	20.9
DDS	198	-178	---	33.9
J230	73	-53	56.7	10.7
J400	45	-25	51.3	6.0
J403	75	-55	48.4	6.0
J700	18	2	38.6	0.56
MY720 CURED WITH:				
J700/J400	40	-20	53.8	5.70
J700/J403	43	-23	48.8	5.62
J700	22	-2	40.8	1.31

change in interfacial shear strength of a given system, the analysis presented by Adamson [103] can be used. Van der Waal's forces, chemical bonding, molecular interactions as

well as frictional forces contribute to the interfacial shear strength. The vertical line drawn in Figure 5.9 represents a constant chemistry system in which only the cure temperature was altered. Thus by equating the frictional force component of the interfacial shear strength to a coefficient of friction times the normal force ($\tau=\mu N$) an estimate of the friction coefficient can be made. From the vertical line in Figure 5.9, it can be seen that the change in interfacial shear strength between the two temperatures is about 13 MPa; the corresponding change in normal force is just the radial compressive stress at 125°C since the contribution from 25°C is negligible (due to ΔT being small). The coefficient of friction calculated in this manner is about 0.6, so that $\Delta\tau=0.6N$. Using this equation, the effect of the normal force on the change in interfacial shear strength can be calculated for all the systems. For example, the DGEBA/mPDA system shows that $\Delta\tau=12$ MPa due to normal forces while the compliant DGEBA/J700 system shows that $\Delta\tau=0.34$ MPa due to normal forces. Generally speaking, the effect of radial compressive stress on interfacial shear strength diminishes as the modulus (and T_g) of the system decreases. Therefore, it can be said that the effect of radial compressive stresses on changes in the interfacial shear strength are significant but generally small. By extrapolating the interfacial shear strengths to zero thermal stresses, it is evident, because of the minor contribution of radial stresses, that a plot of G versus $\Delta\tau$ will be very similar to the G versus τ curve shown in Figure 5.9. It can then be concluded that the changes in interfacial shear strengths seen in this study are mainly due to the modulus differences in the various systems and not to the effect of residual thermal stresses.

These epoxy polymers are glasses below T_g. At temperatures above T_g the polymer is soft and flexible. Mechanical properties show profound changes in the region of glass transition. For instance, the elastic modulus may decrease by a factor of over 1000 times as the temperature is raised through T_g [12]. Above T_g virtually all possible motions for a polymer chain occur while below T_g many molecular motions are frozen and cannot

occur. Because the glass transition temperatures are a parameter characteristic of a given matrix system and are different for each of the matrix systems chosen for this study, the interfacial shear strength has been measured at different temperatures in relation to the glass transition temperature. A plot of $T-T_g$ (where T is the temperature at which the experiments are conducted and T_g is the glass transition temperature of the fully cured matrix) versus the interfacial shear strength would compare the interfacial shear strength results at equivalent matrix conditions.

Figure 5.10 is a plot of the interfacial shear strength versus difference in temperature between test temperature and T_g. It can be seen that a nearly linear relationship exists over the entire range of matrix systems tested.

It is evident that as the T_g of the matrix increases, the interfacial shear strength also increases. From a network structure point of view, materials which have a higher T_g would tend to have a higher modulus and transfer stress better to the interface leading to an increase in the interfacial shear strength. Materials with a higher transition temperature would, in general, also lead to higher thermal stresses in the system which would cause shrinkage of the matrix around the fiber and consequently increase the interfacial shear strength a noted earlier by Kalantar and Drzal [39]. For constant interfacial chemistry, Figure 5.10 also shows that the interfacial shear strength can be predicted by knowing a fundamental material parameter such as the T_g. By conducting experiments such as these at different temperatures it may be possible to predict the interfacial shear strength as a function of modulus or temperature. This is the subject of the next chapter.

In the above discussion, it has been shown that the changes in interfacial shear strength seen in the experiments conducted in this chapter are mainly due to modulus changes of the bulk matrix (and interphase). Recently, however, experimenters have published results [104,105,106] indicating that wetting of the matrix and fiber, as well

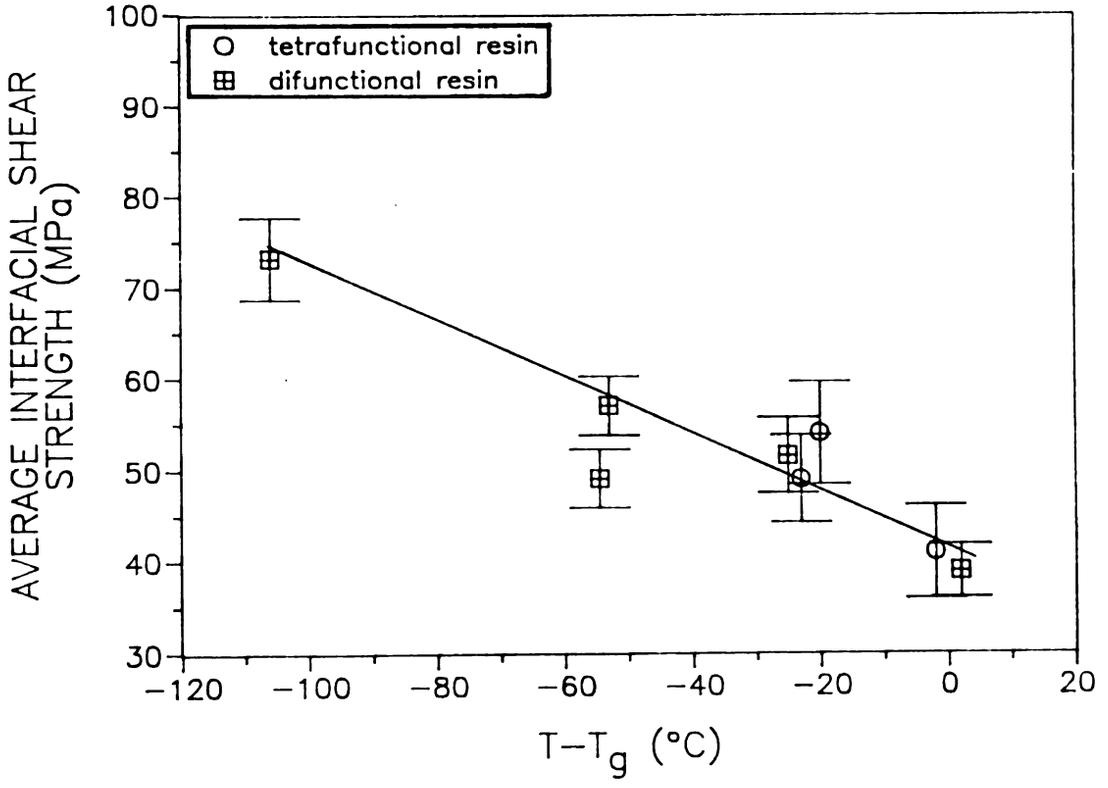

Figure 5.10: Interfacial shear strength as a function of T_g of the fully cured matrix

as the acid-base characteristics of the fiber-matrix combination, could play a major role on determining the final level of fiber-matrix adhesion.

Using deionized water, ethylene glycol and methylene iodide as the liquids, a dispersive and polar component of fibers and matrices were calculated. The results are tabulated below in Table 5.4. It can be seen that the changes in the polar component

TABLE 5.4: Wetting characteristics of matrices and fibers

MATERIAL	γ^D (mj/m^2)	γ^P (mj/m^2)	γ^{TOTAL} (mj/m^2)
AS4 FIBER	35.8±3.0	11.5±1.8	47.3±4.2
mPDA/DGEBA	34.3±3.1	13.1±1.7	47.8±4.9
J230/DGEBA	25.4±4.6	11.9±3.5	37.3±6.8
J400/DGEBA	26.7±4.5	12.2±1.9	38.9±5.9
J403/DGEBA	25.9±3.9	13.0±2.7	38.9±5.3
J700/DGEBA	20.8±2.5	10.8±1.7	31.6±4.3

(which is the parameter most sensitive to changes in level of fiber/matrix adhesion [27]) of the surface free energies is quite small for the different systems (only the J700 system-which has the lowest fiber-matrix adhesion shows a significant decrease in the polar component--and even that is only a change of about 5%) and thus it can be concluded that the changes seen in interfacial shear strengths in this chapter were due to modulus changes in the matrix materials.

5.4 CONCLUSIONS

In this chapter, a series of experiments were conducted wherein the fiber-matrix interfacial chemistry was kept constant while the matrix modulus was altered. A monotonically increasing dependence of interfacial shear strength on the shear modulus of the matrix was determined for both a difunctional and a tetrafunctional epoxy system

cured with polyamines using carbon fibers (AS4) as reinforcement. A linear dependence is observed between the interfacial shear strength and the product of the strain to failure at the critical length of the system times the square root of the shear modulus until the shear modulus decreases below approximately 1 GPa. When the interfacial shear strength is plotted against the difference between the test temperature and the glass transition temperature of the fully cured matrix, a linear relationship also results. The conclusions from these results are that a dependence exists between matrix modulus and interfacial shear strength because of the stress transfer function of the matrix. A decrease in modulus, all other things being equal, causes a corresponding decrease in interfacial shear strength.

CHAPTER 6

THE DEPENDENCE OF INTERFACIAL SHEAR STRENGTH ON TEMPERATURE AND ASSOCIATED INTERPHASE FORMATION

In this chapter, the dependence of interfacial shear strength on temperature will be will be investigated. The same epoxy matrices (reinforced with carbon, AS4 fibers) studied in Chapter 5 will be used to construct a master curve which has the ability to predict the interfacial shear strength by knowing the test and glass transition temperature of the matrix. Additionally, a diffusion model will be presented to predict the formation of an interphase using epoxy-sized carbon fibers in mPDA/DGEBA matrix. Most of the work presented in this chapter has been published separately by Rao and Drzal [58].

6.1 INTRODUCTION

As described in Chapter 1, the ability of the matrix to transmit stresses from fiber to fiber at the microscopic level is responsible for internal stress development in the composite during processing which in turn, may be responsible for generating defects. During the early stages in processing, the matrix is in a fluid state and can only transmit minimal amount of stresses (Chapter 3). As processing progresses, however, there is an increase in modulus with time and temperature. Interfacial properties have been shown to be heavily dependent on the matrix modulus and the interactions at the fiber matrix interface [55]. In thick parts, with an exothermic reacting matrix, simultaneously the matrix properties, and consequently the interfacial properties, can vary throughout the thickness of the material because of temperature non-uniformity. Hence it is critical that the mechanism by which the interfacial (and adhesive) properties are generated during composite processing is understood so that the mechanical properties can be known as a function of temperature and time in order to optimize composite processing.

Though various authors [36,58,59] have studied how temperature and modulus affect polymeric composites, the role that residual stresses [107] play in determining the final mechanical properties of composites as well as the dependence of temperature on mechanical strength of composites [108], little work has been done to elucidate the alteration of interfacial shear strength as a function of processing conditions.

An added complexity results from the fact that in most cases an "interphase" exists at the fiber-matrix interface. This region, first introduced by Sharpe [109], is a three dimensional region of some finite thickness extending, depending on the system constituents, from within the fiber surface to some point in the matrix where local properties approach bulk properties. Its size and composition can vary with each system and can include unreacted polymer components, polymer reaction byproducts, weak surface layers of the fiber, amongst other things. Throughout this chapter the term "interface" will mean the actual contact surface between the fiber and matrix while the term "interphase" will be the region near and on both sides of the interface. Numerous other publications referenced throughout this dissertation, have shown the effect of this interphase itself on fiber-matrix adhesion and composite performance.

It is the objective of this chapter to determine the influence of processing temperature on the interfacial shear strength of various model, polymeric matrices (see "materials" section-Chapter 2) reinforced with AS4 carbon fibers. An AS4-C fiber (embedded in mPDA/DGEBA matrix) was selected to investigate the effect of a low temperature epoxy sizing on the interfacial shear strength behavior at elevated temperatures. The data from the AS4C system will be used to model the formation of an interphase region. Linear superposition methods will be used to generate a master curve (for the AS4 systems) from which the interfacial shear strength can be predicted as a function of the processing temperature of the composite material.

6.2 EXPERIMENTAL

Two carbon fibers (AS4 and AS4C), described in Chapter 2, were used for the studies in this chapter. The representative polymeric matrices used in this chapter are described in detail in Chapters 2 and 5. A brief summary of the interfacial, mechanical and thermal properties of the matrices used in this chapter are shown below in Table 6.1.

It can be seen from Table 6.1 that the thermoset matrices used in this chapter have a wide range of mechanical and interfacial properties. The mPDA system is seen to have a strain to failure of about 6% and a fully cured T_g of about 135°C while the compliant J700 system is seen to have a strain to failure of over 90% and a T_g just below room temperature. It can also be seen that lower adhesion results in systems with lower moduli (Chapter 5). Finally, it can be observed that the AS4C/mPDA/DGEBA system has a higher level of adhesion at ambient temperatures when compared to the same AS4 system.

Table 6.1: Interfacial, mechanical and thermal properties of the DGEBA system

DGEBA CURED WITH:	AMBIENT τ (MPa)	AMBIENT BULK SHEAR MODULUS (GPa)	T_g (°C)	FIBER
mPDA	70.5	1.17	135	AS4
J230	56.7	1.09	74	AS4
J700/J403	42.1	---	46	AS4
J403	46.9	0.85	75	AS4
J700	38.6	0.23	20	AS4
mPDA	80.0	1.17	135	AS4C

As mentioned previously in Chapter 5, an important factor in selecting these curing agents to increase the polyether amine length as opposed to the epoxy length is the

preservation of epoxy-amine chemistry throughout the series by the use of polyether diamines (Jeffamine based curing agents). If epoxy oligomers are selected, additional hydroxyl functional groups are present along the oligomer backbone. These hydroxyls, could in fact interact (e.g. hydrogen bonding) with each other as well as the fiber surface and unnecessarily complicate the analysis.

The single fiber fragmentation test was used to quantify the interface in all the tests. The specially designed heated cell (described in Chapter 2) was used to conduct the high temperature experiments. A dynamic mechanical analyzer (DMA-9900) was used to gather modulus data for the DGEBA/mPDA system as a function of temperature. The procedure is outlined in section 2.2.6.

6.3 RESULTS AND DISCUSSION

6.3.1 CHEMICAL BONDING

New surface analytical techniques allow the chemical nature of the carbon surface to be determined. X-ray photoelectron spectroscopy [100,110] provides not only atomic information but also molecular information about the surface characteristics and can be used to determine the extent of chemical bonding between matrix and reinforcing fiber.

As discussed briefly in Chapter 5, to determine the extent of chemical bonding, a series of experiments were performed with model monofunctional epoxy compounds, amines and epoxy-amine adducts whereby these components were dissolved in an inert aromatic solvent and placed in contact with carbon fibers under the same temperature conditions experienced in the processing of the composite [100]. Afterwards, the fibers were extracted with pure solvent, dried and then their surface composition determined with XPS. Subsequent comparison of the carbon fiber spectra before and after this exposure to the matrix components confirmed that chemical adsorption had taken place. Both the epoxy group and the amine group can chemically react with the surface oxygen

present. Surprisingly, on an absolute basis only about 5% of the surface sites of the carbon fiber were found to be involved in chemical bonding. One would expect chemical bonding to create a stronger interaction than physical bonding.

For the epoxy-amine-carbon fiber system studied here, it is expected that chemical bonding would be similar for all systems and because of the small number of chemical bonds formed, it is expected that the role of chemical bonding between fiber and matrix would be small and constant. At most, under the processing conditions of interest in this study (up to about 125°C), only 5% of the available carbon fiber surface sites can react with the epoxy matrix. Moreover, previous work has shown [55] that the bulk properties of the matrix and interphase properties themselves play a much more significant role on fiber-matrix adhesion than does the chemical bonding between fiber and matrix itself. Since temperature significantly alters the bulk mechanical properties of the matrix, one would expect it to play a more important role than chemical bonding in affecting fiber-matrix adhesion in these systems studied in this chapter.

6.3.2 INTERFACIAL SHEAR STRENGTH

At ambient temperatures the interfacial shear strength was measured for all the formulations and averaged according to Equation 2.2. The data is plotted in Figure 5.1 as interfacial shear strength vs. shear modulus of the bulk matrix. Since the T_g of a material is related to the crosslink density of a material, the difference in compliance in the matrices studied can be seen by examining the T_g's listed for the various formulation in Table 6.1. From Figure 5.1 it is seen that all of the matrix formulations fall on a single smooth curve showing an increasing interfacial shear strength with increasing shear modulus of the matrix (and of the interphase). Further discussion on the relationship is presented in Chapter 5.

For elevated temperature measurements, using the specially designed cell, measurements were made at 30°C increments up to the T_g for each of the different

DGEBA formulations listed in Table 6.1. At each temperature replicate samples (a minimum of 5 samples were tested at each fiber/matrix/temperature combination) were tested to insure statistical significance. Tables 6.2-6.6 below provide a summary of the critical length distribution and data for all of the various formulations tested.

Table 6.2: Critical length data for DGEBA/mPDA system at elevated temperatures

T (°C)	d_{avg} (microns)	l_c/d_{avg} (β_{wci})	α	τ (MPa)
AMBIENT	7.3±0.26	392/7.3	2.7032	68.4±5.0
44.9±1.6	7.2±0.34	384/7.2	2.8169	67.0±4.3
57.8±1.9	7.3±0.30	409/7.3	2.8986	62.8±5.8
65.2±1.9	7.4±0.19	422/7.4	2.9418	61.2±4.3
79.2±2.5	7.2±0.21	412/7.2	2.9420	61.0±4.3
99.8±2.9	7.1±0.32	438/7.1	2.9851	56.2±4.0
114.2±3.6	7.0±0.18	667/7.0	2.7030	38.3±7.8

Table 6.3: Critical length data for DGEBA/J230 system at elevated temperatures

T (°C)	d_{avg} (microns)	l_c/d_{avg} (β_{wci})	α	τ (MPa)
AMBIENT	7.2±0.26	393/7.2	3.9234	57.9±5.9
36.2±1.8	7.1±0.13	404/7.1	3.3714	56.9±6.0
45.3±1.9	7.4±0.20	454/7.4	3.3333	54.1±4.9

59.3±2.3	7.2±0.18	469/7.2	3.2787	51.3±5.8
71.3±3.0	7.0±0.22	583/7.0	2.8571	42.6±6.3

Table 6.4: Critical length data for DGEBA/J403 system at elevated temperatures

T (°C)	d_{avg} (microns)	l_c/d_{avg} (β_{avg})	α	τ (MPa)
AMBIENT	7.1±0.20	469/7.1	4.0006	47.6±5.3
35.8±2.1	7.4±0.23	502/7.4	4.1667	46.6±5.1
43.9±3.0	7.3±0.16	497/7.3	3.7037	45.8±4.9
54.5±3.1	7.3±0.18	557/7.3	4.0003	41.1±3.9
69.8±3.3	7.5±0.20	634/7.5	4.3478	36.2±5.8

Table 6.5: Critical length data for DGEBA/J403/J700 system at elevated temperatures

T (°C)	d_{avg} (microns)	l_c/d_{avg} (B_{avg})	α	τ (MPa)
AMBIENT	7.2±0.20	525/7.2	4.5454	41.6±4.2
29.8±2.6	7.3±0.19	531/7.3	4.7619	41.3±4.0
36.3±3.3	7.4±0.16	550/7.4	4.5386	40.8±4.1
41.2±3.6	7.1±0.20	589/7.1	4.6329	36.3±6.3
43.0±3.0	7.2±0.23	701/7.2	5.1237	30.9±6.9

Table 6.6: Critical length data for DGEBA/J700 system at elevated temperatures

T (°C)	d_{avg} (microns)	l_c/d_{avg} (β_{wei})	α	τ (MPa)
AMBIENT	7.0±0.22	525/7.0	5.2632	39.2±5.0
31.2±2.8	7.5±0.21	611/7.5	5.1924	36.3±6.3
38.3±3.3	7.4±0.13	702/7.4	5.3333	30.9±8.3

In all these data, the tensile strength of the carbon AS4 fiber is assumed to be approximately 5101 MPa [38] at the critical length. Each measurement corresponds to an average of between 8-16 samples. The α and B shown in the tables above corresponds to the shape and scale parameters in the Weibull statistical model [30,36]. These parameters define the distribution of critical lengths according to Equation 2 in Chapter 2.

The interfacial shear strength, for all the matrix formulations reinforced with AS4 fibers, as a function of test temperature is shown in Figure 6.1. It can be seen that in all cases the interfacial shear strength slowly decreases (as the modulus of the matrix also slowly decreases--Chapter 5) with increasing temperature until at some point a significant decrease in the interfacial shear strength is noted. This point is near the bulk T_g of the matrix. These results are similar to those obtained by Wimolkiatsak and Bell [36] where it was shown that for uncoated carbon fibers embedded in a thermoset matrix, the interfacial shear strength decreased with increasing temperature slowly initially (they suggest that the interfacial shear strength is interface controlled in this regime) with a steep decrease at higher temperatures (in this regime, they suggest that the interfacial shear strength is matrix controlled). In our experimental protocol, interfacial shear

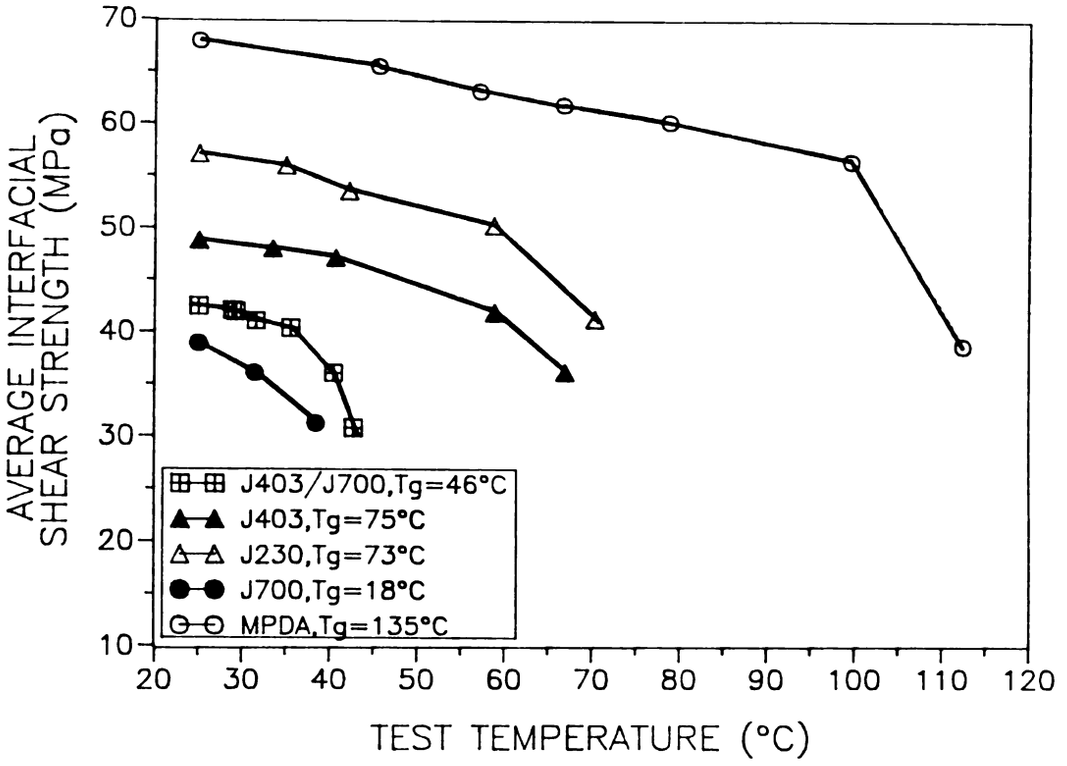

Figure 6.1: Interfacial shear strength as a function of test temperature for DGEBA resin cured with different amine curing agents

strength measurements were difficult to make at or above T_g of the bulk matrix due to the matrix being too ductile causing an excessive amount of necking and tearing upon tensile load application. Since the Jeffamine based systems have lower bulk glass transition, less interfacial shear strength data could be obtained at elevated temperatures for these more ductile systems. Previous work by Rao and Drzal [55] has shown that decreasing the modulus of the matrix (and interphase) leads to lower values of interfacial shear strength for systems with constant interfacial chemistry. As the temperature of the matrix is increased from room temperature towards T_g of the matrix, the modulus of the matrix decreases thereby reducing the ability of the matrix adjacent to the fiber surface to transfer stress.

The glass transition temperatures for all of the different thermoset formulations used in this Chapter are listed in Table 6.1. In all cases it can be seen from Figure 6.1 that the interfacial shear strength is seen to decrease as the T_g of each system is approached. It would be expected that at T_g, since the modulus of the matrix drops by orders of magnitude [12], the interfacial shear strength would also rapidly decrease at that point. However, in all cases, and especially in the case of the brittle mPDA/DGEBA system, the interfacial shear strength is seen to decrease well before T_g of the bulk matrix is reached. The mPDA/DGEBA system is seen to have a bulk T_g of about 135-140°C, but the interfacial shear strength is seen to decrease steeply well before this at a temperature of about 100-110°C. These results support the concept of the formation of an interphase whose glass transition temperature, and thus its mechanical properties [111,112], are different than that of the bulk matrix. Other experimenters [113] have also reported the formation of an interphase having mechanical and viscoelastic properties different from the bulk matrix material.

6.3.3 LINEAR SUPERPOSITION

Since all the matrices used in this study and this chapter are cured with diamine type curing agents and the fiber-matrix chemical interactions would be constant, it should be possible to combine all of the data from Figure 6.1 into one "master" curve. The interfacial shear strength data was analyzed using linear superposition in the same manner that the WLF equation [12] of state is used to describe polymer matrix temperature dependence. The J230 system was chosen randomly as the reference system and all of the other data in Figure 6.1 were either shifted to the left or to the right to coincide with the chosen reference matrix. The shift factor was "best-fit" and manually optimized with temperature and the resulting plot is shown in Figure 6.2. These shift factors were then used to linearly superpose the data. The resulting plot in shown in Figure 6.3. The ordinate in Figure 6.3 is the "corrected" interfacial shear strength; the data has all been multiplied by the numerical factor T/T_o. In this notation T is the measured temperature and T_o is the reference temperature chosen (T_g of the J230 system), 346°K. This T/T_o factor is the standard factor used [12] for correcting data with the WLF equation of state for superpositioning data. It can be seen that the shifted data is seen to cover a wide range of temperatures and interfacial shear strengths. As expected, at lower temperatures (and higher moduli) the interfacial shear strength is seen to be higher. Figure 6.3 then allows for the prediction of interfacial shear strength by knowing just the modulus (or processing temperature at a given time) and the glass transition temperature.

6.3.4 RESIDUAL STRESSES

In addition to chemical and structural considerations, the state of stresses which result from the processing of the material itself can influence the degree of fiber-matrix adhesion. In the case of carbon fibers, the coefficient of thermal expansion is quite small and can actually be negative [114]. The fiber itself is anisotropic and the radial and longitudinal thermal expansions can be quite different. The matrix is isotropic but has

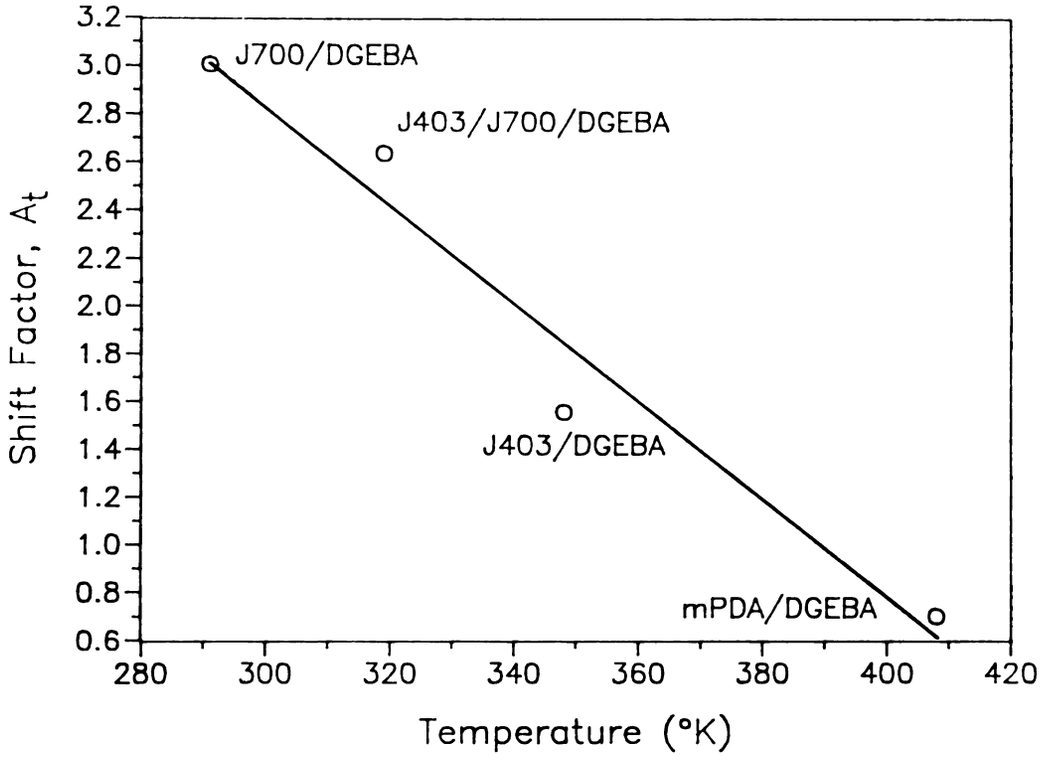

Figure 6.2: Shift factor as a function of temperature

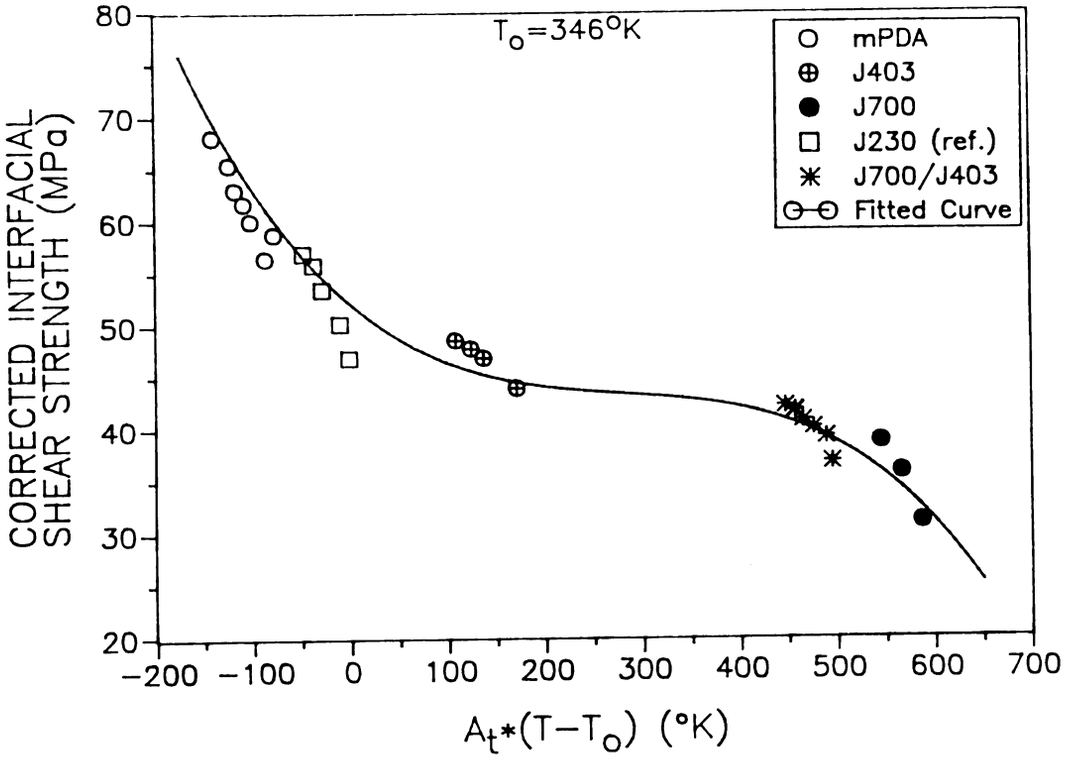

Figure 6.3: Master curve for prediction of interfacial shear strength as a function of shift factor and temperature

a coefficient of thermal expansion a factor of thirty larger than the fiber. As described previously in Chapter 5, this disparity becomes increasingly significant as higher processing temperatures are reached with the absolute difference between the glass transition temperature and the use temperature determining the magnitude of these residual thermal stresses [55].

Epoxy matrices also reduce their volume as they begin to crosslink. This volumetric shrinkage also contributes to the state of stress at the fiber-matrix interphase. For fibers surrounded by matrix, the resulting cure shrinkage produces a beneficial compressive interfacial force while for matrix confined between a row of fibers, a net tensile interfacial state of stress may result. The resulting state of stress can reduce the level of adhesion attainable between fiber and matrix. Calculations of interfacial stresses have been made previously for these thermoset systems and are discussed in depth in Chapter 5. The calculations show that although the radial component of the stress changes in the same manner as the measured interfacial shear stress, the magnitude of the radial compressive stress is small and is considered to be a minor factor. Thus, it is concluded that it is the changes in the matrix material properties themselves, that are primarily responsible for the changes in the interfacial shear strengths in this chapter.

6.3.5 FORMATION OF AN INTERPHASE (AS4C-mPDA-DGEBA SYSTEM)

The AS4-C/epoxy system was chosen as an example where an interphase of known composition different than the bulk is present. It has been proposed and indirectly verified [115] that this interphase consists of a low T_g epoxy material. Kalantar and Drzal [116] have given an excellent review of the possible interphase interactions that may control the level of fiber-matrix adhesion.

The plot of interfacial shear strength versus temperature for this particular system is shown in Figure 6.4. For comparison purposes, both the AS4/mPDA/DGEBA as well as the AS4C/mPDA/DGEBA data is shown. At ambient temperatures, it can be seen that

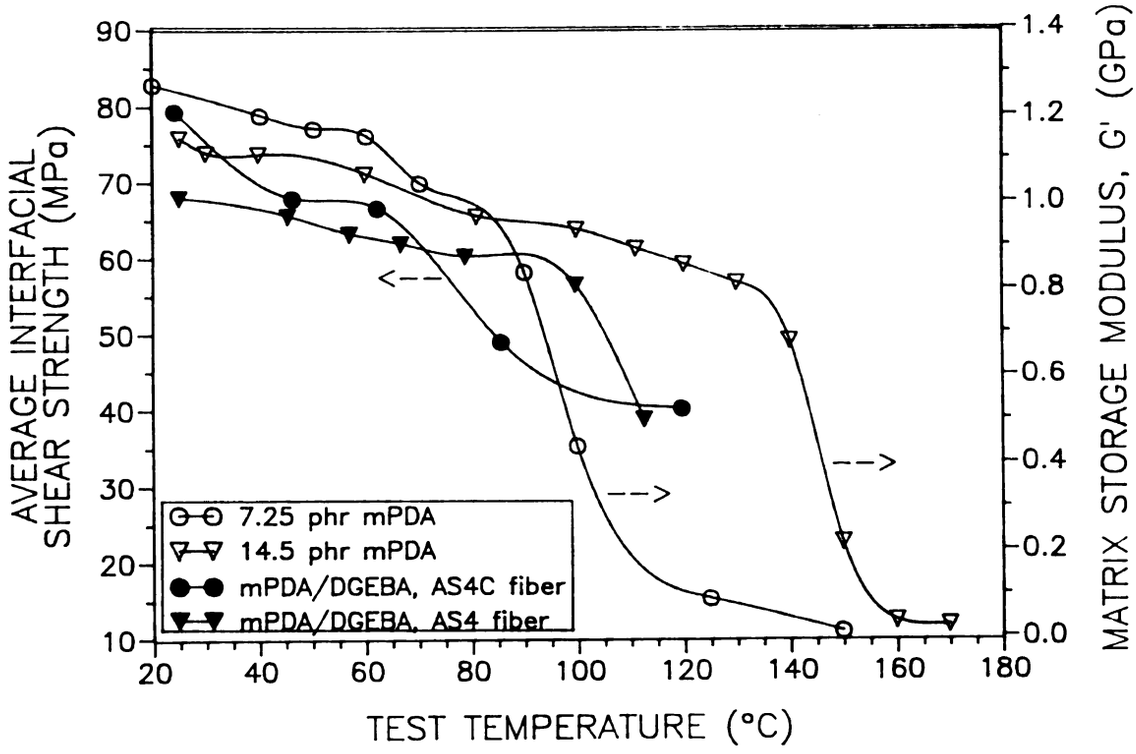

Figure 6.4: Loss modulus of mPDA/DGEBA matrix and interfacial shear strength of mPDA/DGEBA matrix reinforced with carbon, AS4, and AS4-C fibers as a function of temperature

the AS4C system has a 15% higher interfacial shear strength due to the interphase resulting from the coating placed on the fiber during processing. Its modulus is higher than the stoichiometric bulk epoxy modulus. As the test temperature is increased, however, the AS4C system is seen to exhibit a measurable decrease in interfacial shear strength (indicating a lower level of adhesion). As the temperature is increased, there is a distinct decrease starting at about 70°C well before the expected decrease in interfacial shear strength when the T_g of the bulk matrix is approached. The drop in measured interfacial shear strength at about 40°C may be attributed to the interphase epoxy softening thereby leading to a lower modulus in the interphase region causing a corresponding lowering of the interfacial shear strength.

The interphase that results from the diffusion controlled interaction of the pure epoxy coating with the bulk stoichiometric matrix will produce a region around the fiber having less than the stoichiometric amount of amine curing agent. A model this phenomenon is presented in the next section in this chapter. Separate measurements of the T_g and the modulus of this material [79,117] which is subject to the same curing schedule as the bulk matrix indicates that the glass transition temperature can decrease from the bulk value to about 70-75°C at 50% of the stoichiometric amine level. Netravali et al. [56] have also shown that interphase interactions play a major role in determining the interfacial shear strength of coated carbon fibers. They speculate, as Drzal et al. [118] did earlier, that the interphase region is more brittle due to migration and diffusion of the curing agent thereby leading to a more brittle interphase with thermal and mechanical properties different than that of the bulk matrix.

Figure 6.4 also shows the relationship between bulk matrix storage modulus and temperature for DGEBA resin cured with a stoichiometric amount (14.5 phr) of mPDA (open inverted triangles in Figure 6.4) as well as DGEBA resin cured with a 50% of stoichiometric amount (7.3 phr; open circles in Figure 6.4) of mPDA. It can be seen

that for the stoichiometrically cured system, the T_g of the matrix falls in the range of 130-145°C while for the 50% stoichiometrically cured system the T_g is in the range 70-90°C.

Since pure DGEBA monomer melts at about 40°C [5], the first drop for the AS4C data in Figure 6.4 at about 40°C may be due to melting of the unreacted excess DGEBA in this region. Following this decrease the interfacial shear strength remains higher than the AS4 system until about 70°C. At this point, a precipitous drop is interfacial shear strength is measured. The temperature at which this occurs corresponds approximately to the T_g of a 50% of stoichiometric amine/epoxy mixture. This indicates that the curing agent has diffused and migrated to the interphase through the initially pure epoxy resin interphase region. Additionally, the decrease in interfacial shear strength at 70°C for the AS4C system indicates that the interface composition is approximately 50% of the stoichiometric (bulk matrix) amount. These results show that the composition of the interphase region is different than that of the bulk matrix and plays a major role in determining the final level of fiber-matrix adhesion.

6.4 MODELING OF THE FORMATION OF THE INTERPHASE

The role of the interface/interphase region in determining the mechanical and adhesive properties of fiber reinforced composite materials has gained increasing attention in recent years [119,120,121,122,123,124,125,126]. The use of simple "rule of mixtures" models in which the properties of matrix and fiber are weighed to predict various composite properties often fails to predict accurate values [127]. Interaction between fiber and matrix extending away from the interface region has a strong effect on composite properties such as interlaminar shear strength [25,94].

Kalantar and Drzal [116] have provided an excellent review of various interfacial factors, both at the microscopic as well as macroscopic level, which could effect the level

of fiber/matrix adhesion. Delong et al. [115] have attempted to quantify the interphase region spectroscopically. Cazeneuve et al. [128] have used Auger microscopy to study the structure of the interface in carbon fiber composites. Others have measured interfacial properties and concluded that the interphase and its properties play a major role in determining the level of adhesion at the interface. For example, Zukas et al. [129] have shown, with metal-matrix composites, that kinetic interactions at the interphase are different than that in the bulk and that these kinetics lead to different levels of exotherm and adhesion at the interface. Robertson [130] has also speculated on the formation of a weak boundary layer leading to low levels of adhesion at the interphase. Recently, Netravali et al. [56,131] have shown that diffusion of the curing agent into the epoxy rich interphase creates a brittle interface giving rise to higher levels of adhesion. Drzal et al. [118] had also noticed this same phenomena earlier with carbon/epoxy microcomposites. It is this phenomena of diffusion that will be modeled here in this section.

Virtually no models exist in describing diffusion of curing agent into an epoxy rich interphase region resulting in alteration of the mechanical properties of the interphase region. Theocaris et al. [132] have presented models relating properties of the bulk matrix to properties in the interphase region using the theory of elasticity and plasticity. Recently [133] he considered the concept of diffusion of material into the interphase causing a change in the mechanical properties of the interface region. While he does not rigorously solve this particular diffusion problem, he suggests a possible solution using some idealized conditions. This analysis has been extended below to arrive at a predictive model for relating the measured interfacial shear strength to the composition of curing agent at the interface between fiber and matrix.

The effect of the interphase region on interfacial properties of a composite can be visualized by considering an epoxy coated fiber embedded in a bulk epoxy/amine matrix,

as shown in Figure 6.5. Here the system initially consists of a stoichiometric mixture of epoxy and amine in the bulk and epoxy only on the fiber coating. During cure, the amine curing agent diffuses into the coating, creating an interphase having a gradient of low amine concentration near the fiber to the stoichiometric concentration in the bulk. Because the material properties of amine cured epoxies are greatly dependent on the amine-epoxy ratio [117,134,135], the interphase will possess unique properties different from the bulk cured epoxy. Quantification of interphase diffusion will enable realistic modelling of the interphase and its effect on material properties, which in turn will facilitate accurate prediction of these properties.

It can be seen from Figure 6.5 that three different physical phenomena are occurring simultaneously in describing the diffusion process into the interphase region and all three must be included in a rigorous mathematical model. Bulk, convective diffusion of the curing agent into the pure epoxy sizing, chemical reaction between epoxy and curing agent, and accumulation of curing agent are all occurring simultaneously in the interphase region. Thus, we have the classical problem of diffusion in a slab (one-dimensional) with reaction

$$\frac{\delta C}{\delta t}=\frac{\delta}{\delta x}(D(C)\frac{\delta C}{\delta x})+R(C) \qquad (6.1)$$

here the concentration, C, represents the concentration of curing agent in the interphase region. As a first step in the analysis, it will be assumed that the diffusivity is constant (represented by an "effective" diffusion coefficient) and the reaction rate linear (i.e. R=kC). With these assumptions we arrive at:

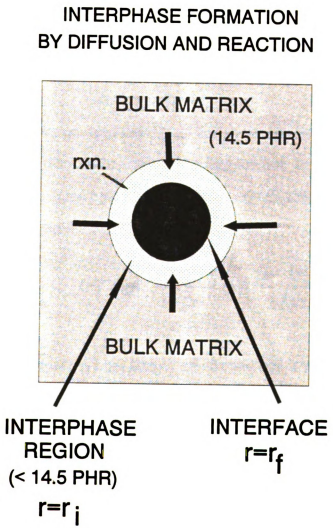

Figure 6.5: Schematic of interphase formation by diffusion of curing agent

$$\frac{\delta C}{\delta t} = D\frac{\delta^2 C}{\delta x^2} - kC \tag{6.2}$$

with the following boundary and initial conditions:

Initial Condition: $C=0$ @ $t=0$, $0<r<r_i$

Boundary Conditions: $C=C_{bulk}$ @ $t\geq 0$, $r=r_i$

$dc/dx=0$ @ $t\geq 0$, $r=r_f$

Because this problem does not lend itself to an analytical solution, usually separation of variables is used to lead to an approximate series solution for the problem (usually solved without reaction). It has been shown by Finlayson [15,136] that the solution to the above problem is given by the following series solution.

$$\frac{C}{C_{bulk}} = \sum (-1^n)\left[erfc\frac{(2n+1)r_i - r}{2\sqrt{(Dt)}} + erfc\frac{(2n+1)r_i + r}{2\sqrt{(Dt)}}\right] \tag{6.3}$$

In Equation (6.3), n is summed from zero to infinity and erfc is the complimentary error function. This solution, though rigorous, has limited capability since the time needed to achieve a concentration of 10% of the bulk at the interface is calculated to be on the order of microseconds. This does not allow for proper analysis for comparison to the interfacial data collected earlier in the chapter. This estimate of time needed to achieve a given concentration at the interface results from the fact that an accurate value for the diffusion coefficient was not available or determined experimentally. The diffusion coefficient could change over orders of magnitude as the reaction proceeds in the interphase and must be accounted for in the model above. The calculated times are very sensitive to the value of diffusion coefficient used in the analysis. While Theocaris [133] has speculated on the numerical value of diffusion coefficients for a reacting system

(they suggest values anywhere from $10^{-12}cm^2/sec$ to $10^{-15}cm^2/sec$), they do not make an effort to estimate the diffusion coefficient as a function of reaction extent. Using a simplified form of Equation (6.2), a model is presented below that allows for both the estimation of interphase thickness as well as well as the variation of diffusion coefficient within the interphase thickness and perhaps most importantly an estimate of an "effective" diffusion coefficient in the interphase region.

As mentioned above, very little experimental work has been done on investigating how the diffusion coefficient changes with extent of cure for a crosslinking reaction. It would be expected that if the curing agent diffuses from the bulk towards the interface in a "reaction-front" type mechanism, the local diffusion coefficient will initially be low (characteristic of liquid-liquid diffusion) and then quickly diminish as reaction occurs and liquid-solid diffusion begins to occur. Liquid-liquid diffusion is characterized by diffusion coefficients in the order of 10^{-7} to 10^{-9} cm^2/sec while liquid-solid diffusion can lead to diffusion coefficients of 10^{-19} cm^2/sec or lower [13,136]. It is difficult to average over such large orders of magnitude; Theocaris [133] has suggested effective values for the diffusion coefficient which fall in the middle of this range (about $10^{-14}cm^2/sec$) without experimentation. In the analysis below, the thermal response and interfacial shear strength data of coated AS4 fiber data will be used, via a simple model. to arrive at a relationship between "effective" diffusion coefficient in the interphase and the thickness of the interphase. It will be shown that the effective diffusion coefficient must be about $10^{-14}cm^2/sec$ to arrive at the approximate interphase thickness specified by the manufacturer.

Because Equation 6.3 above gives a minimal understanding of the physical situation that is occurring (due to limitations in determining the diffusion coefficient as well as lack of an analytical solution for the model in Equation 6.2), a suggestion made by

Theocaris [133] is used to arrive at an analytical solution for the diffusion of curing agent into the interphase region for epoxy coated fibers.

The following assumptions are made:

1. One-dimensional diffusion
2. Slab geometry can be approximated (interphase region small)
3. First-order reaction
4. Adsorption of curing agent onto fiber surface (no accumulation of curing agent in the interphase region.
5. Diffusion coefficient constant (effective diffusion coefficient)

These assumptions lead to Equation 6.1 being simplified to:

$$D\frac{\delta^2 C}{\delta^2 r} - kC = 0 \qquad (6.4)$$

here, C is the concentration of curing agent in the interphase, D is the diffusion coefficient of the curing agent into the liquid epoxy, r is the radial direction outward from the fiber surface and k is the pseudo-first order reaction rate constant for the mPDA/DGEBA matrix. The following boundary conditions are valid in this case

$$\text{at } r=r_f \quad dC/dr=0$$

$$\text{at } r=r_i \quad C=C_{bulk}$$

the first boundary condition is the "no-slip" (i.e. no net flux) condition at the fiber surface and the second boundary condition simply states that bulk concentration (14.5 phr) of curing agent exists at the interphase boundary with matrix. After some involved mathematical manipulations (see Appendix C for appropriate derivation), it can be shown that a closed form analytical solution of the following form is obtained:

$$\frac{C}{C_{bulk}} = \frac{e^{-\phi(1-\psi)} + e^{\phi(1-\psi)}}{e^{\phi} + e^{-\phi}} \tag{6.5}$$

here C is the concentration of curing agent in the interphase region, and the greek symbols are the following dimensionless quantities:

$$\phi = a\Delta r = a(r_i - r_f) = (k/D)^{1/2}\,(r_i - r_f)$$

$$\psi = r_i - r / r_i - r_f = r_i - r / \Delta r$$

Figure 6.6 shows the relationship between the concentration of curing agent in the interphase (normalized to the bulk concentration) and the radial distance in from the interphase to the fiber surface according to Equation 6.5 above. In Figure 6.6 the value of phi, ϕ (ratio of the squareroot of reaction rate constant to diffusion coefficient) is randomly varied from 0.5 to 2.5. It can be seen that the gradient is essentially flat (unchanging) for low values of ϕ and changes to an exponential type behavior for higher values of ϕ. It was seen in section 6.3.5 above that the concentration of curing agent at the interface for AS4C (coated) fibers was estimated to be approximately 50% of stoichiometric value (based on the point at which the interfacial shear strength began to decrease). From Figure 6.5 it can be seen that a ϕ value of 1.45 can be extrapolated back to a value of approximately 50% of stoichiometric value of curing agent concentration at the interface (at $r = r_f$).

Slight rearrangement of the definition of ϕ above gives:

$$D_e = \frac{k}{\left(\frac{\phi}{\Delta r}\right)^2} \tag{6.6}$$

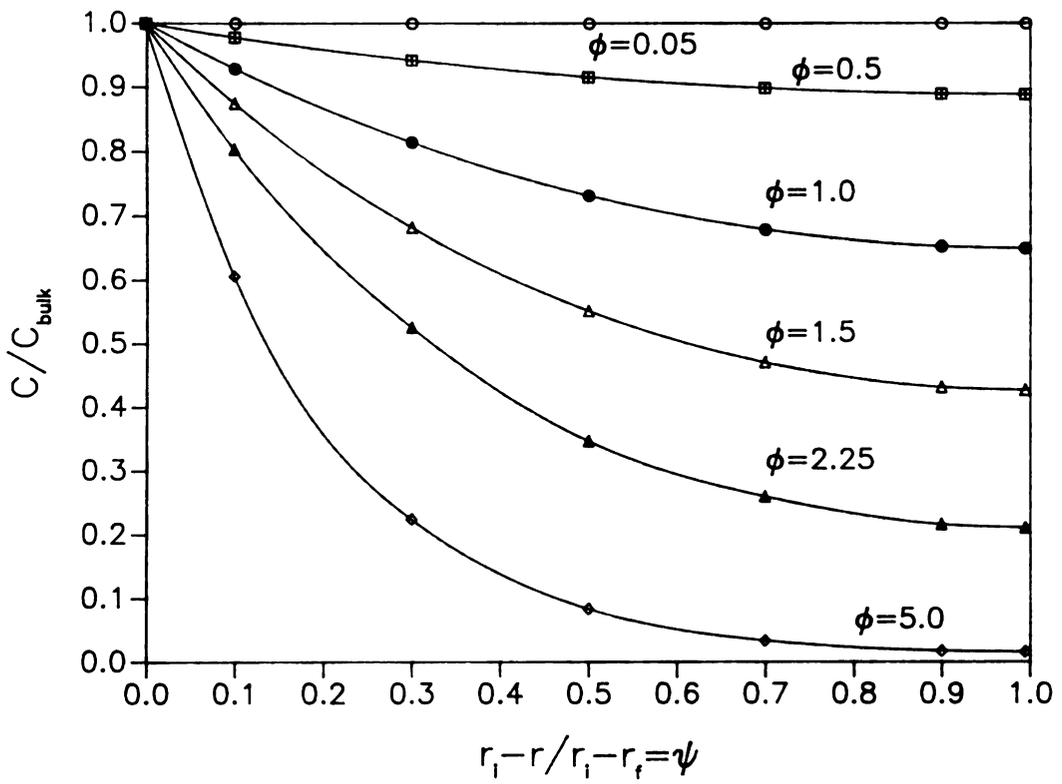

Figure 6.6: Model prediction curing agent concentration profile within interphase region as a function of diffusion coefficient, reaction rate constant and temperature

Since the pseudo-first order constant for the crosslinking reaction can be calculated to be approximately 1.58×10^{-4} sec^{-1} from the data in Chapter 3, Equation 6.6 can be used to derive a relationship between the effective diffusion coefficient in the interphase region and the thickness of the interphase. Figure 6.7 shows this relationship. It can be seen from Figure 6.7 that for the interphase thickness to be 100-300 nm (the approximate value of the initial epoxy layer reported by the manufacturer, Hercules Corporation, placed on the fiber is about 100 nm) the effective diffusion coefficient in the interphase region calculates to be between $10^{-13} cm^2/sec$ and $10^{-14} cm^2/sec$ (as suggested without proof by Theocaris [133]). Thus, for the AS4C data taken here, if D_e is taken to be an average value of 5.5×10^{-14} cm^2/sec, Δr calculates to be about 250 nm. Also, it is noted from Figure 6.6 that as the interphase thickness becomes small (on the order of angstroms) that the effective diffusion coefficient is about $10^{-19} cm^2/sec$ which is characteristic of liquid-solid diffusion. On the other hand, as the interphase thickness approaches a large value (on the order of microns) the effective diffusion coefficient increases to about $10^{-9} cm^2/sec$ which is more characteristic of liquid-liquid diffusion.

This analysis thus gives a valuable starting point for the value of effective diffusion coefficient for mPDA/DGEBA matrix. If the cure temperature or matrix is changed, only the new reaction rate constant is needed (in Equation 6.6) to arrive at a new effective diffusion coefficient. Furthermore, by measuring the interfacial shear strengths at elevated temperatures and by using the "effective" diffusion coefficient calculated above, an interphase thickness can be computed for any type of epoxy sizing placed on a fiber.

Thus, this rather simplified model seems to predict the thickness of the interphase rather accurately based on the diffusion characteristics of the curing agent and measurement of the interfacial shear strength. This model has the advantage of providing a closed, analytical solution for the concentration of curing agent in the interphase

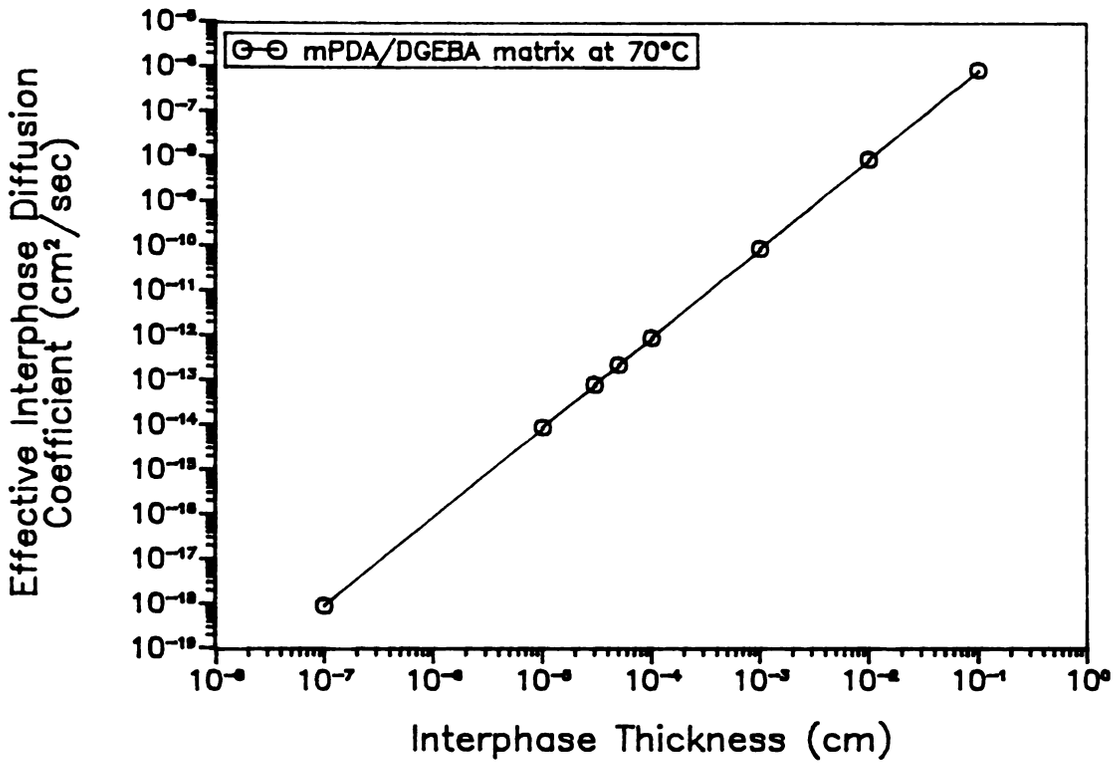

Figure 6.7: Effective diffusion coefficient as a function of interphase thickness

region. The predictive capability of the model (which is based on "average" values of diffusion coefficient and reaction rate constant in the interphase region) can be further improved by experimentally determining the diffusion coefficient as a function of extent of cure (i.e. determination of the concentration profile of curing agent in the interphase region). This would provide a relationship between diffusion coefficient and time which could be used in Equation 6.1 above to arrive at a more complete solution. In addition, a more complete non-stoichiometric kinetic study could be conducted to more accurately describe the epoxy/amine reaction occurring in the interphase region.

The solution presented above is strictly applicable only to sized (or coated) fibers in which there is a region of pure epoxy initially where the curing agent is free to diffuse into. From section 6.3.5 it was seen that the AS4 fiber/epoxy interface behaved as though the stoichiometry was about 70-75% of bulk. If this model applied here, it results in an interphase thickness of about 140 nm using an effective diffusion coefficient of $5.5 \times 10^{-14} cm^2/sec$. While the trend of the interphase thickness being smaller for a unsized fiber is expected, the model is apparently not able to differentiate between the two systems to any great deal. This is due to the fact that one of the boundary conditions may no longer be valid for AS4 fibers. Since there is no pure epoxy sizing (initially), there is no boundary (no interphase) where the concentration of curing agent can be set to the standard stoichiometric value. It is therefore difficult to gage the accuracy of this model for the unsized AS4 system.

With AS4 fibers, the curing agent diffuses to the interface (during the time that it takes for the matrix to gel at 70°C) and adsorbs onto the fiber surface by either chemisorption, physisorption or both. This process leaves behind a concentration of curing agent at the interface which is less than stoichiometric. This is clearly a more complicated situation to model than the sized system described above because the boundary conditions are difficult to enforce with any degree of accuracy. The

stoichiometry at the interface has been inferred from the interfacial shear strength measurements earlier in this chapter to be about 75-80% of stoichiometric for this AS4/mPDA/DGEBA system. In this procedure below, different methods will be attempted to try and estimate interphase thickness from the inferred interfacial stoichiometry. It will be seen that because the boundary conditions are difficult to define, a more accurate model of how the diffusion coefficient changes with time and concentration of curing agent is required for accurate results.

Initially if we consider a steady-state situation with no reaction (the diffusion is much slower than chemisorption and thus rate limiting) and a constant diffusion coefficient, Equation (6.1) can be reduced to:

$$\frac{d^2C}{dr^2}=0 \qquad (6.7)$$

here, C is the concentration of curing agent in the interphase region and r is the radial distance outward from the fiber surface, with boundary conditions:

$$\text{at } r=r_f,\ C=xC_{bulk}$$

$$\text{at } r=r_i,\ C=C_{bulk}$$

the first boundary condition contains a factor, x, which corresponds to the amount of curing agent adsorbed onto the fiber surface by chemisorption, physisorption or both. The second boundary condition is an inferred one because it is assumed that bulk properties are reached at the interphase boundary. The solution to Equation (6.7) with these boundary conditions is straightforward. The final solution reduces to:

$$\frac{C}{C_{bulk}}=1-\psi(1-x) \qquad (6.8)$$

where ψ is the dimensionless radial distance defined earlier. Equation (6.8) suggests that for the stoichiometry to be 80% (as suggested by the elevated high temperature data) that

the amount of curing agent adsorbed onto the fiber surface, x, must also be about 80% since the solution is linear. Since earlier ESCA studies (Chapter 5) revealed that chemisorption contributes only 5% of the total interactions at the interface, there must also be physisorption occurring whereby a monolayer or more of curing agent adsorbs onto the fiber according to this model. The interphase thickness can only be estimated if an assumption is made that the amount adsorbed onto the fiber (x) is slightly different than the actual fraction (C/C_{bulk}) of curing agent at the interface. If this difference is assumed to be very small (1%), then Equation (6.8) can be solved for a interphase thickness.

Obviously, the above solution is oversimplified because the diffusion coefficient drops out of the analysis. If Equation (6.1) is recast in a form with the diffusion coefficient being a function of concentration of the curing agent, we arrive at the following steady-state equation to describe the diffusion process:

$$0=\frac{\delta}{\delta r}(D(C)\frac{\delta C}{\delta r}) \tag{6.9}$$

with the same boundary conditions as with Equation 6.7. If it is assumed that $D(C) \sim e^{-C/Cbulk}$, Equation (6.9) can be solved by separation of variables to arrive at a solution. However, again because of the nature of the boundary conditions, the solution suggests that about 80% of the curing agent must be adsorbed onto the fiber surface to arrive at the measured thermal response of the polymer in the interfacial region. Equation (6.9) presents the best method to attack this rather complicated problem. The problem is difficult because the boundary conditions are not clear cut. Obviously, the diffusion coefficient cannot be modeled as a function of concentration alone; a time factor must also be included and a different functionality (other than exponential) must be used to relate the diffusion coefficient to the reacting properties of the matrix.

While sorption, drying and uptake data for various liquids into cured epoxy networks are available in the literature [137,138], the author was not able to find any existing literature describing the change in the diffusion coefficient with extent of cure, concentration of curing agent or time of reaction. Once this relationship is experimentally elucidated, Equation (6.9) can be used to arrive at a interphase thickness by a numerical trial and error procedure of systematically varying the interphase thickness until it matches the observed changes in the interfacial stoichiometry.

Another way this process can be visualized is by considering transient behavior. Essentially we have the following situation (see Appendix B):

$$\frac{\delta C}{\delta t} = D\frac{\delta^2 C}{\delta r^2} \tag{6.10}$$

with the following boundary conditions:

$$\text{at } t=0, \text{ all } r,\ C=C_\infty=C_{bulk}$$

$$\text{at } t>0,\ r=r_f,\ C=C_i$$

$$\text{at } t>0,\ r=r_i,\ C=C_{bulk}$$

then the following small time solution [13] can be obtained:

$$\frac{C}{C_{bulk}} = erf\left(\frac{r}{4Dt}\right)^{1/2} \tag{6.11}$$

here t is time, D is the effective diffusion coefficient (10^{-14}cm^2/sec), and r is radial distance outward from the fiber surface. To achieve $C/C_{bulk} \sim 0.8$, r can be estimated to be very small (10^{-4} nm) at the time of gelation (at 70°C). However, this is a very approximate solution and strictly holds only for very small times. It can therefore be seen that it is difficult to model the formation of an interphase region for an unsized AS4 fiber system because the system boundaries are difficult to define. To arrive at a

accurate solution also requires a correlation between the diffusion coefficient and reacting parameters of the matrix which are not yet available.

6.5 CONCLUSIONS

The dependence of the fiber-matrix interfacial shear strength on temperature for epoxy matrices reinforced with AS4 and AS4-C carbon fibers was studied in this chapter. The results indicate that the interfacial shear strength decreases with increasing temperature because of the decreasing interphase modulus. At a temperature slightly below the bulk T_g of the matrix, a significant decrease in the interfacial shear strength was detected. This drop, seen in all the systems, is most likely related to the structure of the polymer (and hence T_g of the polymer) in the interphase region, whose composition can be different than that of the bulk matrix and whose mechanical properties control the level of fiber-matrix adhesion. Linear superposition was used to reduce all of the thermoset data into one master curve making possible the prediction of interfacial shear strength under any thermal conditions such as during temperature excursions encountered by the composite material. Additionally, the AS4-C system has been shown to exhibit a distinct decrease in interfacial shear strength at low temperatures (i.e. low T_g) indicating the formation of a low modulus interphase layer. A model derived from first principles has been proposed to explain the results. By making some simplifying assumptions on the diffusive and reactive characteristics of the bulk matrix, and by assuming steady-state behavior, an estimate is made on interphase properties and thickness. This model has the advantage of providing a closed, analytical solution relating concentration of curing agent at the interface to the reactive characteristics of the matrix and to the diffusive characteristics of curing agent in epoxy.

CHAPTER 7

INTERFACIAL TRANSVERSE STRENGTH MEASUREMENTS

In this chapter, a method will be outlined for the measurement of interfacial transverse strength of single fiber microcomposites.

7.1 INTRODUCTION

In addition to the shear stresses, normal stresses are also important contributors to the generation of defects during processing at the fiber-matrix interface. It is necessary to know the value of these normal stresses and to be able to measure their magnitude with changes in interphase and bulk composition. While various authors [102,139] have presented 3-dimensional models and empirical relationships relating matrix properties to compressive radial stresses, little or no experimental work has been done in an attempt to elucidate the relationship between fiber-matrix interfacial transverse strength and properties of the matrix. It will be shown in this chapter that new a single fiber transverse strength technique can be used to qualitatively determine this quantity.

7.2 EXPERIMENTAL

As described in Chapter 2 (section 2.2.4), the experimental technique for the determination of interfacial shear strength outlined previously in Chapter 2 has been modified. Basically, these "transverse" tests were performed by mounting the fiber of interest transverse to the coupon axis. in the standard dogbone shaped mold described earlier. The matrix was then poured in and cured. After appropriate curing, the edges of the samples were polished to create a very smooth surface (using 100 grit sandpaper). The specimens were then tested, using an optical microscope, under reflected light. By focusing the light directly down onto the fiber, and by subjecting the matrix to increasing

strain (in this particular set-up a pneumatic controller was used so that the amount of load applied can be directly measured), changes in the light pattern can be noticed when the first sign of debonding from the matrix under transverse loading occurs. By assuming the fiber to be a rigid, cylindrical inclusion, and by knowing the applied load, the actual load (at debonding) can be calculated using a stress concentration factor [45,140]. Because the moduli of the fibers are large [1] in comparison to the modulus of the matrix, the stress concentration factor has a constant value of approximately 1.8. Four different types of fiber were tested in the standard mPDA/DGEBA matrix. AS4, AU4, Kevlar and silicone-coated fibers were used to vary the level of fiber matrix adhesion and to subsequently investigate the transverse strength at the interface. A minimum of 35 samples were analyzed with each fiber/matrix combination to ensure statistically significant transverse strengths.

7.3 RESULTS AND DISCUSSION

Table 7.1 contains the actual transverse loads at debonding for all of the systems studied. All transverse loads (at debonding) were calculated by multiplying the measured load at debonding by an appropriate stress concentration factor as suggested by Chua et al. [45]. For all the systems studied here, the stress concentration factor is about 1.8. Carbon AS4 fibers were tested initially in a matrix of DGEBA resin cured with a stoichiometric amount of mPDA curing agent. Because of the relatively high interfacial shear strength (Chapter 5) of AS4 fibers in this matrix, transverse debonding was difficult to detect in all of the specimens tested (about 40 in all) until very high strains were reached in the matrix. Frequently, no debonding was detected up to the point of matrix failure. Since the specimens did not exhibit debonding up to the point of matrix failure, a load at debonding of 20,300 psi was computed using the failure stress of the

matrix as an estimate for the lower limit for the load needed to transversely debond these specimens.

In a further attempt to elucidate the transverse properties of AS4 fibers, the AS4 fibers were coated with a silicone-based release agent (by manually dipping the fibers in the chosen release agent; Silicone Z6020 release agent--Dow Corning) in an effort to decrease the interfacial and therefore the transverse bond strength. Interfacial shear strength (using the fragmentation test described in Chapter 5) measurements on the AS4-silicone coated samples (with mPDA/DGEBA matrix) have shown a reduction in shear strength of 65-70%. Figure 7.1 shows "before" and "after" photomicrographs illustrating the debonding of these fibers. The transverse strengths of these fibers (about 35 tested in all) are shown in Table 7.1. The actual load at debonding is seen to be about 7300 psi, a decrease of at least 60% when compared to the load at debonding for "as-received" AS4 fibers. This shows that the coating agent applied to the AS4 fibers has drastically decreased the transverse properties. An equally effective method for elucidating the transverse interfacial properties of AS4 fibers would be to embed the fibers in a more ductile matrix.

Kevlar 49 (polyaramid) fibers were also analyzed using the same matrix and test. These fibers were seen to debond at very low loads. The results from Table 7.1 (for a total of about 45 samples) indicate that the load at debonding for K-49 fibers is about 5300 psi. This indicates a very weak interface when compared to AS4/epoxy interfaces. Kalantar and Drzal [39] have shown that the interfacial shear strength of Kevlar fibers is about a third of AS4 fibers. The results indicate that the K-49 fibers debond at about the same level as the weak-interfaced silicone based AS4 fibers. Figure 7.2 shows ("before" and "after") photomicrographs indicating the debonding that occurs for the Kevlar-49 fibers under transverse load. The failure mode is again seen to occur at the interface between fiber and matrix as with the coated-AS4 fibers in Figure 7.1.

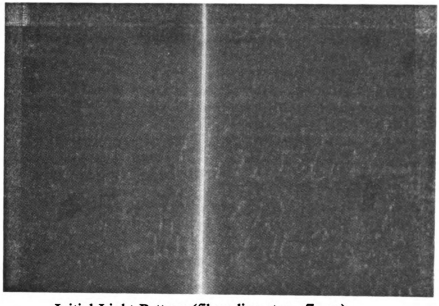

Initial Light Pattern (fiber diameter ~ 7 μm)

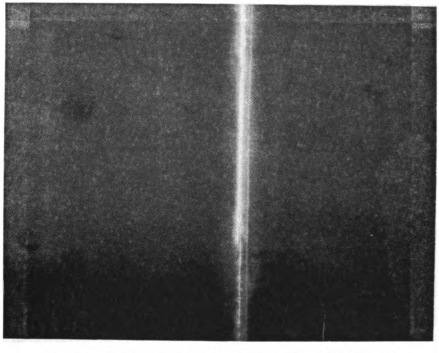

Transmitted Light Pattern at First Sign of Debonding

Figure 7.1: Transverse interfacial mode of failure for
Si Coated AS4 fiber in mPDA/DGEBA matrix

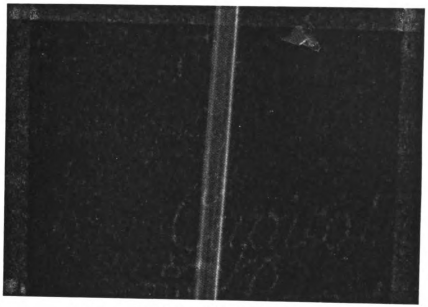

Initial Light Pattern (fiber diameter ~ 12 μm)

Transmitted Light Pattern at First Sign of Debonding

Figure 7.2: Transverse interfacial mode of failure for Kevlar fiber in mPDA/DGEBA matrix

Finally, AU4 carbon fibers were also tested with same protocol. AU4 fibers are untreated carbon fibers and have an interfacial shear strength lower than the AS4 fibers (but they exhibit a higher level of adhesion than do the Kevlar and Silicone-coated AS4 fibers). The average values of transverse strengths for the AU4 fibers (about 55 samples) is about 17.5 ksi.

In Table 7.1 the matrix used was mPDA/DGEBA cured under the normal curing conditions listed in Chapter 2. To convert from applied load at debonding (column 3 in Table 7.1) to actual transverse stress at debonding (column 4 in Table 7.1), the applied load was divided by the minimum cross sectional area of the specimen and then multiplied by a stress concentration factor of 1.8. It can also be noted from Table 7.1

Table 7.1 Transverse strengths in DGEBA/mPDA matrix

FIBER	# OF SAMPLES	APPLIED LOAD AT DEBONDING (lbs)	ACTUAL STRESS AT DEBONDING (ksi)	% OF SPECIMENS LOST DUE TO MATRIX FAILURE
AS4	65	> 130	> 21	95
AU4	40	100.4	17.5±3.5	10
K-49	35	39.5	5.9±0.76	5
Silicone Coated AS4	60	44.4	8.4±0.92	5

that the percentage of samples lost due to matrix failure is very high for systems with strong interfaces and reduces as the interfacial shear strength decreases. All the data from Table 7.1 are summarized in bar graph form in Figure 7.3.

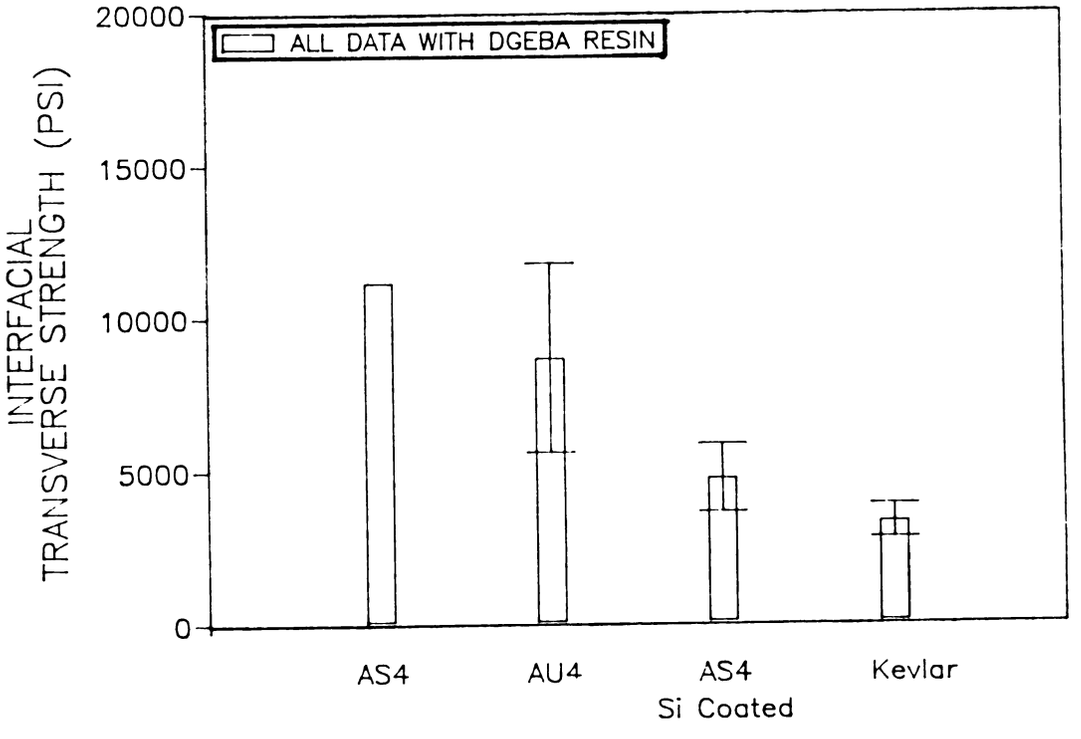

Figure 7.3: Interfacial transverse strengths of carbon, Kevlar and Si-coated carbon fibers in mPDA/DGEBA matrix

7.4 CONCLUSIONS

In this chapter, a single fiber method for determining the transverse interfacial strength was developed. The results show that the transverse interfacial strength closely follows changes in the interfacial shear strength. With the data shown in this Chapter, it can generally be said that the transverse interfacial strength decreases as the interfacial shear strength decreases. All other things being constant, a system with a high interfacial shear strength would be expected to exhibit a high transverse interfacial strength.

CHAPTER 8

ADHESIVE BEHAVIOR OF CARBON FIBERS IN A THERMOPLASTIC POLYCARBONATE MATRIX

In this chapter, a brief study will be conducted on the variation of interfacial shear strength with temperature in thermoplastic matrices. Using a polycarbonate matrix reinforced with carbon--AS4 fibers, the experimental protocol used in Chapter 6 will be used to determine the influence of temperature on the measured interfacial shear strength.

8.1 INTRODUCTION

Thermoplastic matrices offer some unique advantages [141] over thermosetting resins in certain applications. These include short molding cycle time, infinite shelf life of prepreg, recyclability and repairability, reduced handling problems, increased moisture resistance and better fracture toughness. In general, thermosetting polymers adhere more strongly to carbon fibers than do thermoplastic polymers. Evidence for these differences in adhesion is based primarily on scanning electron microscopy of failed carbon fiber reinforced polymer composites [142]. The fibers in the SEM micrographs of epoxy and other thermosetting polymer composites are coated with the matrix polymer whereas in similar SEM micrographs of thermoplastic matrix composites the fibers appear to have cleanly separated from the matrix [142,143]. Many authors have tried to use various explanations to describe these photographic differences. Hunston et al. [144] and Parker et al. [145] compared the interlaminar fracture energy as a function of the matrix fracture energy and found that Carbon Fiber Reinforced Plastics did not fit the general trend exhibited by thermoset matrix composites. Bascom et al. [142,143] observed that these differences in adhesion are not necessarily universal. They used SEM to show that highly cross-linked epoxy and bisamelemimide matrices suggested interfacial failure. They suggest that these observations may be due to limitations in the resolution of the

SEM or to micromechanical effects that focus failure into the interfacial region but not actually at the interface. Bascom et al. [143] have done further experimentation on the adhesion of three different carbon fibers to epoxy polymers and to a variety of thermoplastic polymers using the single fiber fragmentation test. They speculate on the following reasons for the data revealing that all three fibers (AS4, AS1 and XAS) exhibited strong adhesion to the thermoset epoxies, but only one (XAS) exhibited strong adhesion to the thermoplastics: (1) formation of a weak boundary layer, (2) surface roughness, (3) differing amounts of surface treatment and (4) fiber surface chemical constitution.

In an attempt to illustrate how the interface between carbon AS4 fiber and thermoplastic matrix behaves under "typical" processing conditions, a brief study will be conducted to study the alteration of interfacial shear strength with temperature using carbon, AS4 fibers embedded in a thermoplastic polycarbonate matrix. It will be seen that the methodology developed in the previous chapters for determining interphase formation from elevated temperature interfacial shear strength data of thermoset materials can also be applied to thermoplastic matrices. Recently, Muzzy et al. [146] have also used the changing viscosity (and modulus) to develop a model for describing the changes that occur during the processing cycle of toughened thermoplastics to predict changing thermal and interfacial properties of the final composite material.

8.2 EXPERIMENTAL

Carbon AS4 fibers, described in detail in previous chapters were used as the reinforcement in a thermoplastic polycarbonate matrix. The specific polycarbonate used was Lexan 8050-MC112 (without anti-oxidant, obtained from Cadillac Plastics Co.--Troy, MI) in the form of 2 mil thick sheets. The glass transition temperature of this material was found to be about 145-150°C.

While the fragmentation test used to quantify the interfacial shear strength is the same as that described in earlier chapters, the specimen preparation technique is quite different with this thermoplastic. For these specimens, the single fiber microcomposite specimens were processed in the following manner. Fibers were carefully aligned in between two thin sheets of Lexan (used as received from supplier) before being enclosed in a aluminum gasket. The sample was subsequently hot pressed at elevated temperature and pressure with a hydraulic press to ensure consolidation of the thermoplastic matrix around the fibers. A careful study of previous work [147] was done to ensure the proper processing conditions (temperature and pressure). The specific processing cycle used is shown below in Table 8.1:

Table 8.1: Processing cycle for Lexan thermoplastic

1. Heat samples to 125°C at 1 atm. and hold 1 hr.
2. Ramp to 240°C.
3. At 230°C, increase pressure to 7500 lbs.
4. Heat samples at 240°C for 40 min. at 7500 lbs.
5. Quench to room temperature at 7500 lbs.
6. At room temperature, release pressure.
7. Remove samples, and cut out specimens with dogbone shaped punch and die.

In Table 8.1, before completing step #7 the samples are carefully examined under an optical microscope and the regions with straight fibers are identified before being punched out. Further details on these fabrication procedures and techniques can be found elsewhere [147].

8.3 RESULTS AND DISCUSSION

Interfacial shear strength measurements were made from room temperature up to 120°C using the specially designed cell discussed in Chapter 6. The critical length data are summarized in Table 8.2 and the interfacial shear strengths are shown in Figure 8.1 as a function of test temperature. An average of eight samples were tested at each temperature. It can be noted from Figure 8.1 that the interfacial shear strength at ambient conditions is about 45 MPa. This level of adhesion is equivalent to the lower modulus based thermoset matrices used earlier. As the test temperature is

Table 8.2: Critical length distribution for Lexan reinforced with AS4 fiber

T (°C)	α_{weib}	β_{weib} (microns)	d_{fiber} (microns)	τ (MPa)
AMBIENT	3.5753	542.05	7.3±0.1	44.4±3.4
45±1.8	2.8767	640.45	7.6±0.3	40.3±2.8
65±2.0	2.8888	716.42	7.3±0.1	36.5±3.7
80±2.3	3.2323	713.45	7.7±0.3	36.7±6.3
97±3.3	2.7876	845.68	7.3±0.2	31.3±3.3
115±3.5	2.9993	867.45	7.4±0.1	29.6±4.5

increased, the interfacial shear strength is seen to decrease. In comparison to the thermoset matrices studied in chapter 6, the decrease is seen to be more linear here with no precipitous decrease seen (as with the thermoset matrices) as T_g of the matrix is approached. This linear decrease in interfacial shear strength with temperature for thermoplastic systems has been noted earlier by Oshawa et al. [59]. This seems to be indicative of a modulus effect on the interfacial shear strength. As the test temperature is increased, the modulus of the matrix is decreasing thereby reducing the ability of the matrix to transfer stress to the interface (Chapter 5). This type of decrease in interfacial

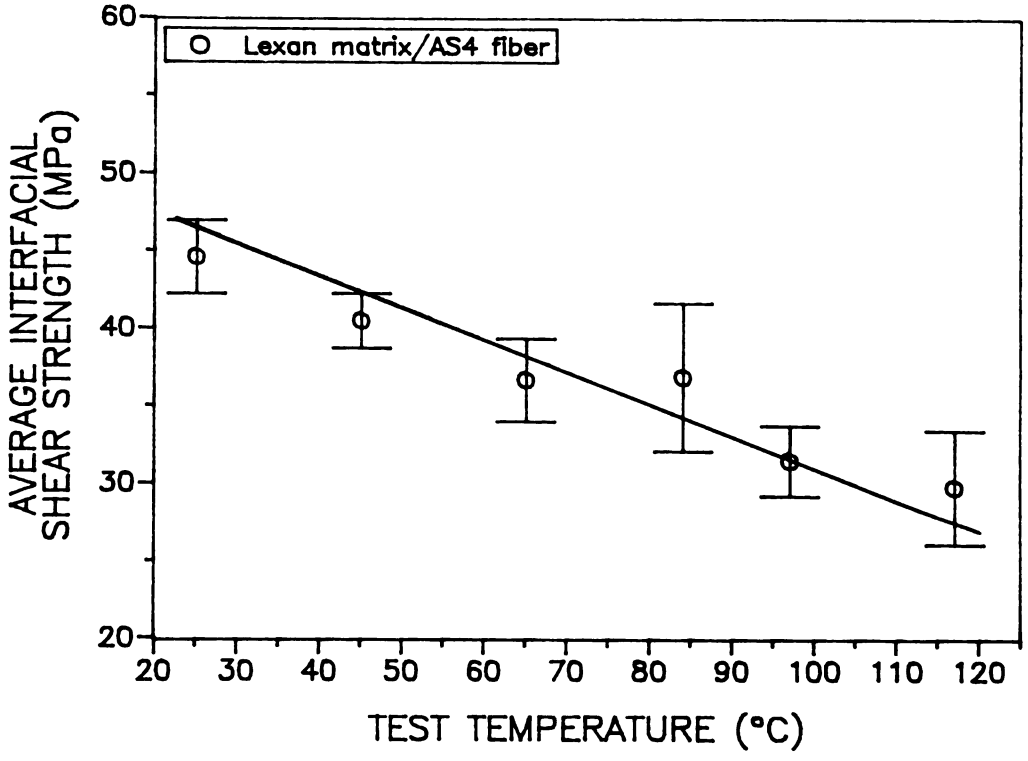

Figure 8.1: Interfacial shear strength as a function of test temperature for thermoplastic Lexan matrix reinforced with carbon, AS4 fibers

shear strength would be expected in this amorphous system since no curing agent is present to diffuse into the interphase region in this matrix and the interphase properties should be very similar to the bulk properties of the matrix itself.

The mode of failure for this particular thermoplastic system is shown in Figures 8.2-8.6 for five different temperatures varying from ambient temperature to 120°C. The birefringent patterns are all seen to be diffuse indicative of weak adhesion at the interface when compared to the thermoset systems studied earlier (see Figures 5.2-5.6). Also, as expected, as the temperature is increased more interfacial damage (larger interfacial cracks) as well as larger amounts of matrix damage is seen to occur. The debonding, at all temperatures tested, is seen to take place interfacially. This is in good agreement with previous work done by Waterbury et al. on a similar polycarbonate thermoplastic system [34,147]. Bascom et al. [53,148] has also shown very similar birefringent patterns for various different thermoplastic microcomposites.

8.4 CONCLUSIONS

In this chapter, the influence of temperature on the interfacial shear strength of a thermoplastic (polycarbonate) matrix reinforced with carbon AS4 fiber was investigated. It was shown that the modulus of the matrix controls the level of adhesion throughout the temperature regime. Failure modes were indicative of interfacial mode of failure and a weak level of interfacial adhesion. No definitive conclusions about the interphase properties being significantly different than the bulk could be made due to the inability to conduct experiments above 120°C (since the T_g of the material is about 150°C, further experiments must be conducted closer to the bulk T_g of the matrix to detect possible differences in the mechanical and thermal properties of the polymer near the fiber/matrix interface).

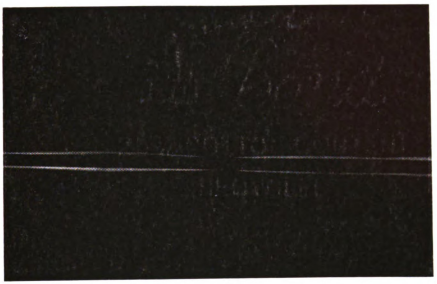

Polarized Light Micrograph
(fiber diameter ~ 7 μm)

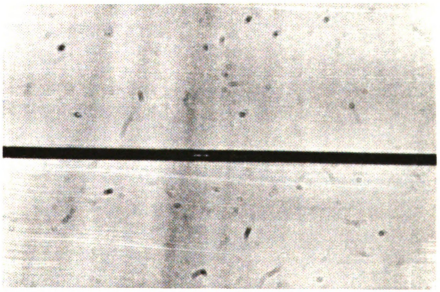

Transmitted Light Micrograph

Figure 8.2: Interfacial failure mode for Lexan/AS4 at 25°C

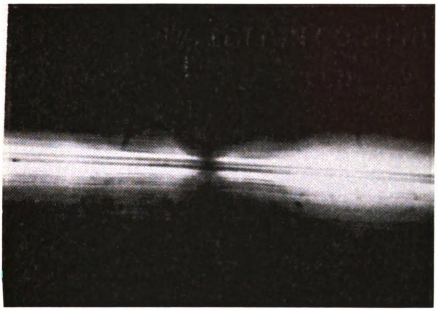

Polarized Light Micrograph
(fiber diameter ~ 7 μm)

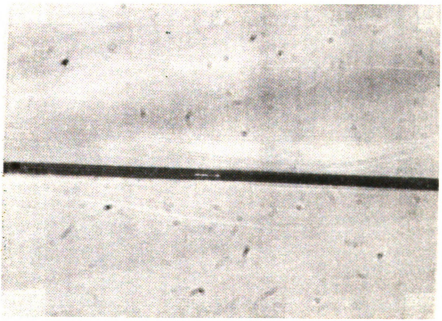

Transmitted Light Micrograph

Figure 8.3: Interfacial failure mode for Lexan/AS4 at 45°C

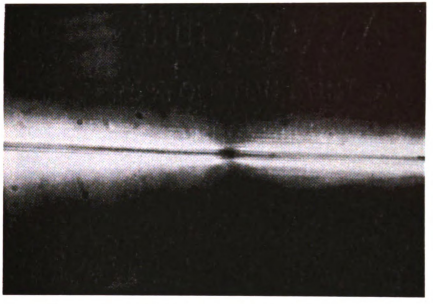

Polarized Light Micrograph
(fiber diameter ~ 7 μm)

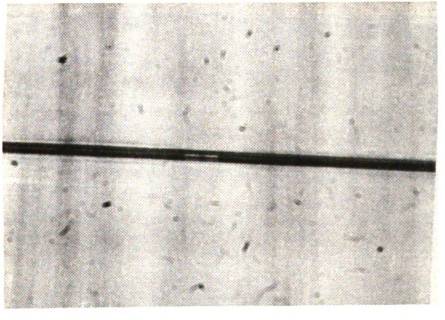

Transmitted Light Micrograph

Figure 8.4: Interfacial failure mode for Lexan/AS4 at 65°C

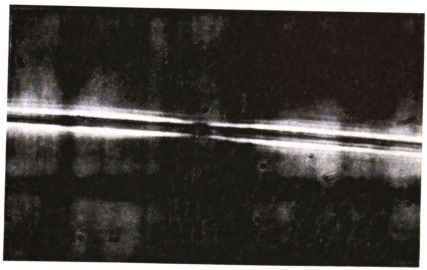

Polarized Light Micrograph
(fiber diameter ~ 7 μm)

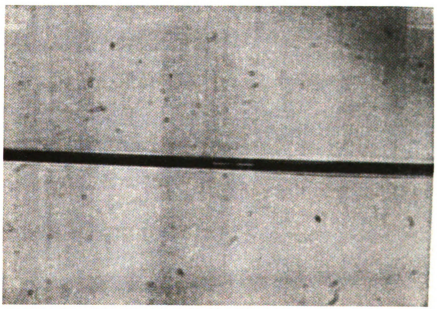

Transmitted Light Micrograph

Figure 8.5: Interfacial failure mode for Lexan/AS4 at 85°C

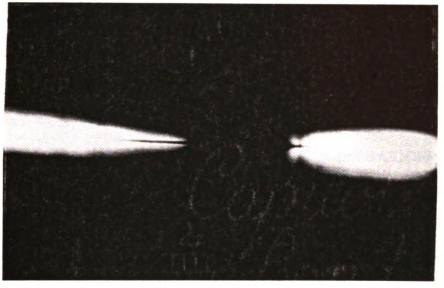

Polarized Light Micrograph
(fiber diameter ~ 7 μm)

Transmitted Light Micrograph

Figure 8.6: Interfacial failure mode for Lexan/AS4 at 120°C

CHAPTER 9

CONCLUSIONS AND RECOMMENDATIONS

9.1 CONCLUSIONS

In this work, the effect of processing variables on the interfacial shear strength was investigated for a typical thermoset epoxy/carbon fiber (mPDA/DGEBA/AS4) system. The processing cycle was conveniently divided into three different regimes; a pre-gelation regime, an ambient temperature regime, and an elevated temperature regime. In each of the three different regimes, readily measurable properties of the matrix and interphase were used to predict the interfacial shear strength. Predictive models were developed in each of the different regimes.

In the pre-gel state, the kinetics of crosslinking and viscokinetic properties of the reacting matrix were related to a interfacial pull-out strength measured with a gravimetric apparatus. A modified WLF equation of state was used to model the changes in viscosity and in pull-out strength as a function of extent of cure.

At ambient conditions, constant interfacial and matrix chemistry was used to systematically vary the matrix properties from ductile, plastic to brittle, elastic in order to simulate the actual processing cycle and to simulate thermoset versus thermoplastic behavior. A single fiber fragmentation test was used to quantify the interfacial shear strength. With all other parameters held constant, it was found that the interfacial shear strength is sensitive to matrix modulus and decreases monotonically with decreasing modulus of bulk matrix. A shear lag model was used to linearly model the changes in interfacial shear strength as a function of matrix and fiber properties.

At elevated temperatures, a specially designed teflon cell was used to conduct the interfacial (single fiber) shear strength measurements. The results confirm the reduction

in interfacial shear strength with a reduction in matrix modulus as found at ambient conditions. As the T_g of the matrix is approached, a corresponding large decrease in interfacial shear strength is noted. The different matrices (with constant interfacial chemistry) used previously were used to generate a master curve to describe changes in interfacial shear strength as a function of temperature. Additionally, epoxy sized fibers were used to study and model the formation of an interphase region by diffusion and reaction of curing agent with the epoxy sizing creating an interphase with different mechanical properties than the bulk matrix. These data are used to arrive at an interphase thickness and effective diffusion coefficient in the interphase region.

Overall, a predictive methodology has been developed for describing changes in the interfacial shear strength [149] throughout the processing cycle of the thermoset composite. This methodology has the advantage of being able to predict the interfacial (shear) properties by measuring fundamental properties of the reacting or reacted matrix.

9.2 RECOMMENDATIONS FOR FUTURE WORK

While most of the experimental work presented in this work is complete, the modeling of the interphase formation presented in Chapter 6 is only a first step. A more complete knowledge of the formation of an interphase could lead to "tailoring" of an interphase for specific composite properties and performance. Future work should include and address improvement of the model by determining the relationship between diffusion coefficient (of curing agent into epoxy resin) and extent of reaction. In other words, the concentration profile of curing agent (or of the epoxy resin) in the interphase must be evaluated either analytically, experimentally or both. Efforts are already underway to elucidate this relationship. Once this data is available, Equation (6.1) can be used to arrive at a more complete final solution. Additionally, alteration and retardation of the kinetics and gelation characteristics of the matrix should allow for

transient behavior to be taken into account. The effect of stoichiometry on the kinetics of the epoxy/amine reaction may also play an important role in the interphase region and must be accounted for. Obviously, the modeling of interphase formation due to migration and diffusion of curing agent is in its infancy stage and the model presented in Chapter 6 should serve as a springboard for a more in-depth mathematical analysis.

Chapter 8 presents a very brief introduction to the effect of temperature on interfacial behavior of a thermoplastic polycarbonate matrix ("Lexan") reinforced with carbon, AS4 fiber. With the advent of new thermoplastic materials capable of increased thermal stability, a knowledge of how the interface changes with the processing of the thermoplastic is paramount for a complete understanding of the final thermoplastic composite. While thermoplastic systems will pose unique characteristics (such as crystallinity and transcrystallinity [150,151,152]--which when occurring in the interphase region could lead to variations in the level of fiber-matrix adhesion; interfacial adhesion could as well be affected by migration and segregation of low molecular weight constituents from the bulk to the interface during processing) compared to thermoset systems, the methodology used in this dissertation should serve as a starting point on the determination of how processing parameters affect interfacial properties in thermoplastic systems.

APPENDICES

APPENDIX A

"PEAK" POINT ANALYSIS OF ISOTHERMAL KINETIC DATA

In Chapter 3, isothermal kinetic data was used to describe the kinetics of crosslinking of the mPDA/DGEBA system. Rigorous numerical regression techniques were employed to arrive at the necessary parameters to describe the reaction kinetics (see Table 3.1). In this section, "peak" isothermal data will be used to arrive at similar kinetic parameters as that shown in Table 3.1. The major advantage to this method, first developed by Kissinger et al. [71] for dynamic (different heating rates) DSC data and later used by others for isothermal data, is that it only involves algebraic manipulation of the assumed kinetic rate equation and peak reaction rate data at different temperatures. Kinetic data must be collected at various isothermal temperatures and the time to reach the peak in reaction rate and the extent of reaction at the peak is all that is required to complete the analysis. It will be shown that, for this particular autocatalytic reaction, the two different methods give rise to similar kinetic parameters.

The starting point for this analysis is the general assumed form of the kinetic reaction rate expression (autocatalytic)

$$\frac{d\alpha}{dt}=(k_1+k_2\alpha^m)(1-\alpha)^n \qquad \text{(A1)}$$

from Equation A1 it is evident that the reaction rate constant k_1 (at a given temperature) can be obtained by plotting α vs. t and calculating the tangent (or initial slope) at t=0 and α=0. Thus, initially, when t=0 and α=0, Equation A1 reduces to

$$k_1 = \frac{d\alpha}{dt} @ t=0, \alpha=0 \qquad \text{(A2)}$$

Equation A2 indicates that the kinetic rate constant k_1 is readily determined directly from isothermal reaction rate data. The maximum (or peak) of the reaction rate curve is defined by

$$\frac{d^2\alpha}{dt^2}=0 \qquad \text{(A3)}$$

Applying this condition to the kinetic expression given by Equation A1 gives

$$\frac{d}{dt}\left(\frac{d\alpha}{dt}\right)=-nk_1(1-\alpha)^{n-1}-nk_2\alpha^m(1-\alpha)^{n-1}+mk_2(1-\alpha)^n\alpha^{m-1} \qquad \text{(A4)}$$

dividing through by $(1-\alpha)^n\alpha^{m-1}$ and setting the left hand side equal to zero (at $\alpha=\alpha_p$) gives

$$0=-nk_1\alpha_p^{1-m}(1-\alpha_p)^{-1}-nk_2\alpha_p(1-\alpha_p)^{-1}+mk_2 \qquad \text{(A5)}$$

multiplying through by $(1-\alpha_p)$ and multiplying the resulting expression by (-1) gives

$$0=nk_1\alpha_p^{1-m}+nk_2\alpha_p-mk_2+mk_2\alpha_p \qquad \text{(A6)}$$

rearranging gives

$$0=nk_1\alpha_p^{1-m}+k_2(m+n)\alpha_p-mk_2 \qquad \text{(A7)}$$

as discussed in Chapter 3, the overall order of the reaction is assumed to be two so that

$$m+n=2 \qquad \text{(A8)}$$

if now the above equation is substituted into Equation A7 and manipulated for k_2 we arrive at

$$k_2 = \frac{(2-m)k_1\alpha_p^{1-m}}{m-2\alpha_p} \tag{A9}$$

note here that m must be greater than $2\alpha_p$ for this relation to hold mathematically; then, solving Equation A1 for m gives (where we define $\dot{\alpha}=d\alpha/dt$)

$$m = \frac{\ln\left[\frac{\frac{\dot{\alpha}}{(1-\alpha)^n} - k_1}{k_2}\right]}{\ln\alpha} \tag{A10}$$

finally, substitution of Equation A9 into A10 at the "peak" gives

$$m = \frac{\ln\left[\frac{\frac{\dot{\alpha}_p}{(1-\alpha_p)^{2-m}} - k_1}{\frac{(2-m)k_1\alpha_p^{1-m}}{m-2\alpha_p}}\right]}{\ln\alpha_p} \tag{A11}$$

here the entire numerator falls into the ln bracket. With this analysis, Equations A2, A9 and A11 give the necessary parameters needed to define the kinetics of reaction. The only data required are the "peak" characteristics at various isothermal times.

Isothermal runs were made in-situ in the DSC at various temperatures and the time to reach a peak in the reaction rate as well as the reaction rate at peak were measured. These data are summarized below in Table A1. The extent of reaction at peak can be obtained from Figure 3.8 and is always around the gelation point (between 0.58 and 0.64 extent of conversion) for this particular system. The time to reach peak reaction rate (t_p) and the peak reaction rate itself $(d\alpha/dt)_p$ listed in Table A1 can be plotted in Arrenhius form [153] resulting in the relationships shown in Table A2.

Usage of Equations A2, A9 and A11 gives the kinetic parameters at the various temperatures once α_p and $(d\alpha/dt)_p$ are known from Table A1. A comparison between the

Table A1: Peak kinetic parameters

T (°C)	T^{-1} ($Kx10^{-3}$)	t_p (sec)	$(d\alpha/dt)_p$ (min^{-1})
50	3.096	220.5	.00466
90	2.755	55.9	.01200
100	2.681	36.3	.01650
110	2.611	19.8	.01910
120	2.545	10.3	.01167
130	2.481	6.80	.09590
140	2.421	2.80	.13333

Table A2: Peak times and reaction rates

$$t_p = 6.96x10^{-7}\exp(6487/T),\ t_p \text{ in min; T in } ^\circ K$$

$$(d\alpha/dt)_p = 1.93x10^{3}\exp(-4196/T),\ (d\alpha/dt)_p \text{ in } min^{-1};\ T \text{ in } ^\circ K$$

more rigorous method presented and used in Chapter 3 and the approximate method used in this chapter is given below in Table A3. It is seen from Table A3 that while the pre-exponential factors vary somewhat, the activation energies are in good agreement using either method. The kinetic exponents are also found to be in good agreement.

Thus, in this section, a rapid estimation technique is proposed for the determination of the kinetic parameters of an autocatalytic reaction of epoxy cure. The method outlined utilizes information from a single characteristic point, namely, the point at maximum rate of cure. The proposed method is a slight modification of the method presented initially

by Kissinger et al. [71] for determination of kinetic parameters using DSC data at different heating rates ("dynamic" data). The proposed method yields results which are in close agreement with the more rigorous numerical technique presented in Chapter 3.

It must be noted that for reaction temperatures below about 85°C, the kinetics of this particular reaction are adequately described by pseudo-first order kinetics (i.e. $d\alpha/dt=k(1-\alpha)$; where $\ln k=13.18-(7610/T)$ for k in sec^{-1} and T in °K) and an autocatalytic model is unnecessary.

Table A3: Comparison of kinetic parameters

METHOD USED IN CHAPTER 3
$k_1=1.693x10^6exp(-7034/T)$
$k_2=9505exp(-4196/T)$
T in °K and $k_{1,2}$ in min^{-1}
$m=-2.75x10^{-3}T+1.43$ (T in °C, for T > 85°C)
METHOD USED HERE
$k_1=8.724x10^5exp(-5700/T)$
$k_2=2.814x10^4exp(-4001/T)$
T in °K and $k_{1,2}$ in min^{-1}

APPENDIX B

MODEL FOR DIFFUSION OF CURING AGENT OUT OF DROPLETS

Figure B1 below schematically represents the physical situation that exists when a microdroplet (0.2 mm) is placed on a carbon fiber. Before the droplet gels, the liquid (mPDA) curing agent diffuses out of the droplet leading to a uncured droplet as discussed in Chapter 4.

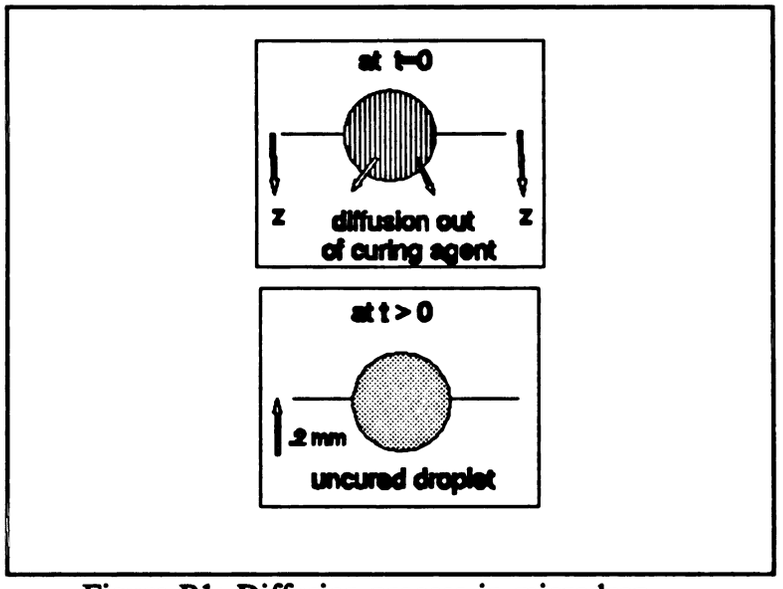

Figure B1: Diffusion process in microdrop

An initial assumption is that the diffusion coefficient, D, is constant and that there *is no* gelation (reaction between curing agent and epoxy resin) from the interface out. It can then be shown that a mass balance (on the curing agent) combined with Fick's law of diffusion gives [13] the following governing partial differential equation describing the process:

$$\frac{\delta C}{\delta t}=D\frac{\delta^2 C}{\delta z^2} \tag{B1}$$

Equation (B1) is subject to the following boundary conditions:

$$\text{at } t=0, \text{ all } z,\ C=C_\infty \sim C_{bulk}$$

$$\text{at } t>0,\ z=0,\ C=C_{bulk}$$

$$\text{at } t>0,\ z=\infty,\ C=C_\infty=0$$

Here, C represents the curing agent concentration. The second boundary condition is only an approximation as the interface is not continuously refreshed with curing agent. However, for small times, it has been shown by Crank [136] that this approximation can be used. The method of combination of variables, to transform the partial differential equation (B1) into an ordinary differential equation, is used to solve this problem. We start by making the following definition of a dimensionless variable

$$\zeta=\frac{z}{(4Dt)^{1/2}} \tag{B2}$$

by using the chain rule of differentiation, we change Equation (B1) to:

$$\frac{dC}{d\zeta}\left(\frac{d\zeta}{dt}\right)=D\frac{d^2C}{d\zeta^2}\left(\frac{d\zeta}{dz}\right)^2 \tag{B3}$$

then from appropriate differentiation of Equation (B2) we have

$$\frac{d\zeta}{dt} = -z\frac{t^{-3/2}}{4(D^{1/2})} \tag{B4}$$

and,

$$(\frac{d\zeta}{dz})^2 = (4Dt)^{-1} \tag{B5}$$

substitution of Equations (B4) and (B5) into (B3) gives the governing ordinary differential equation:

$$\frac{d^2C}{d\zeta^2} + 2\zeta\frac{dC}{d\zeta} = 0 \tag{B6}$$

In other words, the partial differential Equation (B1) has been transformed into an ordinary differential equation with the following boundary conditions:

at $\zeta = 0$, $C = C_{bulk}$

at $\zeta = \infty$, $C = C_{\infty} = 0$

The solution is now straightforward. One integration of Equation (B6) gives:

$$\frac{dC}{d\zeta} = ae^{-\zeta^2} \tag{B7}$$

where a is an integration constant. A second integration and use of the above boundary conditions gives:

$$\frac{C - C_{bulk}}{C_{\infty} - C_{bulk}} = erf(\zeta) \tag{B8}$$

here erf is the error function whose values can be found in any standard mathematical handbook. In our situation, $C_{\infty} \sim 0$, so that the final solution becomes:

$$\frac{C}{C_{bulk}} = 1 - erf(\zeta) \qquad \text{(B9)}$$

By assuming a diffusion coefficient of $10^{-7}cm^2/sec$ [93] for liquid mPDA diffusing out of liquid epoxy resin, we can derive the time required to achieve a very low concentration of mPDA curing agent at the interface (uncured droplet). The time required to reach a 20% of bulk concentration at the interface for a 200 micron droplet can be calculated to be 0.02 minutes. The experimental protocol for placing droplets on the fiber is on the order of minutes so that diffusion of curing agent out of small droplets is expected to occur.

For the more viscous J700 curing agent, the diffusion coefficient is expected [13,93] to be at least a magnitude of order lower ($10^{-8}cm^2/sec$) than for the volatile mPDA curing agent. For a 200 micron droplet, the time to reach a 20% concentration at the interface can be calculated to be .45 minutes. It can be seen that the time required for the same amount of curing agent to diffuse out are an order of magnitude higher. The analysis presented here thus validates and explains some of the curing observations made earlier in Chapter 4 with these two different systems.

APPENDIX C

A MODEL TO DESCRIBE INTERPHASE FORMATION

The physical situation of diffusion of curing agent is discussed in Chapter 6 and is illustrated in Figure 6.5. An attempt is made here to derive a model to describe the preferential diffusion of curing agent into the interphase region of thickness Δr. We start by making the following assumptions to simplify the analysis:

1. Small thickness (slab geometry-1 dimensional)
2. First order reaction between epoxy and curing agent, mPDA
3. Constant, "effective" diffusion coefficient, D
4. No accumulation of curing agent in interphase (steady-state)

With these assumptions, the governing diffusion equation takes the form:

$$D\frac{d^2C(r)}{dr^2}-kC(r)=0 \qquad \text{(D1)}$$

here C(r) is the concentration of curing agent in the interphase region, k is the pseudo first order rate constant (@ ~70°C) for the epoxy-amine reaction, D is the diffusion coefficient of curing agent into the epoxy-rich interphase, and r is the radial distance. Equation (D1) is subject to the following boundary conditions:

$$\text{at } r=r_i,\ C=C_{bulk}$$

$$\text{at } r=r_f,\ dC/dr=0$$

The first boundary condition implies a bulk concentration (14.5 phr) of curing agent at the boundary between interphase and bulk matrix. The second boundary condition is the "no-slip" (no net-flux) condition at the solid fiber surface. If we make the following definition:

$$a^2=\frac{k}{D} \tag{D2}$$

Equation (D1) becomes:

$$\frac{d^2C}{dr^2}-a^2C=0 \tag{D3}$$

the general solution to Equation (D3) is [15,136]:

$$C=C_1e^{-ar}+C_2e^{ar} \tag{D4}$$

here C_1 and C_2 are integration constants. The first boundary condition inserted into Equation (D4) gives:

$$C_{bulk}=C_1e^{-ar_i}+C_2e^{ar_i} \tag{D5}$$

and the second boundary condition with Equation (D4) gives:

$$0=\frac{dC}{dr}=-aC_1e^{-ar_f}+aC_2e^{ar_f} \tag{D6}$$

solving (D6) for the constant C_1 gives:

$$C_1=C_2\frac{e^{ar_f}}{e^{-ar_f}} \tag{D7}$$

and solving (D5) for the constant C_2 gives:

Substitution of Equation (D7) into (D8) and solving for C_{bulk} gives:

$$C_2=\frac{C_{bulk}-C_1e^{-\alpha r_i}}{e^{\alpha r_i}} \tag{D8}$$

$$C_{bulk}=C_2e^{\alpha r_i}+C_2\frac{e^{\alpha r_f}}{e^{-\alpha r_f}}e^{-\alpha r_i} \tag{D9}$$

solving Equation (D9) for C_2 and rearrangement results in:

$$C_2=C_{bulk}\frac{e^{-\alpha r_f}}{e^{\alpha(r_i-r_f)}+e^{\alpha(r_f-r_i)}} \tag{D10}$$

substitution of Equation (D10) into (D7) gives:

$$C_1=C_{bulk}\frac{e^{\alpha r_f}}{e^{\alpha(r_i-r_f)}+e^{\alpha(r_f-r_i)}} \tag{D11}$$

Equations (D10) and (D11) substituted into Equation (D4) gives us the final analytical solution:

$$\frac{C}{C_{bulk}}=\frac{e^{\alpha(r_f-r)}+e^{\alpha(r-r_f)}}{e^{\alpha(r_i-r_f)}+e^{\alpha(r_f-r_i)}} \tag{D12}$$

It is more convenient to make Equation (D12) non-dimensional. Thus we make the following dimensionless definitions:

$$\phi=\alpha(r_i-r_f) \tag{D13}$$

and,

$$\psi=\frac{r_i-r}{r_i-r_f} \tag{D14}$$

with these definitions, it is easily shown that Equation (D12) reduces to the form shown in Chapter 6:

$$\frac{C}{C_{bulk}} = \frac{e^{-\phi(1-\psi)} + e^{\phi(1-\psi)}}{e^{\phi} + e^{-\phi}} \qquad \text{(D15)}$$

This completes the derivation of the model to describe diffusion into the interphase region. Equation (D15) gives the curing agent concentration profile in the interphase by knowing the diffusion coefficient, reaction rate constant and the radial position in the interphase region. Some simplifying assumptions suggested by Theocaris et al. [133] were used to derive this analytical solution.

In this model, there are two adjustable parameters only. While the reaction rate constant was determined experimentally (from the data in Chapter 3, it can be shown that the pseudo-first order reaction rate constant at 70°C is approximately 1.58×10^{-4} sec^{-1}), the diffusion coefficient, D, was obtained from the literature as discussed in Chapter 6. Obviously, if the diffusion coefficient is determined experimentally and known more accurately and a more in-depth kinetic analysis is used, a correspondingly more accurate solution can be obtained. Even though Equation (D15) predicts proper interphase thickness based on inferred interfacial stoichiometry (for coated fibers), a more realistic model would also include the dependence of the diffusion coefficient on extent of reaction and concentration of curing agent as the epoxy-amine reaction proceeds. Separate experiments must be conducted to ascertain these data. A more realistic approach could also include the possibility of a moving interphase boundary by diffusion of polymer out of the interphase into the bulk.

LIST OF REFERENCES

LIST OF REFERENCES

1. Hull, D., *An Introduction to Composite Materials*, Cambridge University Press, New York (1981).

2. Iyer, S. R., "*Continuous Processing of Unidirectional Prepreg*," Ph.D. Dissertation, Michigan State University, Department of Chemical Engineering, November (1990).

3. Lubin, G., *Handbook of Composites*, Van Nostrand Reinhold Co., New York (1982).

4. Seferis, J. C. and L. Nicolais, *The Role of the Polymeric Matrix on the Processing and Structural Properties of Composite Materials*, Plenum Press, New York (1983).

5. Rao, V. and L. T. Drzal, "*Thick-Section Composites*," Ph.D. Dissertation Preproposal, Department of Chemical Engineering, May (1987).

6. Mijovic, J. and J. Wijaya, "Effects of Graphite Fiber and Epoxy Matrix Physical Properties on the Temperature Profile Inside their Composite During Cure," *SAMPE Journal*, Vol. 25(2), 35, Mar/April (1989).

7. Wood, A. S., "Patience: Key to Big Volume in Advanced Composites?," *Modern Plastics*, 44, March (1986).

8. Asmussen, J., Beck, J., Drzal, L. T., Hawley, M. C., Osman, A., Scott, E., Schwalm, C., DeLong, J. and V. Rao, "Interface/Interphase and their Interrelationships to Processing of Thick-Section Composites," **Proceedings of the 1987 Annual Review (National Center for Composite Materials Research)**, Office of Naval Research Initiative Program, November 9-10 (1987).

9. Prime, R. B., in *Thermal Characterization of Polymeric Materials*, Edited by E. A. Turi, Academic Press, Chapter 5, New York (1981).

10. Palmese, G. R. and J. K. Gillham, "Time-Temperature-Transformation (TTT) Cure Diagrams: Relationship between T_g and the Temperature and Time of Cure for a Polyamic Acid/Polyimide System," *J. Appl. Poly. Sci.*, Vol. 34, 1925 (1987).

11. Narkis, M., Chen, J. H. and R. B. Pipes, "Review of Methods for Characterization of Interfacial Fiber-Matrix Interactions," *Polym. Comp.*, Vol. 9(4), 245, August (1988).

12. Nielesen, L. E., *Mechanical Properties of Polymers and Composites*, Volumes 1 and 2, Marcel-Dekker, Inc., New York (1974).

13. Cussler, E. L, *Diffusion: Mass transfer in Fluid Systems*, Cambridge University Press, New York (1984).

14. Cooke, T. F., "High Performance Fiber Composites with Special Emphasis on the Interface: A Review of the Literature," *J. of Polymer Processing*, Vol. 793, 199 (1987).

15. Finlayson, B. A., *Nonlinear Analysis in Chemical Engineering*, McGraw-Hill, New York (1980).

16. Morgan, R. J. and C. M. Walkup, "Epoxy Matrices for Filament-Wound Carbon Fiber Composites," *J. of Appl. Poly. Sci.*, Vol. 34, 37 (1987).

17. Vratsanos, M. S. and R. J. Farris, "Network Mechanical Properties of Amine-Cured Epoxies," *Poly. Engr. and Sci.*, Vol. 29(17), 806, June (1989).

18. Tanaka, E. A. and M. Mika, in *Epoxy Resins: Chemistry and Technology* (Ed. C. A. May), Chapters 2 and 3, Marcel Dekker, Inc., New York (1988).

19. M. Mika, **Ibid**, Chapter 4.

20. Lee, H. and K. Neville, *Handbook of Epoxy Resins*, McGraw-Hill, New York (1967).

21. Pauley, C. R., "Face the Facts About Amine Foaming," *Chem. Engr. Prog.*, 33, July (1991).

22. Dorey, G., "Carbon Fibres and their Applications," *J. Phys. D: Appl. Phys.*, (Printed in the UK), Vol. 20, 245 (1987).

23. Hughes, J. D. H., "The Evaluation of Current Carbon Fibres," *J. Phys. D: Appl. Phys.*, (Printed in the UK), Vol. 20, 276 (1987).

24. Fitzer, E. and H. -P. Rensch, "Carbon Fibre Surfaces and their Analysis," in **Controlled Interphases in Composite Materials** (Edited by H. Ishida), Third International Conference on Composite Interfaces, Elsevier, New York (1990).

25. Madhukar, M. and L. T. Drzal, "Fiber-Matrix Adhesion and its effect on Composite Mechanical Properties: I. Inplane and Interlaminar Shear Behavior of Graphite/Epoxy Composites and II. Longitudinal (0°) and Transverse (90°) Tensile and Flexure behavior of Graphite/Epoxy Composites," *J. of Comp. Matls.*, Vol. 25, August (1991).

26. Donnet, L. B. and R. C. Bansal, *Carbon Fibers*, Marcel Dekker, Inc., New York (1984).

27. Hammer, G. E. and L. T. Drzal, "Graphite Fiber Surface Analysis by X-Ray Photoelectron Spectroscopy and Polar/Dispersive Free Energy Analysis," *Appl. of Surf. Sci.*, Vol. 4, 340 (1980).

28. Drzal, L. T. and P. J. Herrera-Franco, "Composite Fiber-Matrix Bond Tests," *Engineered Materials Handbook*, Volume 3: Adhesives and Sealants, ASM International, 391 (1991).

29. Kelly, A. and W. R. Tyson, "Tensile Properties of Fiber-Reinforced Metals: Copper/Tungsten and Copper/Molybdenum," *J. Mech. Phys. Solids*, Vol. 13, 329 (1965).

30. Rich, M. J. and L. T. Drzal, "Interfacial Properties of Some High-Strain Carbon Fibers in an Epoxy Matrix," **Proceedings for the 41st Annual Conference**, Reinforced Plastics/Composites Institute, The Society of the Plastics Industry, 1, January (1986).

31. Netravali, A. N. and A. Manji, "Effect of ^{60}Co Gamma Radiation on the Mechanical Properties of Epoxy Blends and Epoxy-Graphite Fiber Interface," *Polym. Comp.*, Vol. 12(3), 153, June (1991).

32. Bascom, W. D. and R. M. Jensen, "Stress Transfer in Single Fiber/Resin Tensile Tests," *J. Adhesion*, Vol. 19, 219 (1986).

33. Folkes, M. J. and W. K. Wong, "Determination of Interfacial Shear Strength in Fibre-Reinforced Thermoplastic Composites," *Polymer*, Vol. 28, 1309, July (1987).

34. Waterbury, M. C and L. T. Drzal, "Interfacial Shear Strengths of Carbon Fibers in Bisphenol-A Polycarbonate," **Proceedings of the third ICCI Conference**, Cleveland, OH., June (1990).

35. Herrera-Franco, P. J., Wu. W-L., Madhukar, M. and L. T. Drzal, "Contemporary Methods for the Measurement of Fiber-Matrix Interfacial Shear Strength," **46th Annual Conference: Composites Institute**, The Society of Plastics Industry, Inc., February (1991).

36. Wimoliatisak, A. S. and J. P. Bell, "Interfacial Shear Strength and Failure Modes of Interphase-Modified Graphite-Epoxy Composites," *Polym. Comp.*, Vol. 10(3), 162, June (1989).

37. Henstenburg, R. B. and S. L. Phoenix, "Interfacial Shear Strength Studies Using the Single-Filament-Composite Test. Part II: A Probability Model and Monte Carlo Simulation," *Polym. Comp.*, Vol. 10(5), 389, December (1989).

38. University of Dayton Research Institute, "*Improved Materials for Composite and Adhesive Joints*," Annual Progress Report, AFWAL TR-82-4182, September 1981-August 1982.

39. Kalantar, J. and L. T. Drzal, "The Bonding Mechanism of Aramid Fibers to Epoxy Matrices. Part II: An Experimental Investigation," *J. Mater. Sci.*, Vol. 25, 4194 (1990).

40. Drzal, L. T., "Composite Interphase Characterization," *SAMPE Journal*, Vol. 19, 7 (1983).

41. Miller, B., Muri, P. and L. Rebenfeld, "A Microbond Method for Determination of the Shear Strength of a Fiber/Resin Interface," *Comp. Sci. and Tech.*, Vol. 28, 17 (1987).

42. Gaur, U. and B. Miller, "Microbond Method for Determination of the Shear Strength of a Fiber/Resin Interface: Evaluation of Experimental Parameters," *Comp. Sci. and Tech.*, Vol. 34, 35 (1989).

43. Piggott, M. R. and D. Andison, "The Carbon Fibre-Epoxy Interface," *J. of Rein. Plas. and Comp.*, Vol. 6, 290, July (1987).

44. Gent, A. N. and G. L. Liu., "Pull-Out and Fragmentation in Model Fibre Composites," *J. Mater. Sci.*, Vol. 26, 2467 (1991).

45. Chu, W. L. and H. D. Conway, "A Numerical Method for Computing the Stresses Around an Axisymmetrical Inclusion," *Intl. J. Mech. Sci.*, Vol. 12, 575 (1970).

46. Jones, R. M., *Mechanics of Composite Materials*, McGraw-Hill, New York (1975).

47. J. L. Thomason, "Investigation of Composite Interphase Using Dynamic Mechanical Analysis: Artifacts and Reality," *Polym. Comp.*, Vol. 11(2), 105, April (1990).

48. Dusi, M. R., Galeos, R. M. and M. G. Maximovich, "Physiorheological Characterization of a Carbon Epoxy Prepreg System," *J. Appl. Poly. Sci.*, Vol. 30, 1847 (1985).

49. Kaelble, P. A., *Physical Chemistry of Adhesion*, Wiley-Interscience Press, New York (1971).

50. Berger, E. J. and Y. Eckstein, "Epoxy Resin Wetting of E-Glass Single Filaments as it Relates to Shear Strength," in **Adhesive Joints Formation, Characteristics and Testing (Edited by K. L. Mittal)**, Plenum Press, 51, New York (1984).

51. Drzal, L. T., Rich, M. J., Camping, J. D. and W. J. Park, "Interfacial Shear Strength and Failure Mechanisms in Graphite Fiber Composites," **35th Annual Technical Conference, Reinforced Plastics/Composites Institute**, The Society of the Plastics Industry, Inc., (1980).

52. Marshall, P. and J. Price, "Fibre/Matrix Interface Property Determination," *Composites*, Vol. 22(1), 53, January (1991).

53. Bascom, W. D. and W-J. Chen, "Effect of Plasma Treatment on the Adhesion of Carbon Fibers to Thermoplastic Polymers," *J. Adhesion*, Vol. 34, 99 (1991).

54. Rao, V., Chmielewski, C. A. and L. T. Drzal, "An Experimental Study of the Viscokinetic Behavior and the Development of Interfacial Strength between mPDA/DGEBA Matrix and Carbon, AS4 Fibers," in preparation for publication.

55. Rao, V. and L. T. Drzal, "The Dependence of Interfacial Shear Strength on Matrix and Interphase Properties," *Polym. Comp.*, Vol. 12(1), 48, February (191).

56. Netravali, A. N., Henstenburg, R. B., Phoenix, S. L. and P. Schwartz, "Interfacial Shear Strength Studies Using the Single-Filament-Composite Test. I: Experiments on Graphite Fibers in Epoxy, *Polym. Comp.*, Vol. 10(4), 226, August (1989).

57. Asloun, El. M., Nardin, M. and J. Schultz, "Stress Transfer in Single-Fibre Composites: Effect of Adhesion, Elastic Modulus of Fibre and Matrix, and Polymer Chain Mobility," *J. Mater. Sci.*, Vol. 24, 1835 (1989).

58. Rao, V. and L. T. Drzal, "The Temperature Dependence of Interfacial Shear Strength for Various Polymeric Matrices Reinforced with Carbon Fibers," accepted for publication in special issue of *J. Adhesion* honoring Dr. L. Sharpe, to appear February (1992).

59. Ohsawa, T., Nakayama, A., Miwa, M. and A. Hasegawa, "Temperature Dependence of Critical Fiber Length for Glass Fiber-Reinforced Thermosetting Resins," *J. Appl. Poly. Sci.*, Vol. 22, 3203 (1978).

60. Berglund, L. A. and J. M. Kenny, "Processing Science for High Performance Thermoset Composites," *SAMPE Journal*, Vol. 27(2), 27, March/April (1991).

61. Tajima, Y. A. and D. A. Crozier, "Chemorheology of an Amine-Cured Epoxy Resin," *Poly. Engr. and Sci.*, Vol. 26(6), 427, March (1986).

62. Lee, D-S. and C. D. Hahn, "A Chemorheological Model for the Cure of Unsaturated Polyester Resin," *Poly. Engr. and Sci.*, Vol. 27(13), 955, July (1987).

63. Billmeyer, F. W., *Textbook of Polymer Science*, John Wiley and Sons, New York (1984).

64. Lee, W. I., Loos, A. C. and G. S. Springer, "Heat of Reaction, Degree of Cure, and Viscosity of Hercules 3501-6 Resin," *J. Comp. Mater.*, Vol. 16, 510, November (1982).

65. Hawley, M. C and J. D. Delong, "*Polymer Reaction Engineering in Composite Materials*," Chemical Reaction Engineering III, Proposal to National Science Foundation, Santa Barbera, CA, February (1990).

66. Moroni, A., Mijovic, J. Pearce, E. M. and C. C. Foun, "Cure Kinetics of Epoxy Resins and Aromatic Diamines," *J. Appl. Poly. Sci.*, Vol. 32, 3761 (1986).

67. R. B. Prime, "Differential Scanning Calorimetry of the Epoxy Cure Reaction," *Poly. Engr. and Sci.*, Vol. 13(5), 365, September (1973).

68. M. R. Kamal, "Thermoset Characterization for Moldability Analysis," *Poly. Engr. and Sci.*, Vol. 1(3), 231, March (1974).

69. Dutta, A. and M. E. Ryan, "Effect of Fillers on Kinetics of Epoxy Cure," *J. Appl. Poly. Sci.*, Vol. 24, 635 (1979).

70. Acitelli, M. A., Prime, R. B. and E. Sacher, "Kinetics of Epoxy Cure: (1) The System Bisphenol-A Diglycidyl Ether/m-Phenylene Diamine, *Polymer*, Vol. 12, 335 (1971).

71. Kissinger, H. E., "A Simplistic approach to the analysis of Kinetic Data," *Anal. Chem.*, Vol. 29, 1702 (1957).

72. Chiou, P. and A. Letton, "Reaction Kinetics and Chemoviscosity of a Thermoset Exhibiting Complex Curing Behavior," **Proceedings of the Sixth Annual ASM/ESD Advanced Composites Conference**, Design and Processing Technologies, Detroit, MI, 217, October (1990).

73. Craido, J. M. and A. Ortega, "Non-Isothermal Transformation Kinetics: Remarks on the Kissinger Method," *Journal of Non-Crystalline Solids*," Vol. 87, 302 (1986).

74. Pascault, J. P. and J. J. Williams, "Relationships between Glass Transition Temperature and Conversion," *Polymer Bulletin*, Vol. 24, 115 (1990).

75. Tung, C-Y. M. and P. J. Dynes, "Relationship between Viscoelastic Properties and Gelation in Thermosetting Systems," *J. Appl. Poly. Sci.*, Vol. 27, 569 (1982).

76. Golding, B., *Polymers and Resins: their Chemistry and Chemical Engineering*, D. Van Nostrand Company, Inc., New York (1959).

77. Flory, P. J., *Principles of Polymer Chemistry*, Cornell University Press, New York (1953).

78. Mijovic, J. and B. Schafran, "Chemorheology of Bismaleimide Resins," *SAMPE Journal*, Vol. 26 (3), May/June (1990).

79. Rao, V., Herrera-Franco, P., Ozzello, A. D. and L. T. Drzal, "A Direct Comparison of the Fragmentation Test and the Microbond Pull-Out Test for Determining the Interfacial Shear Strength," *J. Adhesion*, Vol. 34, 65 (1991).

80. Rao, V. and L. T. Drzal, "Note: Loss of Curing Agent During Thin Film (Droplet) Curing of Thermoset Material," accepted for publication in *J. Adhesion* as a NOTE (Vol. 35), (1991).

81. Herrera-Franco, P., Rao, V., Chiang, M. Y-M. and L. T. Drzal, "Bond Strength Measurement in Composites-Analysis of Experimental Techniques," accepted for publication in *Composite Technology* (1991).

82. Frazer, W. A., Ancker, F. H., DiBenedetto, A. T. and B. Eberli, *Polym. Comp.*, Vol. 4, 3203 (1978).

83. Drzal, L. T. and M. J. Rich, "Effect of Graphite Fiber/Epoxy Matrix Adhesion on Composite Fracture Behavior," Research Advances in Composites in the United States and Japan, **ASTM STP 864**, J. R. Vinson and M. Taya, Eds., American Society for Testing and Materials, Philadelphia, 16 (1985).

84. Lee, S. M. and S. Holguin, "A New Single Fiber/Resin Interface Test for Highly Cross-Linked Resin Systems," *J. Adhesion*, Vol. 31, 91 (1990).

85. Piggott, M. R., Chua, P. S. and D. Andison, "The Interface between Glass and Carbon Fibers and Thermosetting Polymers," *Polym. Comp.*, Vol. 6(4), 242, October (1985).

86. Eagles, D. B., Blumentritt, B. F. and S. L. Cooper, "Interfacial properties of Kevlar-49 Fiber-Reinforced Thermoplastics," *J. Appl. Poly. Sci.*, Vol. 20, 435 (1976).

87. Jarvela, P., "The three-fibre method in determining environmental resistance of a fibre-resin bond," *J. Mater. Sci.*, Vol. 20, 4001 (1985).

88. Penn, L. S., Tesoro, G. C. and H. X. Zhou, "Some Effects of Surface-Controlled Reactions of Kevlar 29 on the Interface in Epoxy Composites," *Polym. Comp.*, Vol. 9(3), 184, June (1988).

89. McAlea, K. P. and G. J. Besio, "Adhesion between Polybutylene Terephthalate and E-Glass Measured With a Microbond Technique," *Polym. Comp.*, Vol. 9(4), 285, August (1988).

90. Biro, D. A., McLean, P. and Y. Deslandes, "Application of the Microbond Technique: Characterization of Carbon Fiber-Epoxy Interfaces," *Poly. Engr. and Sci.*, Vol. 37(17), 1250, Mid-September (1991).

91. Ozzello, A., Grummon, D. S., Drzal, L. T., Kalantar, J. S., Loh, I. H. and R. A. Moody, "Interfacial Shear Strength of Ion Beam Modified UHMW-PE Fibers in Epoxy Matrix Composites," in Interface between Polymers, Metals and Ceramics (B. M. Dekoven, A. J. Gellman and R. Rosenberg, Eds.), **Materials Research Society Symposium Proceedings**, Pittsburgh, PA, Vol. 153, 217 (1989).

92. Haaksma, R. A. and M. J. Cehelnik, "A Critical Evaluation of the Use of the Microbond Method for Determination of Composite Interfacial Properties," **MRS Meeting**, Boston, MA, December (1989).

93. Private Communication with Dr. E. A. Grulke, Department of Chemical Engineering, Michigan State University (1991).

94. Piggott, M. R., "The Effect of the Interface/Interphase on Fiber Composite Properties," *Polym. Comp.*, Vol. 8(5), 291, October (1987).

95. Cox, H. L., "The Elasticity and Strength of Paper and other Fibrous Materials," *Br. J. Appl. Physics*, Vol. 3(1), 122 (1952).

96. Kendall, K., "Model Experiments Illustrating Fibre Pull-out," *J. Mater. Sci.*, Vol. 10, 1011 (1975).

97. Theocaris, P. S., *The Mesophase Concept in Composites*, Springer-Verlag Press, New York (1987).

98. Rosen, B. W., "Mechanics of Composite Strengthening in Fibre Composite Materials," Chapter 3 in *Fiber Composite Materials*, Amer. Soc. for Metals, 72 (1964).

99. Dow, N. F., "*Study of Stresses near a Discontinuity of a Filament-Reinforced Composite Material*," General Electronic Company, Report TIS R635D61 (1963).

100. Hook, K. J., Agrawal, R. K. and L. T. Drzal, "Effects of Microwave Processing on Fiber-Matrix Adhesion. II. Enhanced Chemical Bonding of Epoxy to Carbon Fibers," *J. Adhesion*, Vol. 32, 157 (1990).

101. Drzal, L. T., Rich, M. J. and P. F. Lloyd, "Adhesion of Graphite Fibers to Epoxy Matrices: I. The Role of Fiber Surface Treatment," *J. Adhesion*, Vol. 16, 1 (1982).

102. Whitney, J. M. and L. T. Drzal, "Three-Dimensional Stress Distribution around an isolated Fiber Fragment," in *Toughened Composites*, ASTM STP 937, 179 (1980).

103. Adamson, W. A., *Physical Chemistry of Surfaces*, Chapter XII, John Wiley and Sons, New York (1982).

104. Schultz, J., Lavielle, L. and C. Martin, "The Role of the Interface in Carbon Fiber-Epoxy Composites," *J. Adhesion*, Vol. 23, 45 (1987).

105. Penn, L. S. and E. R. Bowler, "A New Approach to Surface Energy Characterization for Adhesive Performance Prediction," *Surface and Interface Analysis*, Vol. 3(4), 161 (1981).

106. Wu, H. F., Biresaw, G. and J. T. Laemmle, "Effect of Surfactant Treatments on Interfacial Adhesion in Single Graphite/Epoxy Composites," *Polym. Comp.*, Vol. 12(4), 281, August (1991).

107. Nimmer, R. F., "Fiber-Matrix Interface Effects in the Presence of Thermally Induced Residual Stresses," *Journal of Composites Technology & Research*, JCTRER, Vol. 12(2), 65, Summer (1990).

108. Miwa, M., Nakayama, A., Ohsawa, T. and A. Hasegawa, "Temperature Dependence of the Tensile Strength of Glass Fiber-Epoxy and Glass Fiber-Unsaturated Polyester Composites," *J. Appl. Poly. Sci.*, Vol. 23, 2957 (1979).

109. Sharpe, L., "The Interphase in Adhesion," *J. Adhesion*, Vol. 3, 51 (1972).

110. Donnet, J. B. and G. Guilpain, "Research Report: Surface Characterization of Carbon Fibers," *Composites*, Vol. 22(1), 59, January (1991).

111. Schultz, J. and M. Nardin, "Interfacial Adhesion, Interphase Formation and Mechanical Properties of Single Fibre Polymer Based Composites," in **Controlled Interphases in Composite Materials** (Edited by H. Ishida), Third International Conference on Composite Interfaces, Elsevier, New York, 561(1990).

112. Gutowski, W., "Effect of Fibre-Matrix Adhesion on Mechanical Properties of Composites," in **Controlled Interphases in Composite Materials** (Edited by H. Ishida), Third International Conference on Composite Interfaces, Elsevier, New York, 505(1990).

113. Gerard, J. F., Amdouni, N., Sautereau, H. and J. P. Pascault, "Introduction of a Rubbery Interphase in Glass/Epoxy Composite Materials: Influence of the Interlayer Thickness on the Viscoelastic and Mechanical Properties of Particulate and Unidirectional Composites," in **Controlled Interphases in Composite Materials** (Edited by H. Ishida), Third International Conference on Composite Interfaces, Elsevier, New York, 441(1990).

114. Kalantar, J. S., "*Bonding Mechanism of Aramid Fibers to Epoxy Matrices*," Masters Thesis, Department of Chemical Engineering, Michigan State University (1988).

115. DeLong, J. D., Hook, K. J., Rich, M. J., Kalantar, J. K. and L. T. Drzal, "Spectroscopic Characterization of Fiber-Polymer Interphases," in **Controlled Interphases in Composite Materials** (Edited by H. Ishida), Third International Conference on Composite Interfaces, Elsevier, New York, 87(1990).

116. Kalantar, J. and L. T. Drzal, "The Bonding Mechanism of Aramid Fibres to Epoxy Matrices, Part I: A review of the literature," *J. Mater. Sci.*, Vol. 25, 4186 (1990).

117. Gupta, V. B., Drzal, L. T., Lee, Y-C. and M. J. Rich, "The Temperature-Dependence of Some Mechanical Properties of a Cured Epoxy Resin System," *Poly. Engr. and Sci.*, Vol. 25(13), 812, September (1985).

118. Drzal, L. T., Rich, M. J., Koenig, M. F. and P. F. Lloyd, "Adhesion of Graphite Fibers to Epoxy Matrices: II. The Effect of Fiber Finish," *J. Adhesion*, Vol. 16, 133 (1983).

119. Drzal, L. T., "The Role of the Fiber-Matrix Interphase on Composite Properties," *Vacuum*, Vol. 41(7-9), 1615 (1990).

120. Sottos, N. R., Scott, W. R. and R. L. McCullough, "Micro-Interferometry for Measurement of Thermal Displacements at Fiber/Matrix Interfaces," *Experimental Mechanics*, Vol. 20, 98, June (1991).

121. Horie, K., Murai, H. and I. Mita, "Bonding of Epoxy Resin to Graphite Fibres," *Fiber Sci. and Tech.*, Vol. 9, 253 (1976).

122. Hughes, J. D. H., "The Carbon Fibre/Epoxy Interface-A Review," *Comp. Sci. and Tech.*, Vol. 41, 13 (1991).

123. Garton, A. and W. T. K. Stevenson, "Crosslinking of Epoxy Resins at Interfaces. IV. Anhydride-Cured Resins at Carbon and Graphite Surfaces," *J. Poly. Sci. Part A: Polymer Chemistry*, Vol. 26, 541 (1988).

124. Chang, J., Bell, J. P. and R. Joseph, "Effects of a Controlled Modulus Interlayer Upon the Properties of Graphite/Epoxy Composite," *SAMPE Quarterly*, Vol. 18(3), 39, April (1987).

125. Kim, J-K. and Y-W. Mai, "High Strength, High Fracture Toughness Fibre Composites with Interface Control- A Review," *Comp. Sci. and Tech.*, Vol. 41, 333 (1991).

126. Gray, R. J., "Experimental Techniques for Measuring Fibre/Matrix Interfacial Bond Shear Strength," *Intl. J. Adhesion and Adhesives*, Vol. 3(4), 197, October (1983).

127. Lee, S. and G. S. Springer, "Effects of Cure on the Mechanical Properties of Composites," *J. Comp. Mater.*, Vol. 22, 15 (1988).

128. Cazeneuve, C., Castle, J. E. and J. F. Watts, "The Structure of the Interface in Carbon Fibre Composites by Scanning Auger Microscopy," *J. Mater. Sci.*, Vol. 25, 1902 (1990).

129. Zukas, W. X., Craven, K. J. and S. E. Wentworth, "Model Adherend Surface Effects on Epoxy Cure Reactions," *J. Adhesion*, Vol. 33, 89 (1990).

130. Robertson, R. E., "The Strength of an Adhesive Weak Boundary Layer," *J. Adhesion*, Vol. 7, 121 (1975).

131. Netravali, A. N., Schwartz, P. and S. L. Phoenix, "Study of Interfaces of High-Performance Glass Fibers and DGEBA-based Epoxy Resins using Single-Fiber-Composite Test," *Polym. Comp.*, Vol. 10(6), 385, December (1989).

132. Theocaris, P. S. and T. P. Philippidis, "Theoretical Evaluation of the Extent of the Mesophase in Particulate and Fibrous Composites," *J. Rein. Plas. and Comp.*, Vol. 4, 173, April (1975).

133. Theocaris, P. S., "Diffusion-Based Adhesive Bonds between Phases in Fibrous Composites," *Colloid Polym. Sci.*, Vol. 268, 414 (1990).

134. Morgan, R. J., Kong, F-M. and C. M. Walkup, "Structure-Property Relations of Polyethertriamine-cured bisphenol-A-diglyicidyl Ether Epoxies, *Polymer*, Vol. 25, 375, March (1984).

135. Gupta, V. B., Drzal, L. T., Lee, Y-C. and M. J. Rich, "The Effects of Stoichiometry and Structure on the Dynamic Torsional Properties of a Cured Epoxy Resin System," *J. Macromol. Sci.-Phys.* Vol. B23(4-6), 435 (1984-85).

136. Crank, J., *The Mathematics of Diffusion*, Clarendon Press, Oxford (1975).

137. Kaplan, M. L., "Solvent Penetration in Cured Epoxy Networks," *Poly. Engr. and Sci.*, Vol. 31(10), 689, May 1991.

138. Munjal, S. and C-I. Kao, "Mathematical Model for Experimental Investigation of Polycarbonate Pellet Drying," *Poly. Engr. and Sci.*, Vol. 30(21), 1352, Mid-November (1990).

139. Miwa, M., Ohsawa, T., Kawade, M. and E. Taushima, "A New Method For Measurement of Carbon Fiber Axial Compressive Strength and Some Applications," **Proceedings for the Seventh ICCM Conference in Beijing**, Beijing, China, August (1989).

140. Peterson, R. E., *Stress Concentration Factors*, John-Wiley and Sons, New York (1974).

141. Middleman, S., *Fundamentals of Polymer Processing*, McGraw-Hill Book Co., New York (1977).

142. Bascom, W. D., "Interfacial Adhesion of Carbon Fibers," **NASA Contractor Report 178306 (Hercules, Inc.)**, Contract NAS1-17918, Magna, Utah (1987).

143. Bascom, W. D., Yon, K-J., Jensen, R. M. and L. Cordner, "The Adhesion of Carbon Fibers to Thermoset and Thermoplastic Polymers," *J. Adhesion*, Vol. 34, 79 (1991).

144. Hunston, D. L., Moulton, R. J., Johnston, N. J. and W. D. Bascom, "Matrix Resin Effects in Composite Delamination: Mode I Fracture Aspects, *Toughened Composites*, STP 937, N. J. Johnston Ed. (American Society for Testing and Materials, Philadelphia, PA), 74 (1987).

145. Parker, D. S. and A. F. Yee, "Factors Influencing the Mode I Interlaminar Toughness of a Rubber Toughened Thermoplastic Matrix Composite," *Journal of Thermoplastic Composite Materials*, Vol. 2, 2, January (1989).

146. Muzzy, J., Norpoth, L. and B. Varughese, "Characterization of Thermoplastic Composites For Processing," *SAMPE Journal*, Vol. 25(1), 23, January/February (1989).

147. Waterbury, M. C., "*The influence of processing, chemistry, and interphase microstructure on the adhesion of carbon fibers to thermoset and thermoplastic*

matrices," Ph.D. Dissertation, Michigan State University, Department of Metallurgy, Mechanics and Materials Science, August (1991).

148. Bascom, W. D., Cordner, L. W., Hinkley, J. L. and N. J. Johnston, "Determination of Carbon Fiber Adhesion to Thermoplastic Polymers Using the Single Fiber/Matrix Tensile Test," **Proceedings of the First ASC Technical Conference**, Dayton, OH, 238, October (1986).

149. Broutman, L. J., "Measurement of the Fiber-Polymer Matrix Interfacial Strength," *Interfaces in Composites*, ASTM STP 452, American Society for Testing and Materials, 27 (1969).

150. Cebe, P., "Non-Isothermal Crystallization of Poly(Etheretherketone) Aromatic Polymer Composite," *Polym. Comp.*, Vol. 9(4), 271, August (1988).

151. Scobbo, J. J. and N. Nakajima, "Strength and Failure of PEEK/Graphite Fiber Composites," *SAMPE Journal.*, 45, January/February (1990).

152. Jang, B., Liu, C. W., Wang, C. Z. and W. K. Shih, "Mechanical Properties and Morphology of Crystalline Polymers and Their Continuous Fiber Composites," *Journal of Thermoplastic Composite Materials*, Vol. 1, 242, July (1988).

153. Ryan, M. E. and A. Dutta, "Kinetics of Epoxy Cure: a Rapid Technique for Kinetic Parameter Estimation," *Polymer*, Vol. 20, 203, February (1979).